



A DIGITAL SPECTRAL ANALYSIS TECHNIQUE AND
ITS APPLICATION TO RADIO ASTRONOMY

by

SANDER WEINREB

B. S., Massachusetts Institute of Technology

SUBMITTED IN PARTIAL FULFILLMENT OF THE
REQUIREMENTS FOR THE DEGREE OF
DOCTOR OF PHILOSOPHY

at the

MASSACHUSETTS INSTITUTE OF TECHNOLOGY

February, 1963

Signature of Author

Department of Electrical Engineering, January 7, 1963

Certified by

Thesis Supervisor

Accepted by

Chairman, Departmental Committee on Graduate Students

A DIGITAL SPECTRAL ANALYSIS TECHNIQUE AND
ITS APPLICATION TO RADIO ASTRONOMY

by

SANDER WEINREB

Submitted to the Department of Electrical Engineering
on January 7, 1963 in partial fulfillment of the re-
quirements for the degree of Doctor of Philosophy.

ABSTRACT

An efficient, digital technique for the measurement of the autocorrelation function and power spectrum of Gaussian random signals is described. As is quite well known, the power spectrum of a signal can be obtained by a Fourier transformation of its autocorrelation function. This paper presents an indirect method of computing the autocorrelation function of a signal having Gaussian statistics; this method greatly reduces the amount of digital processing that is required.

The signal, $x(t)$, is first "infinitely clipped"; that is, a signal, $y(t)$, is produced, where $y(t) = 1$ when $x(t) > 0$ and $y(t) = -1$ when $x(t) < 0$. The normalized autocorrelation function, $\rho_y(\tau)$, of the clipped signal is then calculated digitally. Since $y(t)$ can be coded into one-bit samples, the autocorrelation processing (delay, storage, multiplication, and summation) can be performed quite easily in real time by a special purpose digital machine — a one-bit digital correlator. The resulting $\rho_y(\tau)$ can then be corrected to give the normalized autocorrelation function, $\rho_x(\tau)$, of the original signal. The relation is due to Van Vleck and is simply $\rho_x(\tau) = \sin[\pi\rho_y(\tau)/2]$.

The paper begins with a review of the measurement of power spectra through the autocorrelation function method. The one-bit technique of computing the autocorrelation function is then presented; in particular the mean and variance of the resulting spectral estimate are investigated.

These results are then applied to the problem of the measurement of spectral lines in radio astronomy. A complete radio astronomy system is described. The advantages of the system are: 1) It is a multichannel system; that is, many points are determined on the spectrum during one time interval, 2) Since digital techniques are used, the system is very accurate and highly versatile. The system that is described was built for the purpose of attempting to detect the galactic deuterium line. The last three chapters describe the results of tests of this system, the deuterium line attempt, and an attempt to measure Zeeman splitting of the 21 cm hydrogen line.

Thesis Supervisor: Jerome B. Wiesner
Title: Institute Professor

ACKNOWLEDGMENT

My first thanks must go to Dr. H.I. Ewen who, in 1957, aroused my interest in radio astronomy and suggested the deuterium-line search to me. Dr. Ewen also made a generous contribution to the initial financing of this work.

Next, I would like to thank my supervisor, Prof. J.B. Wiesner, for encouraging me to undertake this research as a doctoral thesis, being ever so helpful in obtaining technical and financial support; and, by his interest and quality of leadership, being a constant source of inspiration for my work. It is fortunate for me that he was present at M.I. T. long enough to fulfill these first two functions and that his presence was not required for the third function.

Many people have been sources of encouragement and helpful technical discussions concerning various aspects of the thesis. I would especially like to thank Dr. R. Price of Lincoln Laboratory, Profs. A.G. Bose and A.H. Barrett of M.I. T., Prof. A.E. Lilley of Harvard College Observatory, and Drs. F.D. Drake, D.S. Heeschen, and T.K. Mennon of the National Radio Astronomy Observatory.

I am thankful to the founders and staff of the National Radio Astronomy Observatory for providing the excellent observing facilities and supporting help. My stay at Green Bank was one of the most pleasant and stimulating periods of my life.

The facilities of the M.I. T. Computation Center were used for part of this work. I appreciate the programming assistance provided by Mr. D.U. Wilde at M.I. T. and by Mr. R. Uphoff at Green Bank.

This work was supported in part by the National Science Foundation (grant G-13904) and in part by the U.S. Army Signal Corps, the Air Force Office of Scientific Research, and the Office of Naval Research.

TABLE OF CONTENTS

	Page
CHAPTER 1. INTRODUCTION	1
1.1 Statistical Preliminaries	2
1.2 Definition of the Power Spectrum	8
1.3 General Form of Estimates of the Power Spectrum	11
1.4 Comparison of Filter and Autocorrelation Methods of Spectral Analysis	13
1.5 Choice of the Spectral Measurement Technique	21
1.6 The One-Bit Autocorrelation Method of Spectral Analysis	27
CHAPTER 2. THE AUTOCORRELATION METHOD OF MEASURING POWER SPECTRA	32
2.1 Introduction	32
2.2 Mean of the Spectral Estimate	36
2.2-1 Relation of $P^*(f)$ to $P(f)$	36
2.2-2 The Weighting Function, $w(n\Delta\tau)$	39
2.2-3 Some Useful Properties of $P^*(f)$	42
2.3 Covariances of Many-Bit Estimates of the Autocorrelation Function and Power Spectrum	44
2.3-1 Definitions: Relation of the Spectral Covariance to the Autocorrelation Covariance	45

TABLE OF CONTENTS (Continued)

	Page
2.3-2 Results of the Autocorrelation Covariance Calculation	46
2.3-3 Results of the Spectral Covariance Calculation	50
2.4 Normalized, Many-Bit Estimates of the Spectrum and Autocorrelation Function	52
2.4-1 Mean and Variance of the Normalized Autocorrelation Function	55
2.4-2 Mean and Variance of the Normalized Spectral Estimate	57
CHAPTER 3. THE ONE-BIT METHOD OF COMPUTING AUTOCORRELATION FUNCTIONS	60
3.1 Introduction	60
3.2 The Van Vleck Relation	64
3.3 Mean and Variance of the One-Bit Autocorre- lation Function Estimate	66
3.4 Mean and Variance of the One-Bit Power Spectrum Estimate	71
CHAPTER 4. THE RADIO-ASTRONOMY SYSTEM	76
4.1 The System Input-Output Equation	76
4.2 Specification of Antenna Temperature	80
4.2-1 Correction of Effect of Receiver Bandpass	81
4.2-2 Measurement of T_{av}	84

TABLE OF CONTENTS (Continued)

	Page
4.2-3 Measurement of $T_r(f+f_o)$	85
4.2-4 Summary	86
4.3 The Switched Mode of Operation	87
4.3-1 Motivation and Description	87
4.3-2 The Antenna Temperature Equation	93
4.4 System Sensitivity	94
 CHAPTER 5. SYSTEM COMPONENTS	 98
5.1 Radio Frequency Portion of the System	98
5.1-1 Front-End Switch and Noise Source	98
5.1-2 Balance Requirements	101
5.1-3 Shape of the Receiver Bandpass, $G(f+f_o)$	103
5.1-4 Frequency Conversion and Filtering	105
5.2 Clippers and Samplers	107
5.3 The Digital Correlator	112
 CHAPTER 6. SYSTEM TESTS	 122
6.1 Introduction - Summary	122
6.2 Computer Simulation of the Signal and the Signal-Processing System	124
6.2-1 Definitions and Terminology	125
6.2-2 Computer Method	128
6.2-3 Results and Conclusions	131

TABLE OF CONTENTS (Continued)

	Page	
6.3	Measurement of a Known Noise Power Spectrum	140
6.3-1	Procedure	140
6.3-2	Results	143
6.4	Measurements of Artificial Deuterium Lines	145
6.5	Analysis of the RMS Deviation of the Deuterium-line Data	150
6.5-1	Theoretical RMS Deviation	150
6.5-2	Experimental Results	153
CHAPTER 7.	THE DEUTERIUM-LINE EXPERIMENT	158
7.1	Introduction	158
7.2	Physical Theory and Assumptions	161
7.3	Results and Conclusions	169
CHAPTER 8.	AN ATTEMPT TO MEASURE ZEEMAN SPLITTING OF THE 21-cm HYDROGEN LINE	173
8.1	Introduction	173
8.2	Experimental Procedure	174
8.3	Results and Conclusions	176

TABLE OF CONTENTS (Continued)

	Page
APPENDIX A	181
Equivalence of the Filter Method and the Autocorrelation Method of Spectral Analysis	
APPENDIX B	186
The E1B Method of Autocorrelation Function Measurement	
APPENDIX C	190
Calculation of the Covariances of Many-Bit Estimates of the Autocorrelation Function and Power Spectrum	
APPENDIX D	196
Computer Programs	
D. 1 Doppler Calculation Program	196
D. 2 Deuterium and Zeeman Data Analysis Program	200
D. 3 Computer Simulation Program	204
REFERENCES	209
BIOGRAPHICAL NOTE	213

LIST OF ILLUSTRATIONS

Figure		Page
1.1	A Random Process	4
1.2	Methods of Spectral Measurement	14
1.3	Filter-Array Equivalent of Autocorrelation System	19
1.4	Analog and Digital Autocorrelation Methods of Spectral Measurement	22
1.5	Analog and Digital Filter Methods of Spectral Measurement	23
1.6	Ranges of Application of Various Spectral Measurement Techniques	25
1.7	The One-Bit Autocorrelation Method of Spectral Analysis	28
2.1	Effect of Sampling and Truncation of the Autocorrelation Function	38
2.2	Three Scanning Functions	41
2.3	General Forms of the RMS Deviations of the Autocorrelation Function and Power Spectrum	48
4.1	The Switched- One-Bit Autocorrelation Radiometer	90
4.2	The Switching Cycle	91
5.1	Radio-Frequency Portion of the Deuterium-Line Detection System	99
5.2	Circuitry Used in the Deuterium-Line Receiver to Perform the Clipping Operation	109
5.3	Sampling Configuration Used in the Deuterium-Line Experiment	110

LIST OF ILLUSTRATIONS (Continued)

Figure		Page
5.4	Effect of Large Gain Changes Upon the Measured Spectrum	110
5.5	Basic Block Diagram of a One-Bit Digital Correlator	113
5.6	Digital Correlator Used for the Deuterium-Line and Zeeman Experiments	119
5.7	Circuit Diagram of a High-Speed Correlator Channel	121
6.1	Block Diagram of Computer Simulation Program	129
6.2	Results of Computer Simulated Autocorrelation Function Measurements	133
6.3	Results of Computer Simulated Spectral Measurements	135
6.4	Procedure for Producing a "Known" Power Spectrum	141
6.5	Procedure Used to Measure $ H(f) $	141
6.6	Results Pertinent to Section 6.3	144
6.7	Artificial Deuterium-Line Generator	147
6.8	Artificial Deuterium-Line Results	149
6.9	Experimental and Theoretical Sensitivity of a Conventional Dicke Radiometer Compared with a One-Bit Autocorrelation Radiometer	157

LIST OF ILLUSTRATIONS (Continued)

Figure		Page
7.1	Configuration for the Deuterium-Line Experiment	164
7.2	Effects of a Spatially-Varying Hydrogen Optical Depth	164
7.3	Results of the Deuterium-Line Experiment	172
8.1	Results of Zeeman Observations in the Cas A Radio Source	179
8.2	Results of Zeeman Observations in the Taurus A Radio Source	180

LIST OF TABLES

Table		Page
1.1	Comparison of Two One-Bit Methods of Autocorrelation Function Measurement	31
2.1	Properties of Three Weighting Functions	40
6.1	Results of Computer Simulation Experiment - Autocorrelation Functions	132
6.2	Results of Computer Simulation Experiment - Power Spectra	134
6.3	Autocorrelation Function RMS Deviation	136
6.4	Spectral RMS Deviation	138
6.5	Analysis of the RMS Deviation of the Deuterium-Line Data	155
8.1	Zeeman Results	178

GLOSSARY

TIME FUNCTIONS

- $x(t)$ A stationary, ergodic, random time function having Gaussian statistics.
- $y(t)$ The function formed by infinite clipping of $x(t)$. That is, $y(t) = 1$ when $x(t) > 0$ and $y(t) = -1$ when $x(t) < 0$.

FREQUENCY AND TIME

Due to their rather standard usage in both communication theory and radio astronomy, the symbols, T and τ , symbolize different quantities in different sections of the paper. In the first 3 chapters, T is a time interval and τ is the autocorrelation function delay variable. In the last 6 chapters, T is temperature and τ is either optical depth or observation time. Some other frequency and time variables are the following:

- $\Delta t, k, K, f_t$ The time function sampling interval is Δt . A sample of the time function, $x(t)$, is $x(k\Delta t)$ where k is an integer. The total number of samples is K . The sampling frequency is $f_t = 1/\Delta t$. In most cases Δt and f_t will be chosen equal to $\Delta\tau$ and f_s , respectively.
- $\Delta\tau, n, N, f_s$ The autocorrelation function sampling interval is $\Delta\tau$. The samples of the autocorrelation function are $R(n\Delta\tau)$ where n is an integer going from 0 to $N-1$. The reciprocal of $\Delta\tau$ is f_s .

Δf	The frequency resolution of a spectral measurement (see Section 1.3). It will be approximately equal to $1/N\Delta\tau$.
B_1, B_{20}	The 1 db and 20 db bandwidths of a radio-meter. The spectrum is analyzed with resolution, Δf , in the band, B_1 . The sampling frequencies, f_t and f_s , are often chosen equal to $2B_{20}$.
f_o	A known combination of local oscillator frequencies.

AUTOCORRELATION FUNCTIONS

$R(\tau)$	The true autocorrelation function of $x(t)$.
$R''(\tau)$	A statistical estimate of $R(\tau)$ based upon unquantized or many-bit samples of $x(t)$.
$\rho(\tau)$ or $\rho_x(\tau)$	The true normalized autocorrelation function; $\rho(\tau) = R(\tau)/R(0)$.
$\rho''(\tau)$	A statistical estimate of $\rho(\tau)$ based upon unquantized or many-bit samples of $x(t)$.
$\rho'(\tau)$ or $\rho'_x(\tau)$	A statistical estimate of $\rho(\tau)$ based upon one-bit samples of $y(t)$.
$\rho_y(\tau)$	The true normalized autocorrelation function of $y(t)$.
$\rho'_y(\tau)$	A statistical estimate of $\rho_y(\tau)$ based upon one-bit samples of $y(t)$.

POWER SPECTRA

(The power spectrum is defined in Section 1.2)

$P(f)$	The true power spectrum of $x(t)$
$P''(f)$	A statistical estimate of $P(f)$ based upon unquantized or many-bit samples of $x(t)$
$P^*(f)$	The expected value of $P''(f)$
$p(f)$	The true normalized power spectrum; $p(f) = P(f)/R(0)$.
$p''(f)$	A statistical estimate of $p(f)$ based upon many-bit or unquantized samples of $x(t)$
$p'(f)$	A statistical estimate of $p(f)$ based upon one-bit samples of $y(t)$
$p^*(f)$	The expected value of $p'(f)$ and $p''(f)$.
$p'_c(f)$	The normalized spectral estimate produced by a one-bit autocorrelation radiometer when its input is connected to a comparison noise source.
$p'_o(f)$	A normalized estimate of the receiver power transfer function, $G(f)$. It is the spectral estimate produced by a one-bit autocorrelation radiometer when the input spectrum and receiver noise spectrum are white.
$\delta p'(f)$	The estimate of the difference spectrum that is determined by a switched radiometer; $\delta p'(f) = p'(f) - p'_c(f)$.

TEMPERATURES

$T_a(f)$	The power spectrum available at the antenna terminals expressed in degrees Kelvin.
$T_r(f)$	The receiver noise temperature spectrum.
$T(f)$	The total temperature spectrum referred to the receiver input. $T(f) = T_a(f) + T_r(f)$
$T_c(f)$	The spectrum of the comparison noise source.
T_{av}	The frequency-averaged value of $T(f)$. The average is weighted with respect to the receiver power transfer function, $G(f)$.
$T_{a\ av}$	The frequency-averaged value of $T_a(f)$.
$T_{c\ av}$	The frequency-averaged value of $T_c(f) + T_r(f)$.
$T_{r\ av}$	The frequency-averaged value of $T_r(f)$.
δT_{av}	The unbalance temperature; $\delta T_{av} = T_{av} - T_{c\ av}$.

RMS DEVIATIONS

A σ with two subscripts will be used to denote an RMS deviation of a statistical estimate. The first subscript will be a P, R, p, or ρ and indicates the variable to which the RMS deviation pertains. The second subscript will be a 1 or an m and indicates whether the statistical estimate is based upon one-bit or many-bit samples. Thus, for example, σ_{p1} is the RMS deviation of $p'(f)$, the one-bit estimate of $p(f)$. Statistical estimates of RMS deviations will have

a single subscript and a prime or double prime indicating whether one-bit or many-bit samples are referred to. For example, $\sigma_p'(f)$ is a statistical estimate of $\sigma_{p1}(f)$.

MISCELLANEOUS

$w(\tau)$	The function that is used to weight the autocorrelation function; see Section 2.2.
$W(f)$	The spectral scanning or smoothing function. It is the Fourier transform of $w(\tau)$; see Figure 2.2.
$G(f+f_0)$	The receiver power transfer function. The spectrum at the clipper input, $P(f)$, is equal to $G(f+f_0)$ times the input temperature spectrum, $T(f+f_0)$.

SPECIAL SYMBOLS

$\overline{x(t)}$	A line over a variable indicates that the statistical average is taken. See Equation 1.1.
$P^*(f)$	An asterisk superscript on a spectrum indicates that it has been smoothed and is repeated about integer multiples of the sampling frequency. This operation is discussed in Section 2.2.
$T^\dagger(f)$	The one-bit autocorrelation radiometer produces a statistical estimate of an input temperature spectrum such as $T(f)$. The statistical average or expected value of this estimate is equal to $T^\dagger(f)$. The relationship between $T(f)$ and $T^\dagger(f)$ is discussed in Section 4.2-1. Under proper conditions, such as a sufficiently fast sampling rate, $T^\dagger(f)$ is simply a smoothed version of $T(f)$.

CHAPTER 1

INTRODUCTION

This report can be divided into three parts which comprise Chapters 1 - 2 - 3, 4 - 5, and 6 - 7 - 8, respectively.

1) A technique for the measurement of the power spectrum and autocorrelation function of a Gaussian random process is presented. This technique, which will be referred to as "the one-bit autocorrelation method," has the property that it is easily performed digitally; hence, the accuracy and flexibility associated with digital instrumentation is achieved. The technique is a multichannel one; that is, many points on the spectrum and autocorrelation function can be determined at one time. A limitation is that the bandwidth analyzed must be less than 10 mc for operation with present-day digital logic elements.

2) The above technique will be applied to the problem of the measurement of spectral lines in radio astronomy. In Chapter 4 the composition and theoretical performance of a practical radio astronomy system utilizing the one-bit digital autocorrelation technique will be presented. The design of components of this system is discussed in Chapter 5.

3) The above system was constructed and extensive experimental results are given. These results are of laboratory tests of the

system, an attempt to detect the galactic deuterium line, and an attempt to measure Zeeman splitting of the 21 cm hydrogen line.

The reader who is interested in the radio astronomy aspects of the report may wish to skip Chapters 2 and 3; the results of these two chapters are summarized in radio astronomy terms in Chapter 4.

The remainder of this chapter will be spent on some background material, a comparison of filter and autocorrelation methods of spectral measurement, a classification of spectral measurement problems, and finally, a brief description of the one-bit autocorrelation method.

1.1 STATISTICAL PRELIMINARIES

A brief presentation of some of the statistical techniques and terminology used in this paper will be given in this section. In addition, some assumptions will be stated regarding the statistical nature of the signals of interest. For an introduction to statistical communication theory techniques, the reader is referred to Davenport and Root,¹ Chapters 1 - 6 (109 pages) or Bendat,² Chapters 1 and 2 (77 pages).

The type of signal which is of interest in this paper is the random time function; that is, a signal whose sources are so numerous, complicated, and unknown that exact prediction or description of the time function is impossible. Our interest is in the study of averages

of functions of the signal, in particular, the power spectrum, which will be defined in the next section.

A random variable, x , is the outcome of an experiment which (at least theoretically) can be repeated many times and has a result that cannot be exactly predicted. The flipping of a coin or the measurement of a noise signal at a given time are two such experiments. The outcome of a particular experiment is called a sample of the random variable; it is implied that there are a large number of samples (although many samples may have the same value).

The random variable is described by a probability density function, $p(x)$. The statistical average (this will sometimes be called the "mean") of a random variable will be denoted by a bar over the quantity being averaged, such as \bar{x} . In terms of the probability density function, the statistical average of x is given by,

$$\bar{x} = \int_{-\infty}^{\infty} x p(x) dx \quad (1.1)$$

In most signal analysis cases the random variable is a function of a parameter such as frequency or time. Thus, there is an infinite number of random variables, one for each value of the parameter. For each random variable there is a large number of samples. This two dimensional array of sample functions is called a random process and is illustrated on the following page.

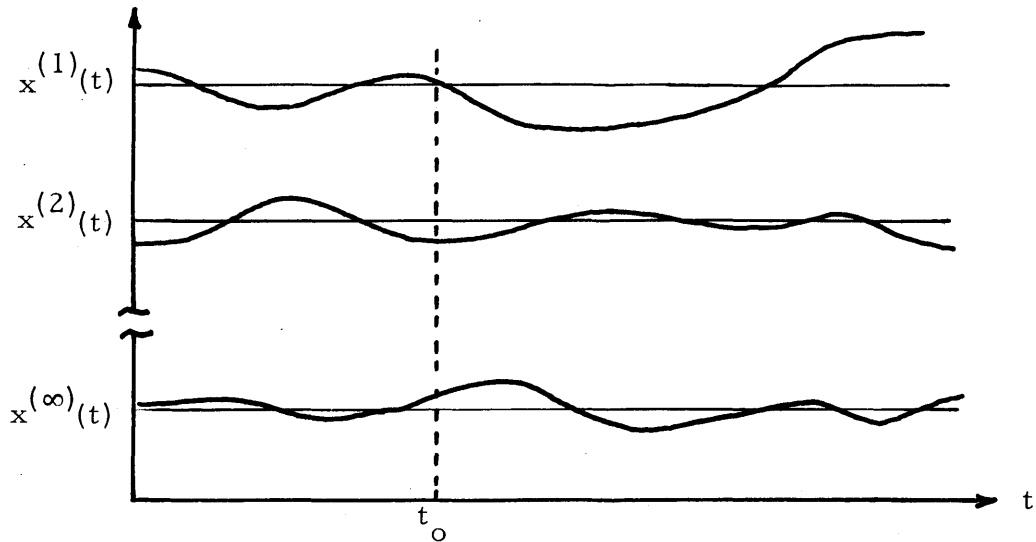


Figure 1.1

The concept of a random process with time as the parameter is shown in Figure 1.1. For each value of time a random variable, x_{t_0} , is defined. Each random variable has an infinite number of samples, $x_{t_0}^{(1)}, x_{t_0}^{(2)}, \dots, x_{t_0}^{(\infty)}$. The random process can also be described as having an infinite number of sample functions, $x^{(1)}(t), x^{(2)}(t), \dots, x^{(\infty)}(t)$. (The superscripts will be dropped when they are not needed for clarity.)

Statistical averages, such as $\overline{x_{t_0}}$, are taken vertically through the random process array and may or may not be a function of time.

Time averages, such as,

$$\frac{1}{T} \int_0^T x(t) dt$$

are taken across the array and may or may not depend on the sample function chosen.

It will be assumed that signals whose power spectra we wish to measure are stationary and ergodic. By this it is meant that statistical averages such as $\overline{x_{t_0}}$, $\overline{x_{t_0}^2}$, and $\overline{x_{t_0} x_{t_0 + \tau}}$ are independent of the time, t_0 , and are equal to the infinite time averages which, in turn, are independent of the particular sample function, i. e.,

$$\overline{x_{t_0}} = \lim_{T \rightarrow \infty} \frac{1}{2T} \int_{-T}^T x(t) dt \quad (1.2)$$

$$\overline{x_{t_0}^2} = \lim_{T \rightarrow \infty} \frac{1}{2T} \int_{-T}^T x^2(t) dt \quad (1.3)$$

$$\overline{x_{t_0} x_{t_0 + \tau}} = \lim_{T \rightarrow \infty} \frac{1}{2T} \int_{-T}^T x(t) x(t+\tau) dt \quad (1.4)$$

These assumptions imply that the power spectrum does not vary with time (at least over the period of time that measurements are made). This is the usual situation in radio astronomy except for the case of solar noise.

Under the stationary and ergodic assumptions the sample functions of the random process have a convenient interpretation, each sample

function is a "record" or length of data obtained during different time intervals. The statistical average then has the interpretation as the average result of an operation repeated on many records.

The quantity, $\overline{x_{t_0} x_{t_0 + \tau}}$, is called the autocorrelation function of the signal. From Equation 1.4 we see that under the stationary and ergodic assumption the autocorrelation function can also be expressed as an infinite time average. Because of the stationary assumption, $\overline{x_{t_0} x_{t_0 + \tau}}$ is not a function of t_0 and the notation, $R_x(\tau)$ or $R(\tau)$, will be used to signify the autocorrelation function.

In words, the autocorrelation function is the (statistical or infinite time) average of the signal multiplied by a delayed replica of itself. $R_x(0)$ is simply the mean square, $\overline{x^2}$, of the signal, while $R_x(\infty)$ is equal to the square of the mean, \bar{x} . It is easily shown that $R_x(0) \geq R_x(\tau) = R_x(-\tau)$. The normalized autocorrelation function, $\rho_x(\tau)$, is equal to $R_x(\tau)/R_x(0)$ and is always less than or equal to unity.

The variance, σ_x^2 , of a random variable is a measure of its dispersion from its mean. It is defined as,

$$\sigma_x^2 \equiv \overline{(x - \bar{x})^2} \quad (1.5)$$

$$= \overline{x^2} - \bar{x}^2 \quad (1.6)$$

The positive square root of the variance is the RMS deviation, σ_x .
 The statistical uncertainty, Δ_x , of a random variable is the RMS deviation divided by the mean,

$$\Delta_x = \frac{\sigma_x}{\bar{x}} \quad (1.7)$$

As is often the case in the analysis of random signals, it will be assumed that the signal has Gaussian statistics in the sense that the joint probability density function, $p(x_t, x_{t+\tau})$, is the bivariate Gaussian distribution,

$$p(x_t, x_{t+\tau}) = \frac{1}{2\pi R_x(0) [1 - \rho_x^2(\tau)]^{1/2}} \cdot \exp \left\{ \frac{x_t^2 - 2\rho_x(\tau)x_t x_{t+\tau} + x_{t+\tau}^2}{-2 R_x(0) [1 - \rho_x^2(\tau)]} \right\} \quad (1.8)$$

This assumption is often justified by the central limit theorem (see Bendat², Chapter 3) which states that a random variable will have a Gaussian distribution if it is formed as the sum of a large number of random variables of arbitrary probability distribution. This is usually true in the mechanism which gives rise to the signals observed in radio astronomy.

1.2 DEFINITION OF THE POWER SPECTRUM

The power spectrum is defined in many ways dependent on: 1) The mathematical rigor necessary in the context of the literature and application in which it is discussed, 2) Whether one wishes to have a single-sided or double-sided power spectrum (positive and negative frequencies, with $P(-f) = P(f)$), 3) Whether one wishes $P(f)\Delta f$ or $2P(f)\Delta f$ to be the power in the narrow bandwidth, Δf .

In this paper, the double-sided power spectrum will be used since it simplifies some of the mathematical equations that are involved. The negative-frequency side of the power spectrum is the mirror image of the positive-frequency side; in most cases it need not be considered. In accordance to common use by radio astronomers and physicists, $P(f)\Delta f$ (or $P(-f)\Delta f$) will be taken to be the time average power in the bandwidth, Δf , in the limit as $\Delta f \rightarrow 0$ and the averaging time, $T \rightarrow \infty$. Thus, the total average power, P_T , is given by,

$$P_T = \int_0^{\infty} P(f) df \quad (1.9)$$

or

$$P_T = \frac{1}{2} \int_{-\infty}^{\infty} P(f) df \quad (1.10)$$

(if an impulse occurs at $f = 0$, half of its area should be considered to be at $f > 0$ for evaluation of Equation 1.9).

The statements of the preceding paragraph are not a sufficiently precise definition of the power spectrum because: 1) The relationship of $P(f)$ to the time function, $x(t)$, is not clear, 2) The two limiting processes ($\Delta f \rightarrow 0$, $T \rightarrow \infty$) cause difficulty; i. e., what happens in the limit to the product, $T\Delta f$?

A more precise definition of the power spectrum is obtained by defining $P(f)$ as twice the Fourier transform of the autocorrelation function, $R(\tau)$, defined in the previous section. Thus, we have

$$P(f) = 2 \int_{-\infty}^{\infty} R(\tau) e^{-j2\pi f\tau} d\tau \quad (1.11)$$

$$R(\tau) = \lim_{T \rightarrow \infty} \frac{1}{2T} \int_{-T}^T x(t) x(t+\tau) d\tau \quad (1.12)$$

The inverse Fourier transform relation gives,

$$R(\tau) = \int_0^{\infty} P(f) \cos 2\pi f\tau df \quad (1.13)$$

$$R(\tau) = \frac{1}{2} \int_{-\infty}^{\infty} P(f) e^{-j2\pi f\tau} df \quad (1.14)$$

This definition of the power spectrum gives no intuitive feeling as to the relation of $P(f)$ to power. We must prove then, that this definition has the properties stated in the second paragraph of this section. Equations 1.9 and 1.10 are easily proved by setting $\tau = 0$ in Equations 1.12, 1.13, and 1.14. We find,

$$R(0) = \lim_{T \rightarrow \infty} \frac{1}{2T} \int_{-T}^T x^2(t) dt \quad (1.15)$$

$$R(0) = \int_0^{\infty} P(f) df \quad (1.16)$$

The right-hand side of Equation 1.15 is identified as P_T , the total average power. Power is used in a loose sense of the word; P_T is the total average power dissipated in a one-ohm resistor if $x(t)$ is the voltage across its terminals, otherwise a constant multiplier is needed.

The proof that $P(f)\Delta f$ is the time average power in the band Δf , as $\Delta f \rightarrow 0$ and $T \rightarrow \infty$ is not as direct. Suppose that $x(t)$ is applied to a filter having a power transfer function, $G(f)$. It can be shown by using only Equations 1.11 and 1.12 that the output power spectrum, $P_o(f)$, is given by (see Davenport and Root,¹ p. 182),

$$P_o(f) = G(f) P(f) \quad (1.17)$$

If $G(f)$ is taken to be equal to unity for narrow bands of width, Δf , centered at $+f$ and $-f$, and zero everywhere else, we find

$$\int_0^{\infty} P_o(f) df = P(f) \Delta f \quad (1.18)$$

as $\Delta f \rightarrow 0$. The left-hand side of Equation 1.18 is simply the average power out of the filter (using Equations 1.15 and 1.16) and, hence, $P(f) \Delta f$ must be the power in the bandwidth Δf .

1.3 THE GENERAL FORM OF ESTIMATES OF THE POWER SPECTRUM

The power spectrum of a random signal cannot be exactly measured by any means (even if the measurement apparatus has perfect accuracy); the signal would have to be available for infinite time. Thus, when the term "measurement of the power spectrum" is used, what is really meant is that a statistical estimate, $P'(f)$, is measured.

The measured quantity, $P'(f)$, is a sample function of a random process; its value depends on the particular time segment of the random signal that is used for the measurement. It is an estimate of $P(f)$ in the sense that its statistical average, $\overline{P'(f)}$, is equal to a function, $P^*(f)$, which approximates $P(f)$. The statistical uncertainty of $P'(f)$ and the manner in which $P^*(f)$ approximates $P(f)$ appear to be invariant to the particular spectral measurement technique and will be briefly discussed in the next two paragraphs.

The function, $P^*(f)$, approximates $P(f)$ in the sense that it is a smoothed version of $P(f)$. It is approximately equal to the average value of $P(f)$ in a band of width, Δf , centered at f ,

$$P^*(f) \sim \frac{1}{\Delta f} \int_{f-\Delta f/2}^{f+\Delta f/2} P(f) df \quad (1.19)$$

The statistical uncertainty, Δ_p , of $P^i(f)$, will be given by an equation of the form

$$\Delta_p(f) \equiv \frac{\sqrt{[P^i(f) - P^*(f)]^2}}{P^*(f)} = \frac{\alpha}{\sqrt{T \Delta f}} \quad (1.20)$$

where T is the time interval that the signal is used for the measurement and α is a numerical factor of the order of unity dependent on the details of the measurement.

Equations 1.19 and 1.20 are the basic uncertainty relations of spectral measurement theory and appear to represent the best performance that can be obtained with any measurement technique (see Grenander and Rosenblatt,³ p. 129). Note that as the frequency resolution, Δf , becomes small making $P^*(f)$ a better approximation of $P(f)$, the statistical uncertainty becomes higher [$P^i(f)$ is a worse estimate of $P^*(f)$]. Optimum values of Δf , with the criterion of minimum mean square error between $P^i(f)$ and $P(f)$ are given by Grenander and Rosenblatt, pp. 153-155. In practice, Δf is usually chosen somewhat narrower than the spectral features

one wishes to examine and T is chosen, if possible, to give the desired accuracy.

1.4 COMPARISON OF FILTER AND AUTOCORRELATION METHODS OF SPECTRAL ANALYSIS

Two general methods have been used in the past to measure the power spectrum. These are the filter method, shown in Figure 1.2 (a) and the autocorrelation method, shown in Figure 1.2 (b). In this section the two methods will first be briefly discussed. A filter-method system that is equivalent to a general autocorrelation-method system will then be found.

This result serves two purposes: 1) It helps to answer the question, "Which method is best?" 2) An intuitive understanding of the filter-method system is quite easily achieved, while this is not true for the autocorrelation-method system. Therefore, it is often helpful to think of the autocorrelation-method system in terms of the equivalent filter-method system.

The filter-method system of Figure 1.2 (a) is quite straight-forward. The input signal is applied in parallel to a bank of N bandpass filters which have center frequencies spaced by δf . The power transfer function of the i 'th bandpass filter ($i = 0$ to $N-1$) is $G_i(f)$ [impulse response, $h_i(t)$], which has passbands centered at $\pm i\delta f$. The N outputs of the filter bank are squared and averaged to give N numbers,

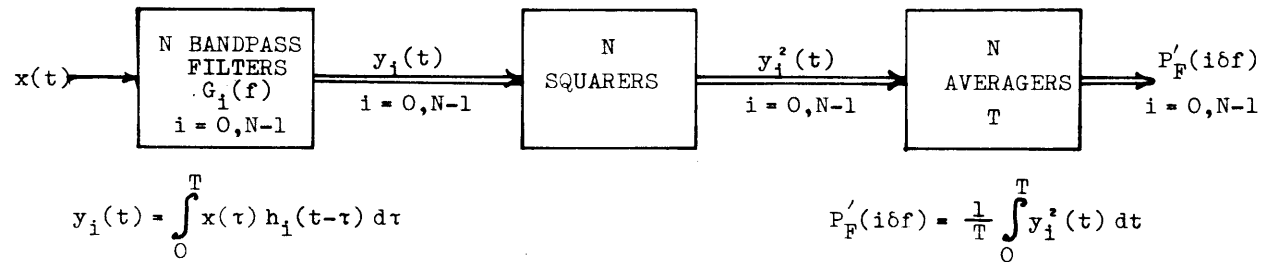


FIG. 1.2(a) - Bandpass-filter method of spectral measurement.

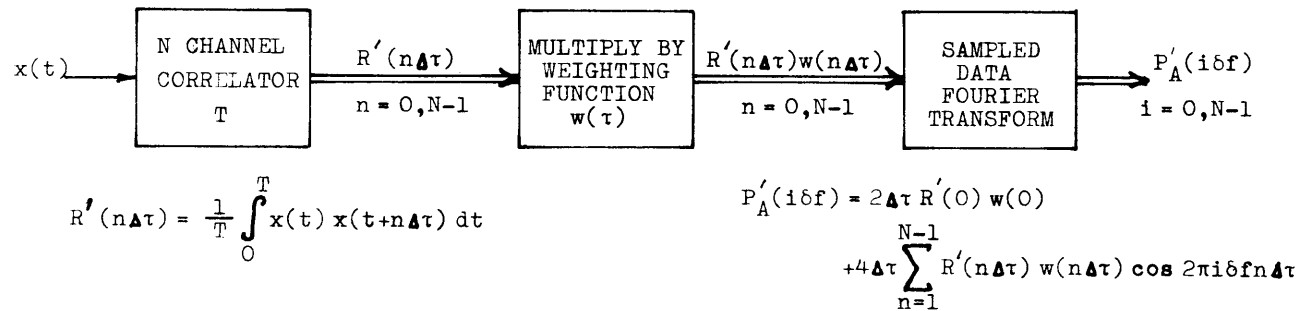


FIG. 1.2(b) - Autocorrelation method of spectral measurement.

$P_F^i(i\delta f)$, $i = 0$ to $N - 1$, which are estimates of the power spectrum, $P(f)$, at $f = i\delta f$.

The relation of the filter-method spectral estimate, $P_F^i(i\delta f)$, to the input signal, $x(t)$, is,

$$P_F^i(i\delta f) = \frac{1}{T} \int_0^T \left[\int_0^T x(t) h_i(\lambda - t) dt \right]^2 d\lambda \quad (1.21)$$

which is the time average of the square of the convolution integral expression for the filter output in terms of the input. It is assumed that $x(t)$ is available for only a finite interval, T , and that the filter input is zero outside of this interval. The relation of $P_F^i(i\delta f)$ to the true spectrum is of the form of Equations 1.19 and 1.20 where Δf is simply the filter bandwidth.

The autocorrelation method of spectral analysis is based upon the expression (called the Wiener-Khintchin theorem) giving the power spectrum as a Fourier transform of the autocorrelation function, $R(\tau)$. Indeed, this is the way we defined the power spectrum in Section 1.2. The expression is repeated below,

$$P(f) = 2 \int_{-\infty}^{\infty} R(\tau) e^{-j 2\pi f \tau} d\tau \quad (1.22)$$

The autocorrelation function can be expressed as a time average of the signal multiplied by a delayed replica of itself,

$$R(\tau) = \lim_{T \rightarrow \infty} \frac{1}{2T} \int_{-T}^T x(t) x(t+\tau) dt \quad (1.23)$$

The operations indicated in Equations 1.22 and 1.23 cannot be performed in practice; an infinite segment of $x(t)$ and an infinite amount of apparatus would be required. An estimate of $R(\tau)$ at a finite number of points, $\tau = n\Delta\tau$, can be determined by a correlator which computes,

$$R'(n\Delta\tau) = \frac{1}{T} \int_0^T x(t) x(t+n\Delta\tau) dt \quad (1.24)$$

A spectral estimate, $P_A^f(i\delta f)$, can then be calculated as a modified Fourier transform of $R'(n\Delta\tau)$,

$$P_A^f(i\delta f) = 2\Delta\tau R'(0) w(0) + 4\Delta\tau \sum_{n=1}^{N-1} R'(n\Delta\tau) \cdot w(n\Delta\tau) \cos(2\pi i\delta f n\Delta\tau) \quad (1.25)$$

The numbers, $w(n\Delta\tau)$, which appear in Equation 1.25 are samples of a weighting function, $w(\tau)$, which must be chosen; the choice is discussed in the next chapter. The weighting function must be even and have $w(\tau) = 0$ for $\tau \geq N\Delta\tau$; its significance will soon become apparent. In order to use all of the information contained in $R'(n\Delta\tau)$, δf should be chosen equal to $1/[2(N-1)\Delta\tau]$. This follows from application of the Nyquist sampling theorem; $P_A^f(i\delta f)$ is a Fourier transform of a function band-limited to $(N-1)\Delta\tau$.

The relation of $P_F^i(i \delta f)$ to the true power spectrum will again be of the form of Equations 1.19 and 1.20 where Δf , the frequency resolution, is approximately equal to $1/[(N-1)\Delta\tau]$. The calculation of the exact relation between $P_F^i(i \delta f)$ and $P(f)$ will be the major topic of Chapter 2. Our major concern in this section is to relate $P_F^i(i \delta f)$ and $P_A^i(i \delta f)$.

It is shown in Appendix A that $P_A^i(i \delta f)$ will be equal to $P_F^i(i \delta f)$ for any common input, $x(t)$, provided the filter responses and the auto-correlation weighting function, $w(\tau)$, are related in a certain way. The only significant assumption that was required for this proof is that the duration of the data, T , be much longer than the filter time constants (or equivalently, $N\Delta\tau$). This requirement must be satisfied in practice in order to obtain a meaningful spectral estimate, and thus, it is not an important restriction.

The required relation between the filter response and the auto-correlation weighting function is most easily stated in terms of $G_i(f)$, the power transfer function of the i 'th filter, and $W(f)$, the Fourier transform of the weighting function,

$$W(f) = 2 \int_0^{\infty} w(\tau) \cos 2\pi f\tau \, d\tau \quad (1.26)$$

The relation is,

$$G_i(f) = \sum_{k=-\infty}^{\infty} W(f - i\delta f - kf_s) + W(f + i\delta f + kf_s) \quad (1.27)$$

where $f_s = 1/\Delta\tau$. This result is illustrated in Figure 1.3; $G_1(f)$ consists of narrow bandpass regions, each having the shape of $W(f)$, centered at $\pm i \delta f$, $f_s \pm i \delta f$, $2f_s \pm i \delta f$, etc.

It is thus obvious that the autocorrelation spectral measurement system has many spurious responses. It can be seen that these spurious responses will have no effect if the input power spectrum is restricted (by prefiltering) such that,

$$\int_{-\infty}^{\infty} P(f') W(f-f') df' = 0 \quad \text{for } |f| > f_s/2 \quad (1.28)$$

This requirement, a necessary consequence of sampling of the autocorrelation function, is, of course, not required with the filter-method system since filters without spurious response are easily constructed.

If the requirement of Equation 1.28 is met, the terms where $k \neq 0$ in Equation 1.27 have no effect and an equivalent set of filter power transfer functions is given by,

$$G_1(f) = W(f-i \delta f) + W(f+i \delta f) \quad (1.29)$$

Furthermore, if we consider only positive frequencies not close to zero, we obtain,

$$G_1(f) \sim W(f-i \delta f) \quad (1.30)$$

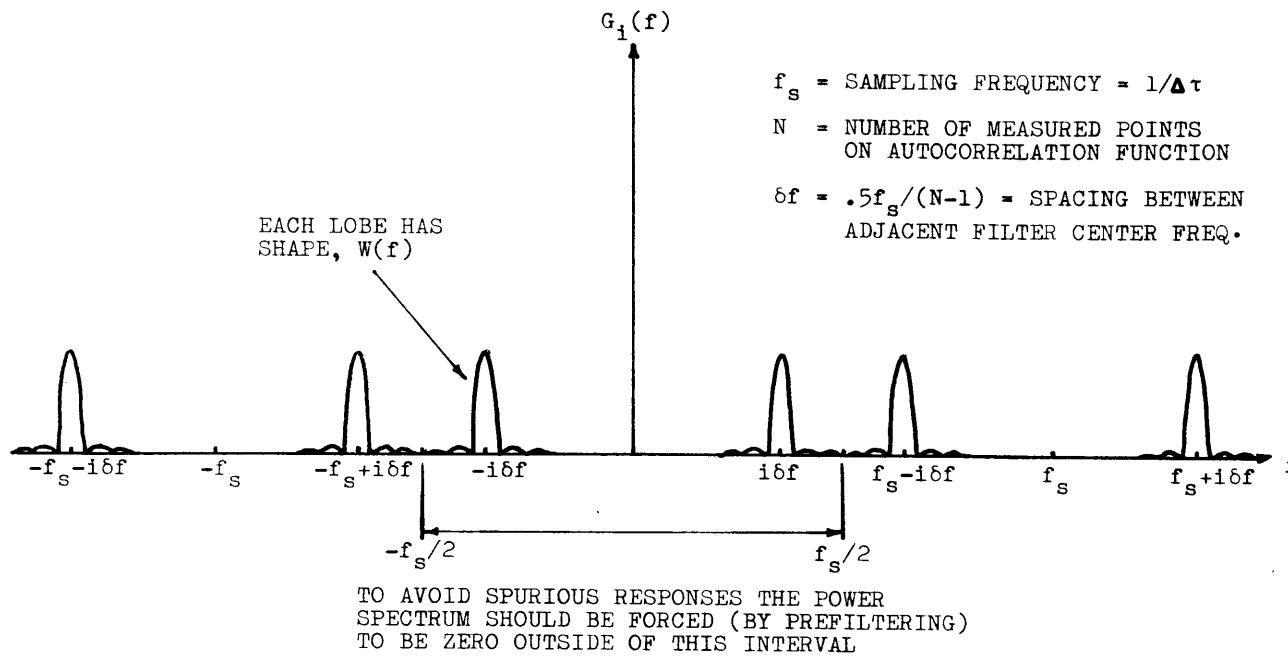


FIG. 1.3 - The autocorrelation method of spectral measurement depicted in Fig. 1.2(b) is equivalent to the filter-array method of Fig. 1.2(a) if the i 'th filter ($i = 0$ to $N-1$) has the power transfer function, $G_i(f)$, shown above. $W(f)$ is the Fourier transform of the autocorrelation weighting function, $w(\tau)$.

To summarize then, we have shown that the estimation of N points on the autocorrelation function (Equation 1.24) followed by a modified Fourier transform (Equation 1.25) is equivalent to an N -filter array spectral measurement system if Equation 1.27 is satisfied. Each method estimates the spectrum over a range of frequencies, $B = (N-1)\delta f = f_s/2$, with δf spacing between points. If the autocorrelation method is used the spectrum must be zero outside of this range.

Note that the $G_i(f)$ which can be realized with practical filters is quite different than the equivalent $G_i(f)$ of an autocorrelation system (to the advantage of the filter system). The restriction on $W(f)$ is that it be the Fourier transform of a function, $w(\tau)$, which must be zero for $\tau \geq N \Delta\tau$. This restriction makes it difficult to realize an equivalent $G_i(f)$ which has half-power bandwidth, Δf , narrower than $2/(N \Delta\tau) \approx 2\delta f$ (high spurious lobes result). No such restriction between the bandwidth, Δf , and the spacing, δf , exists for the filter system.

In most filter-array spectrum analyzers, δf is equal to Δf ; that is, adjacent filters overlap at the half-power points. This cannot be done with the autocorrelation method; δf will be .4 to .8 times Δf dependent on the spurious lobes which can be tolerated. This closer spacing gives a more accurate representation of the spectrum, but is wasteful in terms of the bandwidth analyzed, $B = (N-1)\delta f$, with a given resolution, Δf . For this reason it appears that 2 autocorrelation points per equivalent filter is a fairer comparison.

1.5 CHOICE OF THE SPECTRAL MEASUREMENT TECHNIQUE

In the previous section we have compared the filter and autocorrelation methods of spectral analysis on a theoretical basis. The major result is that if we desire to estimate N points on the spectrum during one time interval, we may use either an N filter array as in Figure 1.2(a) or a $2N$ point autocorrelation system as in Figure 1.2(b). The estimates of the power spectrum obtained by the two methods are equivalent; there is no theoretical advantage of one method over the other.

Both methods of spectral analysis can be performed with both analog and digital instrumentation as is indicated in Figures 1.4 and 1.5. In addition, if digital instrumentation is chosen, a choice must be made between performing the calculations in a general purpose digital computer or in a special purpose digital spectrum analyzer or correlator.

The digital filter method* shown in Figure 1.5 deserves special mention as it is not too well known. The procedure indicated in the block diagram simulates a single-tuned circuit; the center frequency and Q are determined by α and β . The digital simulation of any analog filter network is discussed by Tou,⁴ pp. 444-464. The digital filter method will be compared with the digital autocorrelation method later in this section.

* I would like to thank M. J. Levin, M. I. T. Lincoln Laboratory, for pointing out this technique to me.

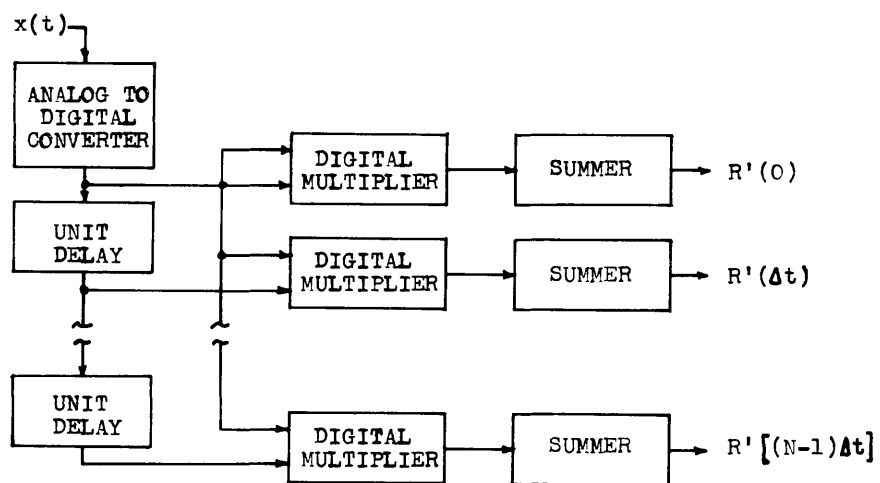
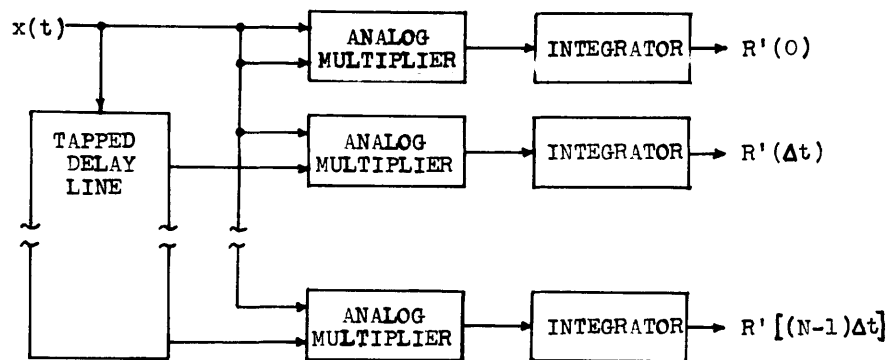


FIG. 1.4 - Analog and digital correlation methods of spectral measurement.

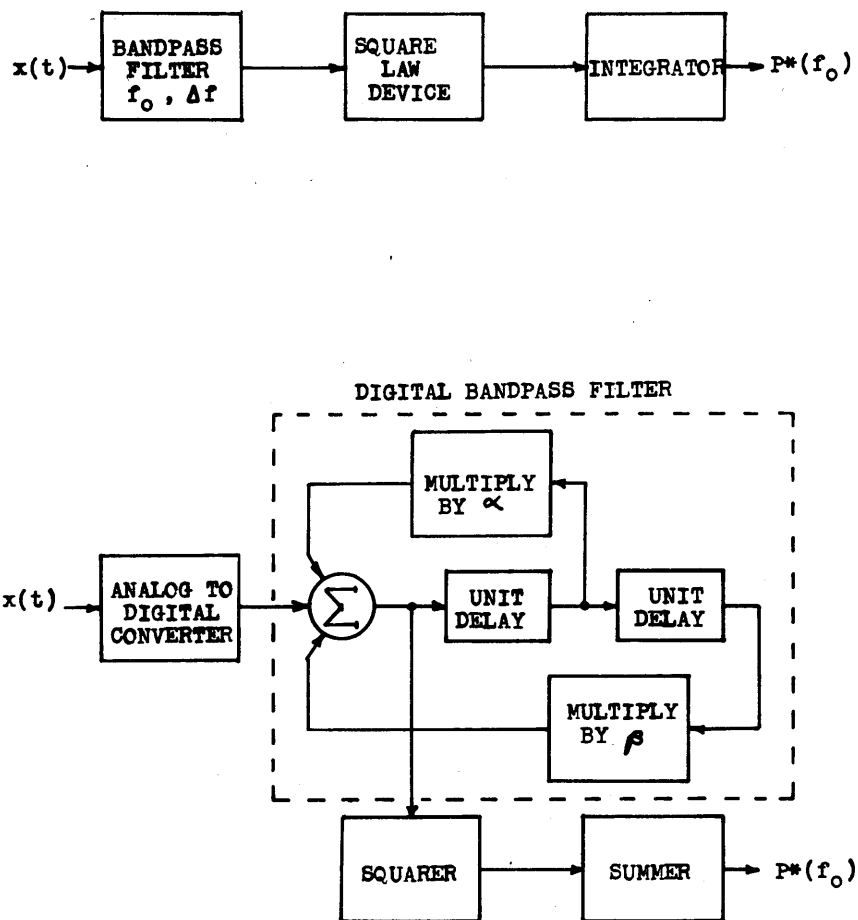


FIG. 1.5 - Analog and digital filter methods of spectral measurement.

A way of classifying spectral measurement problems into ranges where various techniques are applicable is indicated in Figure 1.6. The ordinate of the graph is N , the number of significant points which are determined on the spectrum and the abscissa is the percent error which can be tolerated in the measurement.

The error in a spectral measurement is due to two causes: 1) The unavoidable statistical fluctuation due to finite duration of data, 2) the error caused by equipment inaccuracy and drift. The statistical fluctuation depends through Equation 1.20 on the frequency resolution-observation time product, $T\Delta f$. The value of $T\Delta f$ that is required for a given accuracy is plotted on the abscissa of Figure 1.6.

The error due to equipment inaccuracy and drift limits the range of application of analog techniques as is indicated in Figure 1.6. These ranges are by no means rigidly fixed; exceptions can be found. However, the line indicates the error level where the analog instrumentation becomes exceedingly difficult.

The range of application of digital-computer spectral analysis is limited by the amount of computer time that is required. The line that is drawn represents one hour computer time on a high speed digital computer performing 10^4 multiplications and 10^4 additions in one second. It is interesting that the required computer time is not highly dependent on whether the autocorrelation method or the filter method is programmed on the computer. This will be shown in the next paragraph.

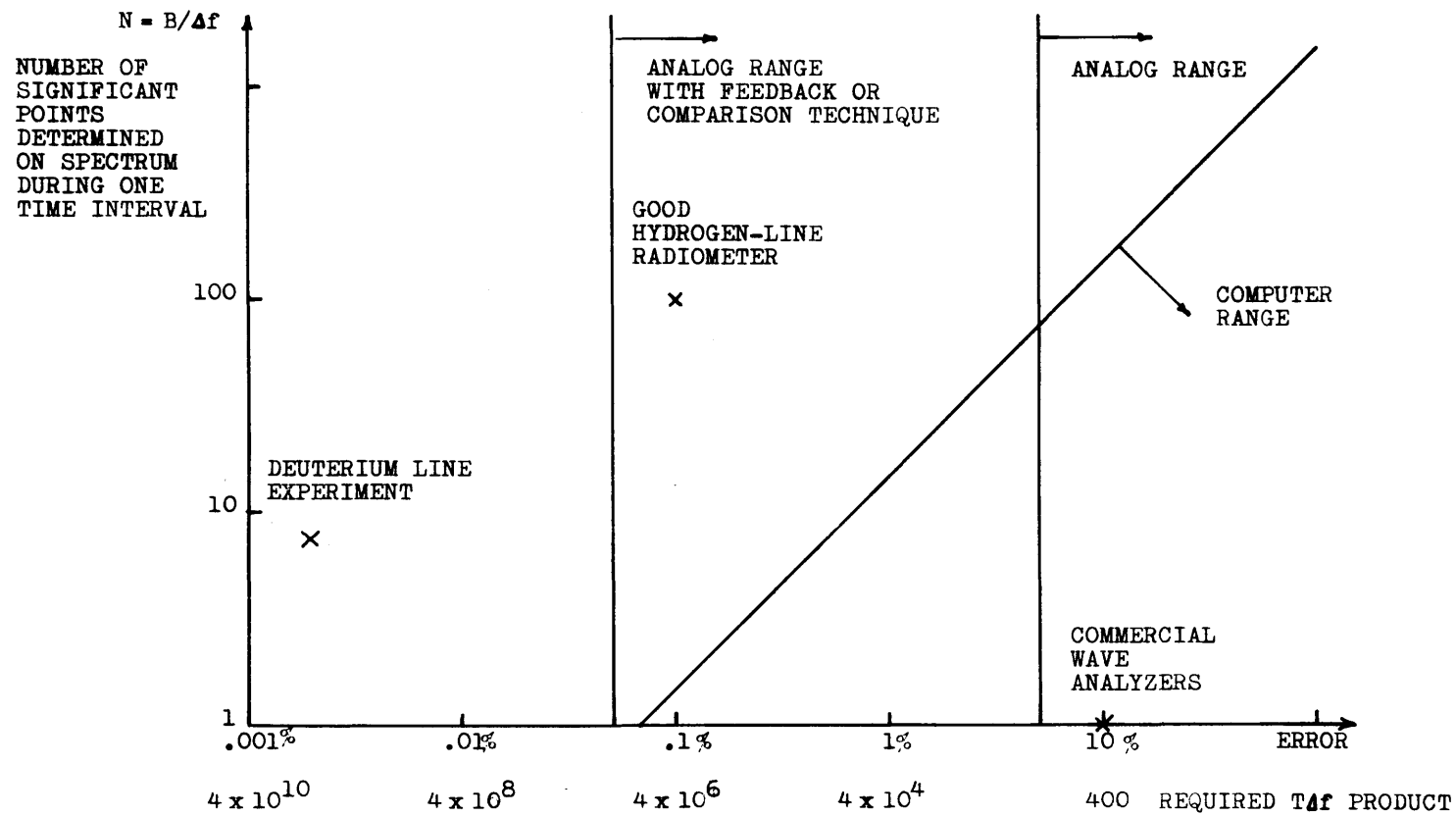


FIG. 1.6 - Range of application of various spectral measurement techniques.

Examination of Figure 1.4 reveals that one multiplication and one addition are required per sample per point on the autocorrelation function. The sampling rate is $2B$, and $2N$ autocorrelation points are required for N spectrum points; thus, $4NB$ multiplications and additions per second of data are required. A similar analysis of the digital-filter method of Figure 1.5 indicates 3 multiplications and 3 additions per sample per point on the spectrum are required. This gives $6NB$ multiplications per second of data. The number of seconds of data that is required is given by solving Equation 1.20 for T in terms of the statistical uncertainty, Δ_p , and the resolution Δf . This gives $T = 4/(\alpha \Delta_p^2 \Delta f)$ where the numerical factor, α , has been assumed equal to 2. We then find $16N^2/\Delta_p^2$ and $24N^2/\Delta_p^2$ as the total number of multiplications and additions required with the autocorrelation method and filter method, respectively. Because of the square dependence on N and Δ_p , the computer time increases very rapidly to the left of the one-hour line of Figure 1.6.

Some additional considerations concerning the choice of a spectral analysis technique are as follows:

- 1) If analog instrumentation is used, the filter method appears to be more easily instrumented and, of course, does not require the Fourier transform. The bandpass filter, squarer, and averager can be realized with less cost and complexity than the delay, multiplier, and averager required by the autocorrelation system. Analog correlation may be applicable to direct computation of autocorrelation functions and cross-correlation functions, but not to spectral analysis.

2) Analog instrumentation is not suited for spectral analysis at very low frequencies (say below one cps) although magnetic tape speed-up techniques can sometimes be used to advantage.

3) Digital instrumentation cannot be used if very large bandwidths are involved. At the present time, it is very difficult to digitally process signals having greater than 10 mc bandwidth.

4) If digital instrumentation or a computer is used for the spectral analysis, there seems to be little difference between the autocorrelation method and the filter method if the same degree of quantization (the number of bits per sample) can be used. This is evident from the computation of the required number of multiplications and additions earlier in this section. However, if the autocorrelation method is used, only one bit per sample is necessary and the multiplications and additions can be performed very easily. This method will be discussed in the next section.

1.6 THE ONE-BIT AUTOCORRELATION METHOD OF SPECTRAL ANALYSIS

The one-bit autocorrelation method of spectral analysis, as it is used in this paper, is presented with explanatory notes in Figure 1.7. Most of the remainder of the paper will be concerned with the analysis of this system, its application to radio astronomy, and experimental results obtained with this system.

The key "clipping correction" equation given in Figure 1.7 was derived by Van Vleck⁵ in 1943. At that time, before the era of digital

THE ONE-BIT AUTOCORRELATION METHOD OF SPECTRAL ANALYSIS

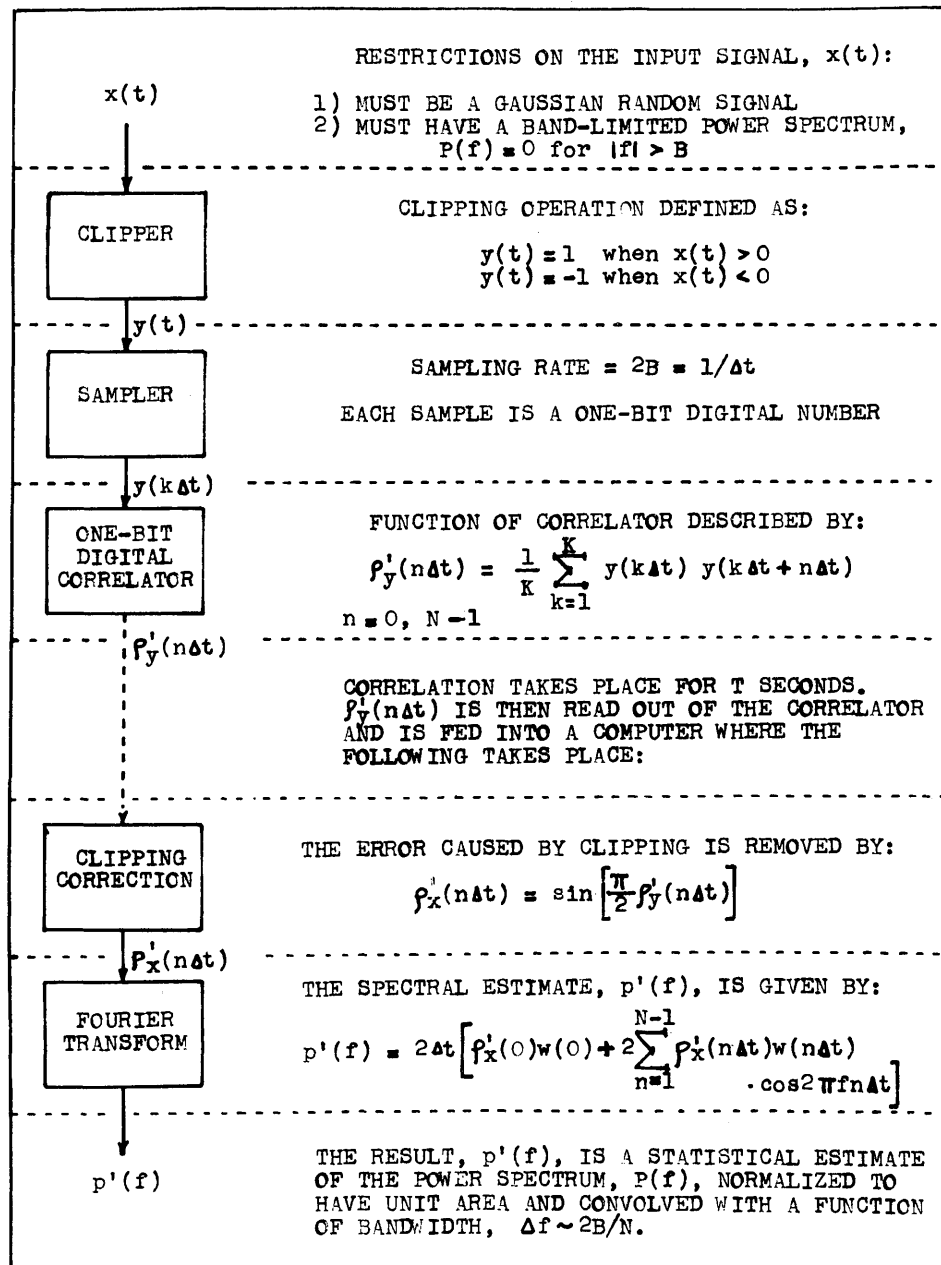


FIG. 1.7

data processing, the present use of the relation was certainly not foreseen; it was simply a means of finding the correlation function at the output of a clipper when the input was Gaussian noise. The use of the relation for the measurement of correlation functions has been noted by Faran and Hills,⁶ Kaiser and Angell,⁷ and Greene.⁸ The principle contributions of this paper are: 1) The investigation of the mean and statistical uncertainty (as in Equation 1.20) of a spectral estimate formed as indicated in Figure 1.7, 2) The application of this technique to the measurement of spectral lines in radio astronomy.

It should be understood that the spectral measurement technique as outlined in Figure 1.7 applies only to time functions with Gaussian statistics (as defined by Equation 1.8). Furthermore, only a normalized autocorrelation function and a normalized (to have unit area) power spectrum are determined. The normalization can, of course, be removed by the measurement of an additional scale factor (such as $\int_0^{\infty} P(f) df$). These restrictions do not hamper the use of the system for the measurement of spectral lines in radio astronomy.

Recently, some remarkable work which removes both of the above restrictions has been done in Europe by Veltmann and Kwackernaak,⁹ and Jespers, Chu, and Fettweis.¹⁰ These authors prove a theorem which allows a one-bit correlator to measure the (unnormalized) autocorrelation function of any bounded time function. The proof of the

theorem and the measurement procedure are summarized in Appendix B. A comparison of this procedure with that of Figure 1.7 is outlined in Table 1.1.

It is suggested (not too seriously) that the above mentioned method of measurement of autocorrelation functions be referred to as the E1B (European one-bit) method, while the procedure of Figure 1.7 be referred to as the A1B (American one-bit) method. Any hybrid of the two procedures could be called the MA1B method for mid-Atlantic one-bit or modified American one-bit dependent on which side of the Atlantic one is on.

TABLE 1.1
COMPARISON OF TWO ONE-BIT METHODS OF
AUTOCORRELATION FUNCTION MEASUREMENT

	A1B METHOD (Fig. 1.7)	E1B METHOD (Appendix B)
Restrictions on signal, $x(t)$	Must have Gaussian statistics.	Must be bounded by $\pm A$.
Differences in procedure	1) Clipping level is 0 volts. 2) SIN correction of one-bit autocorrelation function.	1) Clipping level is randomly varied from $-A$ to $+A$. 2) No correction.
Mean of result	Normalized autocorrelation function.	Unnormalized autocorrelation function.
RMS deviation of result compared with RMS deviation of many-bit autocorrelation	Increased by less than $\pi/2$.	A preliminary analysis indicates increase depends on $A^2/\overline{x^2}$.

CHAPTER 2
THE AUTOCORRELATION FUNCTION METHOD
OF MEASURING POWER SPECTRA

2.1 INTRODUCTION

The theory of measuring the power spectrum through the use of the autocorrelation function will be presented in this chapter. We will start with the defining equations, repeated below, of the power spectrum, $P(f)$, of a time function, $x(t)$;

$$P(f) = 2 \int_{-\infty}^{\infty} R(\tau) e^{-j2\pi f\tau} d\tau \quad (2.1)$$

$$R(\tau) = \lim_{T \rightarrow \infty} \frac{1}{2T} \int_{-T}^T x(t) x(t+\tau) dt \quad (2.2)$$

If these equations are examined with the thought of measuring $P(f)$ by directly performing the indicated operations, the following conclusions are reached:

1) In practice, the time function is available for only a finite time interval, and thus the limits on τ and t cannot be infinite as in Equations 2.1 and 2.2. Both the time function and the autocorrelation function must be truncated.

2) If the operation of Equation 2.2 is to be performed by a finite number of multipliers and integrators, then τ cannot assume a continuous range of values. The autocorrelation function, $R(\tau)$, must be sampled; that is, it will be measured only for $\tau = n\Delta\tau$ where n is an integer between 0 and $N-1$.

3) If digital processing is to be used, two more modifications must be made. The time function will be sampled periodically giving samples, $x(k\Delta t)$ where k is an integer between 1 and $(K+N)$, the total number of samples. Each of these samples must be quantized. If its amplitude falls in a certain interval (say $x_m - \Delta/2$ to $x_m + \Delta/2$) a discrete value (x_m) is assigned to it. It will be shown in the next chapter that the quantization can be done extremely coarsely; just two intervals, $x(k\Delta t) < 0$ and $x(k\Delta t) > 0$ can be used with little effect on the spectral measurement.

These considerations lead us to define the following estimates of the power spectrum and autocorrelation function,

$$P''(f) \equiv 2\Delta\tau \sum_{n=-\infty}^{\infty} R''(n\Delta\tau) w(n\Delta\tau) e^{-j2\pi f n\Delta\tau} \quad (2.3)$$

$$R''(n\Delta\tau) \equiv \frac{1}{K} \sum_{k=1}^K x(k\Delta t) x(k\Delta t + |n|\Delta\tau) \quad (2.4)$$

The function, $w(n\Delta\tau)$, is an even function of n , chosen by the observer, which is zero for $|n| \geq N$ and has $w(0) = 1$. It is included in the

definition as a convenient method of handling the truncation of the autocorrelation function measurement; $R''(n\Delta\tau)$ need not be known for $|n| \geq N$. The choice of $w(n\Delta\tau)$ will be discussed in Section 2.2-2.

The estimates given by Equations 2.3 and 2.4 contain all of the modifications (sampling and truncation of the time function and autocorrelation function) discussed above except for quantization of samples which will be discussed in the next chapter. We will call these estimates the many-bit estimates (denoted by a double prime) as contrasted with the one-bit estimates (denoted by a single prime) of the next chapter.

The main objective of this chapter will be to relate the many-bit estimates, $P''(f)$ and $R''(n\Delta\tau)$ to the true values, $P(f)$ and $R(n\Delta\tau)$. Many of the results will be applicable to the discussion of the one-bit estimates in the next chapter; other results are found for the sake of comparison with the one-bit results.

It is assumed, of course, that $x(t)$ is a random signal having Gaussian statistics. The estimates, $P''(f)$ and $R''(n\Delta\tau)$, are therefore random variables since they are based on time averages (over a finite interval) of functions of $x(t)$. The particular values of $P''(f)$ and $R''(n\Delta\tau)$ depend on the particular finite time segment of $x(t)$ that they are based on.

The mean and variance of $P''(f)$ and $R''(f)$ describe, for our purposes, their properties as estimates of $P(f)$ and $R(n\Delta\tau)$. The mean, $\overline{R''(n\Delta\tau)}$, of $R''(n\Delta\tau)$, is easily found,

$$\overline{R''(n\Delta\tau)} = \frac{1}{K} \sum_{k=1}^K \overline{x(k\Delta t) x(k\Delta t + |n| \Delta\tau)} \quad (2.5)$$

$$= R(n\Delta\tau) \quad (2.6)$$

where we have made use of the fact that the statistical average of $x(k\Delta t) x(k\Delta t + |n| \Delta\tau)$ is simply $R(n\Delta\tau)$. $R''(n\Delta\tau)$ is called an unbiased estimate of $R(n\Delta\tau)$.

The mean of $P''(f)$ is also easily found by taking the statistical average of both sides of Equation 2.3 and using Equation 2.6. Defining $P^*(f)$ as the mean of $P''(f)$, we find,

$$P^*(f) \equiv \overline{P''(f)} = 2\Delta\tau \sum_{n=-\infty}^{\infty} R(n\Delta\tau) w(n\Delta\tau) e^{-j2\pi f n\Delta\tau} \quad (2.7)$$

If it were not for the sampling and truncation of $R(\tau)$, $P^*(f)$ would simply be equal to $P(f)$ and, hence, $P''(f)$ would be an unbiased estimate of $P(f)$. The relationship of $P^*(f)$ to $P(f)$ will be discussed in the next section. In later sections, the variances of $P''(f)$ and $R''(n\Delta\tau)$ will be found.

Much of the material presented in this chapter is contained in a different form in the small book, The Measurement of Power Spectra, by Blackman and Tukey.¹¹ For the sake of completeness this material has been included here. An extensive bibliography to past work in this field is given by Blackman and Tukey.

2.2 MEAN OF THE SPECTRAL ESTIMATE

2.2-1 Relation of $P^*(f)$ to $P(f)$

In the previous section it was shown that the mean, $P^*(f)$, of the many-bit spectral estimate is given (Equation 2.7) as the Fourier transform of the truncated and sampled autocorrelation function. We will find in the next chapter that the mean of the one-bit spectral estimate is equal to $P^*(f)$ divided by a normalization factor. It is, thus, quite important that the relationship between $P^*(f)$ (the quantity we estimate) and $P(f)$, the true power spectrum, be well understood.

This relationship is found by substituting the following Fourier transform relations for $R(n\Delta\tau)$ and $w(n\Delta\tau)$ into Equation 2.7:

$$R(n\Delta\tau) = \frac{1}{2} \int_{-\infty}^{\infty} P(\alpha) e^{j2\pi\alpha n\Delta\tau} d\alpha \quad (2.8)$$

$$w(n\Delta\tau) = \int_{-\infty}^{\infty} W(\beta) e^{j2\pi\beta n\Delta\tau} d\beta \quad (2.9)$$

The result is,

$$P^*(f) = \sum_{i=-\infty}^{\infty} \int_{-\infty}^{\infty} P(\alpha) W(f-\alpha - if_s) d\alpha \quad (2.10)$$

where $f_s = 1/\Delta\tau$ and we have made use of the relation,

$$\Delta\tau \sum_{n=-\infty}^{\infty} e^{j2\pi n\Delta\tau(\alpha+\beta-f)} = \sum_{i=-\infty}^{\infty} \delta(\alpha+\beta-f+if_s) \quad (2.10)$$

Equation 2.10 not only specifies $P^*(f)$ in terms of $P(f)$, but it also should be considered as the general definition of the $*$ operator which will be used in later chapters. This operation is described in Figure 2.1. Two modifications of $P(f)$ are involved; the first is a consequence of truncation of the autocorrelation function and the second is a consequence of sampling of the autocorrelation function:

1) The spectrum is convolved with $W(f)$, a narrow-spike type function of bandwidth, $\Delta f \approx f_s/N$. This convolution should be considered as a smoothing or scanning operation. Features in the spectrum narrower than Δf are smoothed out.

2) The smoothed spectrum is repeated periodically about integer multiples of f_s . If the convolution of $P(f)$ and $W(f)$ is zero for $|f| > f_s/2$, then Equation 2.10 simplifies to,

$$P^*(f) = \int_{-\infty}^{\infty} P(\alpha) W(\alpha-f) d\alpha \quad |f| \leq f_s/2 \quad (2.11)$$

In practice f_s will be chosen to be twice the frequency at which the smoothed spectrum is 20 db below its midband value. In this case, little error (<1% in the midband region) occurs due to sampling and

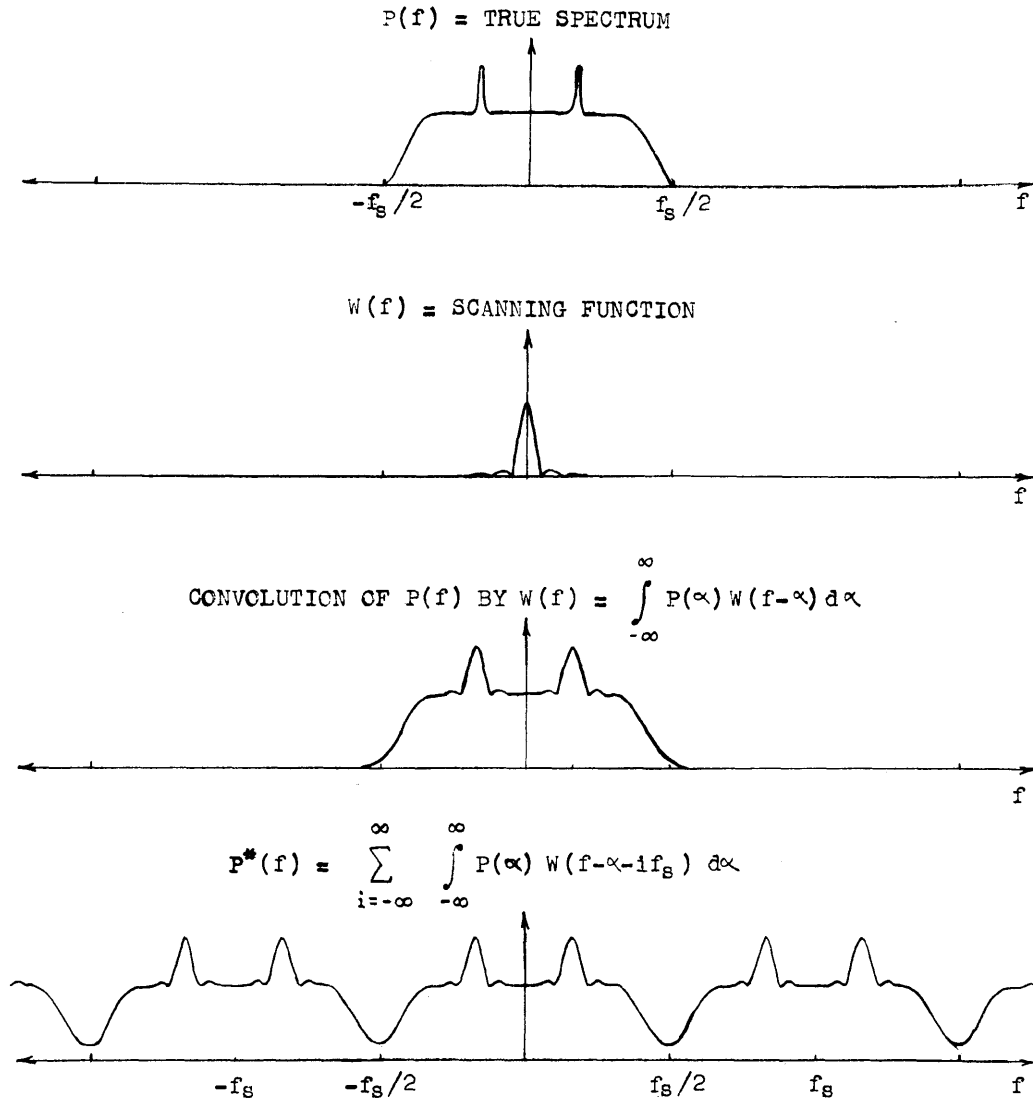


FIG. 2.1 - The effect of truncation and sampling of the autocorrelation function is indicated in the above figure. The quantity, $P^*(f)$, is the mean of a spectral measurement performed with an autocorrelation system.

$P^*(f)$ can be considered as simply a smoothed version of $P(f)$. If $P(f)$ does not change much in a band of width, Δf , then,

$$P^*(f) \approx P(f) \quad (2.12)$$

The relationship between $P^*(f)$ and $P(f)$ should be quite familiar to those versed in the theory of antenna arrays (or multiple slit diffraction theory). The function $\sum_{i=-\infty}^{\infty} W(f - if_s)$ is analogous to the antenna field pattern of a line array of N point sources with amplitudes weighted by $w(n\Delta\tau)$.

2.2-2 The Weighting Function, $w(n\Delta\tau)$

The shape of the spectral scanning function, $W(f)$, is determined by the choice of its Fourier transform, the autocorrelation weighting function, $w(n\Delta\tau)$. The weighting function can be arbitrarily chosen except for the following restrictions:

$$w(0) = 1 = \int_{-\infty}^{\infty} W(f) df \quad (2.13)$$

$$w(n\Delta\tau) = w(-n\Delta\tau) \quad (2.14)$$

$$w(n\Delta\tau) = 0 \quad \text{for } |n| \geq N \quad (2.15)$$

The choice of $w(n\Delta\tau)$ is usually a compromise between obtaining a $W(f)$ with a narrow main lobe and high spurious lobes or a $W(f)$ with a broadened main lobe and low spurious lobes.

TABLE 2.1 PROPERTIES OF THREE WEIGHTING FUNCTIONS

Name	Weighting Function $w(n\Delta\tau)$	Scanning Function $W(f)$	RMS Deviation Factor α	Half Power Bandwidth Δf	Strongest Spurious Response
Uniform	$w(n\Delta\tau) = 1 \quad n < N$ $w(n\Delta\tau) = 0 \quad n \geq N$	$W(f) \equiv W_o(f) =$ $2N\Delta\tau \frac{\sin 2\pi Nf/f_s}{2\pi Nf/f_s}$	1.099	$\frac{0.604 f_s}{N}$	-7 db
Cos or Hanning	$w(n\Delta\tau) = 0.5 + 0.5 \cos \frac{\pi n}{N}$ $ n < N$ $w(n\Delta\tau) = 0 \quad n \geq N$	$W(f) = 0.5 W_o(f)$ $+ 0.25 W_o(f + \frac{f_s}{2N})$ $+ 0.25 W_o(f - \frac{f_s}{2N})$	0.866	$\frac{f_s}{N}$	-16 db
Blackman	$w(n\Delta\tau) = 0.42 + 0.5 \cos \frac{\pi n}{N}$ $+ 0.08 \cos \frac{2\pi n}{N} \quad n < N$ $w(n\Delta\tau) = 0 \quad n \geq N$	$W(f) = 0.42 W_o(f)$ $+ 0.25 W_o(f + f_s/2N)$ $+ 0.25 W_o(f - f_s/2N)$ $+ 0.04 W_o(f + f_s/N)$ $+ 0.04 W_o(f - f_s/N)$	0.686	$\frac{1.13 f_s}{N}$	-29 db

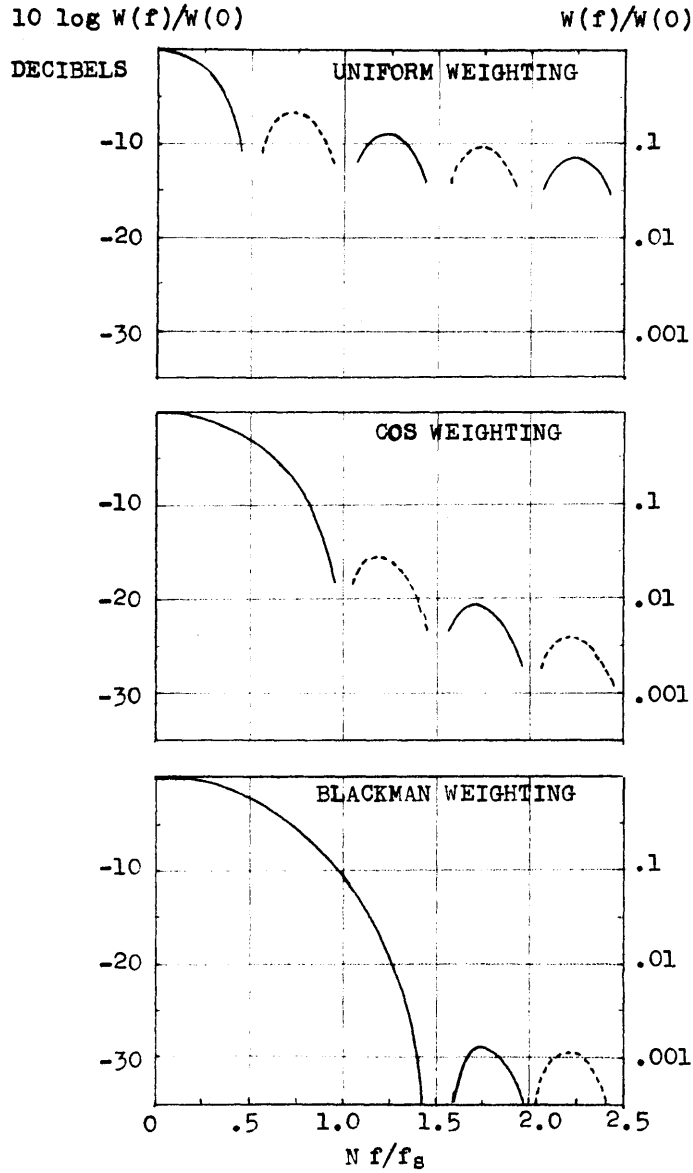


FIG. 2.2 - The scanning functions which result from the uniform, cos, and Blackman weighting functions are shown above (from Blackman and Tukey¹¹). See Table 2.1 for further information. The broken lines indicate $W(f)$ is negative.

This problem is a common one in antenna theory and optics. The "optimum" $w(n\Delta\tau)$ obviously depends on some exact specification of the performance of $W(f)$. This criterion will usually depend on the particular measurement that is being made. Some weighting functions which appear to be optimum in some sense are: 1) The uniform weighting function (to be discussed below) which gives a narrow main lobe, 2) The binomial weighting function (Kraus,¹² p. 94) which gives no spurious lobes, and 3) the Tchebycheff weighting function (see Dolph¹³) which gives equal spurious lobes.

It appears that little can be gained by making a very careful choice of $w(n\Delta\tau)$. Blackman and Tukey (pp. 95-100) describe five weighting functions; three of these should be adequate for most applications and are given in Table 2.1 and Figure 2.2. The cos weighting function appears to be a good compromise for most spectral line observations in radio astronomy; the uniform weighting function gives sharper resolution, whereas the Blackman weighting function gives low (-29 db) spurious lobes.

2.2-3 Some Useful Properties of $P^*(f)$

Some useful relations between $P^*(f)$ and $R(n\Delta\tau)$ can be obtained by using conventional Fourier techniques. These relations are all derived from Equation 2.7, repeated below.

$$P^*(f) = 2\Delta\tau \sum_{n=-\infty}^{\infty} R(n\Delta\tau) w(n\Delta\tau) e^{-j2\pi f n\Delta\tau} \quad (2.7)$$

This equation, with $P^*(f)$ and $R(n\Delta\tau)$ replaced by different quantities, will often occur (such as Equation 2.3), and hence, the results of this section will also apply to the following quantities which replace $P^*(f)$ and $R(n\Delta\tau)$:

- $P''(f)$ and $R''(n\Delta\tau)$ - The many-bit estimates of $P^*(f)$ and $R(n\Delta\tau)$.
- $p''(f)$ and $\rho''(n\Delta\tau)$ - Normalized many-bit estimates which will be discussed at the end of this chapter.
- $p^*(f)$ and $\rho(n\Delta\tau)$ - Normalized quantities analogous to $P^*(f)$ and $R(n\Delta\tau)$.
- $p'(f)$ and $\rho'(n\Delta\tau)$ - Normalized one-bit estimates which will be defined in the next chapter.

If Equation 2.7 is multiplied by $e^{j2\pi f k\Delta\tau}$ and the result is integrated from 0 to $f_s/2$, we find

$$R(n\Delta\tau) w(n\Delta\tau) = \int_0^{f_s/2} P^*(f) \cos 2\pi f n\Delta\tau \, df \quad (2.16)$$

This is analogous to the inverse transform relationship, Equation 1.14, between $R(\tau)$ and $P(f)$. Setting $n=0$ in Equation 2.16 and $\tau=0$ in Equation 1.14 gives,

$$R(0) = \int_0^{f_s/2} P^*(f) \, df \quad (2.17)$$

and

$$R(0) = \int_0^{\infty} P(f) df \quad (2.18)$$

where $R(0)$ is, of course, the total time average power.

The Parseval theorem for $P^*(f)$ can be derived by substituting Equation 2.7 for one $P^*(f)$ in the quantity $\int_0^{f_s/2} P^*(f) \cdot P^*(f) df$. The result is easily recognized if Equation 2.16 is used. The result is,

$$\int_0^{f_s/2} [P^*(f)]^2 df = 2\Delta\tau \sum_{n=-\infty}^{\infty} R^2(n\Delta\tau) w^2(n\Delta\tau) \quad (2.19)$$

which is sometimes useful.

2.3 COVARIANCES OF MANY-BIT ESTIMATES OF THE AUTO-CORRELATION FUNCTION AND POWER SPECTRUM

In this section we will examine the covariances, $\sigma_{Pm}^2(f_1, f_2)$ and $\sigma_{Rm}^2(n, m)$, of estimates, $P''(f)$ and $R''(n\Delta\tau)$ (defined in Equations 2.3 and 2.4), of the power spectrum and autocorrelation function, respectively. These estimates are based on many-bit (or unquantized) samples of the time function as opposed to estimates based on one-bit samples which are the major topic of this paper. The calculations of the covariances in the many-bit case are included for the sake of comparison. The following Section 2.3-1 applies to both many-bit and one-bit cases.

2.3-1 Definitions; Relation of the Spectral Covariance to the Autocorrelation Covariance

The covariance of the power spectrum estimate is defined as,

$$\sigma_{P_m}^2(f_1, f_2) \equiv \overline{[P''(f_1) - P^*(f_1)] [P''(f_2) - P^*(f_2)]} \quad (2.20)$$

$$= \overline{P''(f_1) P''(f_2) - P^*(f_1) P^*(f_2)} \quad (2.21)$$

A special case arises when $f_1 = f_2 = f$ and the covariance becomes the variance, $\sigma_{P_m}^2(f)$. The positive square root of the variance is the RMS deviation, $\sigma_{P_m}(f)$. The variance and RMS deviation specify how much $P''(f)$ is likely to vary from its mean, $P^*(f)$. The covariance specifies, in addition, how the statistical error at one frequency, f_1 , is correlated with the statistical error at another frequency, f_2 .

The definition of the autocorrelation covariance is quite similar,

$$\sigma_{R_m}^2(n, m) \equiv \overline{[R''(n\Delta\tau) - R(n\Delta\tau)] [R''(m\Delta\tau) - R(m\Delta\tau)]} \quad (2.22)$$

$$= \overline{R''(n\Delta\tau)R''(m\Delta\tau) - R(n\Delta\tau)R(m\Delta\tau)} \quad (2.23)$$

and the meaning of the autocorrelation variance and RMS deviation follow accordingly.

The spectral covariance or variance can be expressed in terms of the autocorrelation covariance by substitution of Equations 2.3 and 2.7 into Equation 2.21. This gives,

$$\sigma_{Pm}^2(f_1, f_2) = 4\Delta\tau^2 \sum_{n=-\infty}^{\infty} \sum_{m=-\infty}^{\infty} \sigma_{Rm}^2(n, m) w(n\Delta\tau) \cdot w(m\Delta\tau) e^{-j2\pi\Delta\tau(nf_1 + mf_2)} \quad (2.24)$$

Our first step, then, will be to calculate the autocorrelation covariance. This is not only needed for the calculation of the spectral covariance, but is also of interest on its own accord.

Note that the autocorrelation covariance is required to calculate the spectral variance or covariance; the autocorrelation variance is not sufficient. However, the integrated (over frequency) spectral variance can be expressed in terms of the autocorrelation variance summed over the time index, n . This relation is found by integrating both sides of Equation 2.24 (with $f_2 = f_1$) from 0 to $f_s/2$. The result is

$$\int_0^{f_s/2} \sigma_{Pm}^2(f_1) df_1 = 2\Delta\tau \sum_{n=-\infty}^{\infty} \sigma_{Rm}^2(n) w^2(n\Delta\tau) \quad (2.25)$$

2.3-2 Results of the Autocorrelation Covariance Calculation

The covariance, $\sigma_{Rm}^2(n, m)$, of the many-bit autocorrelation function estimate is calculated in Appendix C; the results will be discussed in this section.

The covariance, expressed in terms of the autocorrelation function, is found to be,

$$\sigma_{Rm}^2(n, m) = \frac{1}{K} \sum_{i=-K}^K \left[R(i\Delta t + |n|\Delta\tau - |m|\Delta\tau) R(i\Delta t) \right. \\ \left. + R(i\Delta t + |n|\Delta\tau) R(i\Delta t - |m|\Delta\tau) \right] \quad (2.26)$$

A plot of a typical autocorrelation function and its RMS deviation, $\sigma_{Rm}(n)$, is given in Figure 2.3.

It is informative to investigate the autocorrelation variance ($n=m$) in two limiting cases:

- 1) Suppose Δt is large enough so that,

$$R(i\Delta t) = 0 \quad \text{for } i \neq 0 \quad (2.27)$$

Equation 2.26 then reduces to

$$\sigma_{Rm}^2(n) = \frac{R^2(0) + R^2(n\Delta\tau)}{K} \quad (2.28)$$

The condition of Equation 2.27 implies that successive products, $x(k\Delta t) x(k\Delta t + |n\Delta\tau|)$, which go into the estimate of the autocorrelation function are linearly independent. There are K such products and the form of Equation 2.28 is a familiar one in statistical estimation problems.

In order to minimize the variance, K should be made as large as possible. If the duration, T , of the data is fixed, then the only recourse is to reduce $\Delta t = T/K$. As Δt is reduced, a point will be reached where Equation 2.27 is not satisfied. The minimum value of Δt which satisfies Equation 2.27 is equal to $1/2B$ if $x(t)$ has a

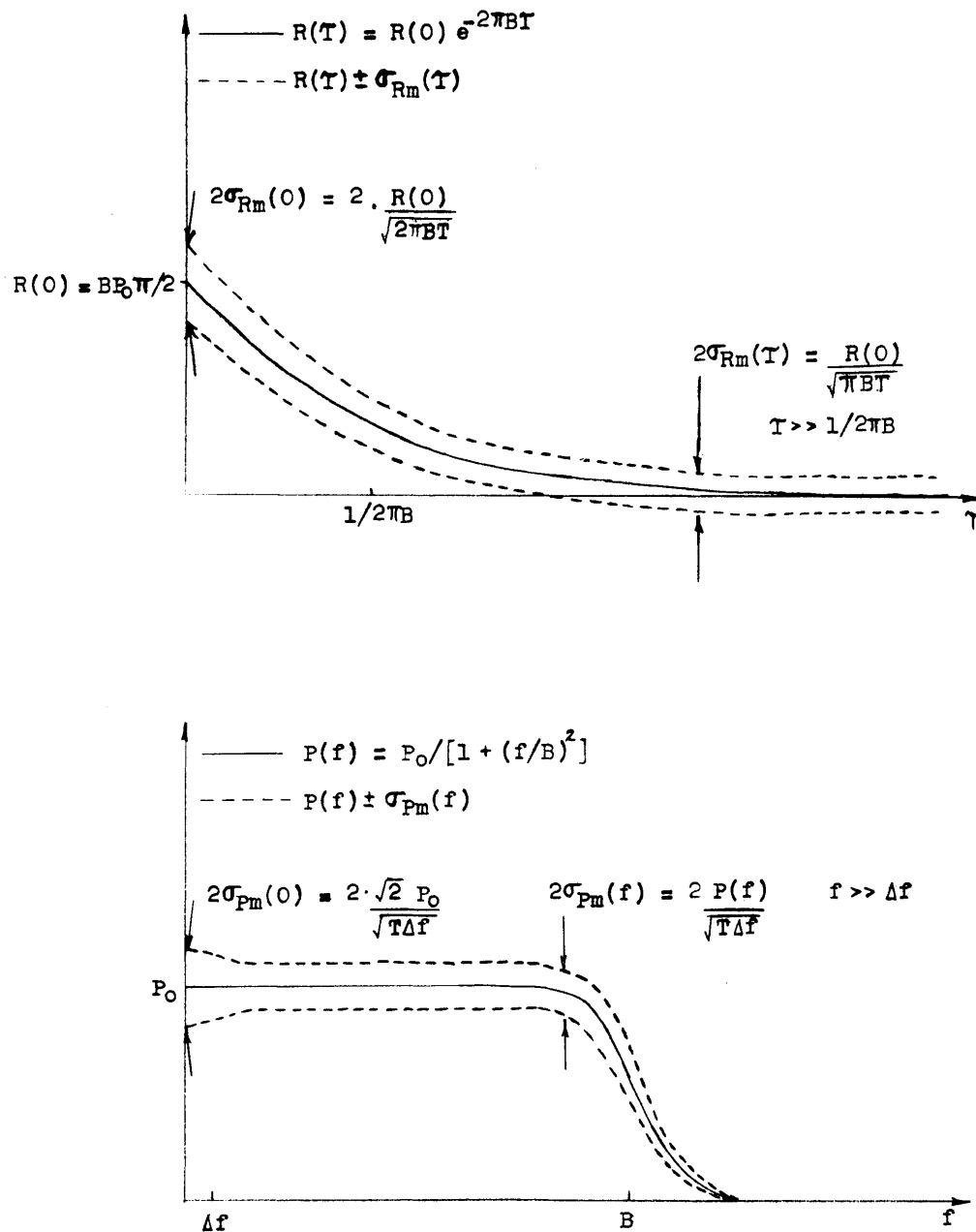


FIG. 2.3 - An autocorrelation function and its transform, the power spectrum, are shown above. The form of the RMS deviations of these functions is indicated. Note that $\sigma_{Pm}(f)$ is proportional to $P(f)$ (except near $f = 0$) whereas $\sigma_{Rm}(\tau)$ is nearly constant.

rectangular power spectrum extending from $-B$ to B and if $\Delta\tau$ is set equal to $1/2B$. The variance at this value of Δt is

$$\sigma_{Rm}^2(n) = \frac{R^2(0) + R^2(n\Delta\tau)}{2BT} \quad (2.29)$$

where $R(n\Delta\tau) = 0$, $n \neq 0$, for the rectangular spectrum with $\Delta\tau = 1/2B$.

The next example will illustrate that the variance cannot be reduced further by reduction of Δt beyond the point required by Equation 2.27.

2) Suppose $\Delta t \rightarrow 0$ and $K \rightarrow \infty$ in such a manner that $K\Delta t = T$ is constant. The case of continuous data (analog correlation) is approached and Equation 2.26 (with $n = m$) becomes,

$$\sigma_{Rm}^2(n) = \frac{1}{T} \int_{-T}^T [R^2(t) + R(t + n\Delta\tau) R(t - n\Delta\tau)] dt \quad (2.30)$$

If we again take the case of a rectangular spectrum between $-B$ and B ; Equation 2.30 gives,

$$\sigma_{Rm}^2(n) = \frac{R^2(0) + R^2(0) (\sin 4\pi B n \Delta\tau) / (4\pi B n \Delta\tau)}{2BT} \quad (2.31)$$

This result, with $\Delta\tau = 1/2B$, agrees exactly with Equation 2.29.

Thus, reducing the time function sampling interval, Δt , from $1/2B$ to 0 has had no effect on $\sigma_{Rm}^2(n)$ in the case of a rectangular spectrum.

Examinations of Equations C. 8 and C. 11 in Appendix C give more general results. These equations show that both the auto-correlation variance and the spectral variance do not change for values of Δt less than $1/2B$ if $P(f) = 0$ for $f \geq B$.

2.3-3 Results of the Spectral Covariance Calculation

The spectral covariance, $\sigma_{Pm}^2(f_1, f_2)$, is calculated in Appendix C with the following result,

$$\sigma_{Pm}^2(f_1, f_2) = \frac{1}{T} \int_{-\infty}^{\infty} P^2(f) W(f+f_1) \cdot [W(f+f_2) + W(f-f_2)] df \quad (2.32)$$

It has been assumed that: 1) The signal has Gaussian statistics, 2) Both $P(f)$ and $W(f)$ are smooth over frequency bands of width $1/T$, 3) The spectrum smoothed by [or convolved with] $W(f)$ is zero for frequencies greater than B , 4) The time function sampling interval, Δt , and the autocorrelation function sampling interval, $\Delta \tau$, have both been chosen equal to $1/2B$, 5) Equation 2.32 is only valid for $|f_1|$ and $|f_2|$ less than B .

The manner in which the spectral estimate covaries is easily observed in Equation 2.32. If f_1 and f_2 are such that $W(f+f_1)$ and $W(f\pm f_2)$ do not overlap, then $\sigma_{Pm}^2(f_1, f_2) = 0$. In other words, the

statistical errors at two frequencies separated by more than Δf , the bandwidth of $W(f)$, are uncorrelated. This result might have been expected from the analogy with the filter-array spectrum analyzer discussed in Chapter 1.

The spectral variance ($f_1 = f_2$) can be put in a simpler form if some further approximations are made. It can be seen that at $f_1 = f_2 = 0$, the variance becomes,

$$\sigma_{Pm}^2(0) = \frac{2}{T} \int_{-\infty}^{\infty} P^2(f) W^2(f) df \quad (2.33)$$

while for $f_1 = f_2 \gg \Delta f$, we obtain,

$$\sigma_{Pm}^2(f_1) = \frac{1}{T} \int_{-\infty}^{\infty} P^2(f) W^2(f+f_1) df \quad (2.34)$$

In what follows we will assume that f_1 is positive and not close to zero so that Equation 2.34 applies.

If the spectrum is smooth over bands of width, Δf , then $P(f)$ can be taken out from under the integral sign in Equation 2.34 to give,

$$\sigma_{Pm}^2(f_1) = \frac{P^2(f_1)}{T} \int_{-\infty}^{\infty} W^2(f') df' \quad (2.35)$$

where a change of variable $f' = f+f_1$ has been made. The integral now depends only on the weighting function, $w(\tau)$, and has dimensions of a

reciprocal bandwidth. It is, therefore, convenient to define a dimensionless parameter, α , such that

$$\frac{\alpha}{\Delta f} \equiv \int_{-\infty}^{\infty} W^2(f') df' = \int_{-\infty}^{\infty} w^2(\tau) d\tau \quad (2.36)$$

where Δf is the half power bandwidth of $W(f)$. The second equality in Equation 2.36 follows from Parseval's theorem for Fourier transforms. It should be remembered that $W(f)$ must have unit area as specified by Equation 2.13.

The numerical factor, α , will be of the order of unity and is specified for various weighting functions in Table 2.1. If $W(f)$ is a rectangular function of width Δf , and height $1/\Delta f$, then $\alpha=1$. The RMS deviation of the spectral measurement can now be put in the familiar form,

$$\sigma_{P_m}(f) = \frac{\alpha}{\sqrt{T \Delta f}} P(f) \quad (2.37)$$

The appearances of a typical spectrum and its RMS deviation are sketched in Figure 2.3.

2.4 NORMALIZED, MANY-BIT ESTIMATES OF THE SPECTRUM AND AUTOCORRELATION FUNCTION

[Reminder concerning notation: A ρ will denote a normalized autocorrelation function; a lower case p will denote a normalized power

spectrum; a double prime or subscript m will denote a quantity determined from many-bit samples; a single prime or subscript 1 will denote a quantity obtained from one-bit samples.]

The one-bit method of spectral analysis produces a spectral estimate, $p'(f)$, and an autocorrelation function estimate, $\rho'(n\Delta\tau)$, which are (unavoidably) normalized such that,

$$\rho'(0) = 1 \quad (2.38)$$

and

$$\int_0^{f_s/2} p'(f) df = 1 \quad (2.39)$$

In order to compare the many-bit results of this chapter with the one-bit results of the next chapter, the many-bit estimates must be similarly normalized. A computer-simulated, experimental comparison of normalized, many-bit estimates with one-bit estimates is given in Chapter 6 and the results of this section will be used there.

It is important to note that $\rho'(0)$ has no statistical fluctuation; it is constrained to equal unity. (This is more stringent than having $\overline{\rho'(0)} = 1$.) The variance, $\sigma_{\rho 1}^2(0)$, must be zero. A quantity derived from many-bit samples that has the same property is

$$\rho''(n\Delta\tau) = \frac{R''(n\Delta\tau)}{R''(0)} \quad (2.40)$$

where $R''(n\Delta\tau)$ is defined in Equation 2.4. Note that $R''(n\Delta\tau)$ has been divided by $R''(0)$, a random variable, and not by $R(0)$, which is constant (but unknown). If $\rho''(n\Delta\tau)$ had been defined as $R''(n\Delta\tau)/R(0)$, only trivial modifications of previous results would be required. However, this definition does not give a $\rho''(n\Delta\tau)$ that is analogous to $\rho'(n\Delta\tau)$.

The normalized many-bit power spectrum estimate, $p''(f)$, is similarly defined as $P''(f)/R''(0)$. The definition of $P''(f)$, Equation 2.3, may be used to give,

$$p''(f) = 2\Delta\tau \sum_{n=-\infty}^{\infty} \rho''(n\Delta\tau) w(n\Delta\tau) e^{-j2\pi f n\Delta\tau} \quad (2.41)$$

This definition will give (see Section 2.2-3),

$$\int_0^{f_s/2} p''(f) df = 1 \quad (2.42)$$

in analogy to Equation 2.39.

Our main purpose in this section will be to find the mean and variance of $\rho''(n\Delta\tau)$ and $p''(f)$. The calculation of the mean or variance of the quotient of two dependent random variables is a difficult problem. However, a drastic simplification results if the denominator random variable, $R''(0)$, has a random fluctuation which is small compared to its mean. This simplification will be used in the next section.

2.4-1 Mean and Variance of the Normalized Autocorrelation Estimate

The mean and variance of $\rho''(n\Delta\tau) = R''(n\Delta\tau)/R''(0)$ can be found by expanding $R''(n\Delta\tau)$ and $R''(0)$ as,

$$R''(n\Delta\tau) = R(n\Delta\tau) + R(0) \epsilon(n) \quad (2.43)$$

where $\epsilon(n)$ is a small $[\epsilon(n) \ll 1]$ random variable. It is easily seen by solving Equation 2.43 for $\epsilon(n)$, that,

$$\overline{\epsilon(n)} = 0 \quad (2.44)$$

$$\overline{\epsilon(n) \epsilon(m)} = \frac{\sigma^2 R_{nm}(n, m)}{R^2(0)} \quad (2.45)$$

The requirement of $\epsilon(n) \ll 1$ is met by assuring that the observation time, T , is long enough so that $\sigma_{R_{nm}}(n)$ is much less than $R(0)$. This must be true in practice if the estimate of $R''(n\Delta\tau)$ is to be of any accuracy.

The normalized autocorrelation function estimate, $\rho''(n\Delta\tau)$, can then be written as,

$$\rho''(n\Delta\tau) = \frac{R(n\Delta\tau) + R(0) \epsilon(n)}{R(0) + R(0) \epsilon(0)} \quad (2.46)$$

Since $\epsilon(n) \ll 1$ (including $n=0$) Equation 2.46 can be expanded and terms of higher order than first in $\epsilon(n)$ or $\epsilon(0)$ are dropped to give,

$$\rho''(n\Delta\tau) = \rho(n\Delta\tau) - \rho(n\Delta\tau)\epsilon(0) + \epsilon(n) \quad (2.47)$$

The mean is now easily found,

$$\overline{\rho''(n\Delta\tau)} = \rho(n\Delta\tau) \quad (2.48)$$

and the covariance, $\sigma_{\rho m}^2(n, m)$, can be expressed as,

$$\sigma_{\rho m}^2(n, m) \equiv \overline{[\rho''(n\Delta\tau) - \rho(n\Delta\tau)] [\rho''(m\Delta\tau) - \rho(m\Delta\tau)]} \quad (2.49)$$

$$\begin{aligned} &= \overline{\epsilon(n)\epsilon(m)} + \overline{\epsilon^2(0)} \rho(n\Delta\tau)\rho(m\Delta\tau) \\ &\quad - \overline{\epsilon(n)\epsilon(0)}\rho(m\Delta\tau) - \overline{\epsilon(m)\epsilon(0)}\rho(n\Delta\tau) \end{aligned} \quad (2.50)$$

The terms, $\overline{\epsilon(n)\epsilon(m)}$ [where n or m may be zero], in Equation 2.50 are expressed in terms of $\sigma_{Rm}^2(n, m)$ by Equation 2.45. This quantity is given by Equation 2.26 and substitution into Equation 2.45 gives,

$$\begin{aligned} \overline{\epsilon(n)\epsilon(m)} &= \frac{1}{K} \sum_{i=-K}^K [\rho(i\Delta t + |n|\Delta\tau - |m|\Delta\tau) \rho(i\Delta\tau) \\ &\quad + \rho(i\Delta t + |n|\Delta\tau) \rho(i\Delta t - |m|\Delta\tau)] \end{aligned} \quad (2.51)$$

Equations 2.50 and 2.51 specify the covariance of the normalized, many-bit estimate of the autocorrelation function. A feeling for this result can be obtained by substitution into Equation 2.50 of an approximate form of Equation 2.51. This approximate form is valid for Δt

large enough so that successive samples are independent (as discussed near Equation 2.28) and is,

$$\overline{\epsilon(n) \epsilon(m)} = \frac{\rho(|n|\Delta\tau - |m|\Delta\tau) + \rho(n\Delta\tau) \rho(m\Delta\tau)}{K} \quad (2.51)$$

Substitution of Equation 2.51 into Equation 2.50 gives a simple result for the variance ($n=m$),

$$\sigma_{\rho m}^2(n) = \frac{1 - \rho^2(n\Delta\tau)}{K} \quad (2.52)$$

This result should be compared with Equation 2.28, which gives $\sigma_{Rm}^2(n)$ with the same approximations. The major result has been the reduction of the variance near $n=0$, as would be expected.

2.4-2 Mean and Variance of the Normalized Spectral Estimate

The mean of the spectral estimate is easily found by taking the mean of both sides of Equation 2.41 and using Equation 2.48. This mean will be denoted as $p^*(f)$ and is given by,

$$p^*(f) = \overline{p''(f)} = 2\Delta\tau \sum_{n=-\infty}^{\infty} \frac{R(n\Delta\tau)}{R(0)} w(n\Delta\tau) e^{-j2\pi f n\Delta\tau} \quad (2.53)$$

$$= \frac{P^*(f)}{R(0)} \quad (2.54)$$

$$= \frac{P^*(f)}{\int_0^{f_s/2} P^*(f) df} = \frac{P^*(f)}{\int_0^{\infty} P(f) df} \quad (2.55)$$

where Equation 2.7 has been used to give Equation 2.54 and Equations 2.17 and 2.18 have been used to give Equation 2.55. $P^*(f)$ is the smoothed spectrum discussed in Section 2.2. The mean of $p''(f)$ is, thus, the smoothed spectrum normalized to have unit area in the range between 0 and $f_s/2$.

The spectral variance or covariance can be calculated in a straightforward manner through the use of Equation 2.24 which relates the spectral variance or covariance to the autocorrelation covariance. The autocorrelation covariance for the normalized estimate is given by Equations 2.50 and 2.51. Combination of these equations gives a very long expression for the spectral variance. This will not be presented in this paper in view of its complexity and minor importance. However, a heuristic argument which gives an approximate, but simple, expression for the spectral variance will be given below.

Suppose that we consider that the normalized spectrum is of uniform height, $1/b$, over a bandwidth, b . The effect of constraining the spectral estimate to have unit area is then equivalent to requiring that the average height of the spectrum is $1/b$, its true value. This is analogous to correcting a set of measured points so that their average value is equal to the true value. In this case (see Kenney and Keeping,¹⁴ Section 8.7) the variance is reduced by $1 - 1/N$ where N is the number of independent points. In Section 2.2 it was shown that points on the spectrum spaced Δf apart are independent; thus, $N = b/\Delta f$. The RMS deviation, $\sigma_{pm}(f_1)$ of the normalized spectral estimate then becomes,

$$\sigma_{\text{pm}}(f_1) = \frac{\alpha}{\sqrt{T \Delta f}} \cdot p(f) \cdot \sqrt{1 - \Delta f/b} \quad (2.56)$$

where Equation 2.37 has been used for the RMS deviation before normalization. This result approximates the result of a formal derivation using Equations 2.24, 2.50, and 2.51.

CHAPTER 3

THE ONE-BIT METHOD OF COMPUTING AUTOCORRELATION FUNCTIONS

3.1 INTRODUCTION

The theory of estimating the power spectrum through the use of a finite number of samples, K , of the input signal, $x(t)$, has been presented in the previous chapter. This theory would be sufficient if analog techniques or very finely quantized digital techniques were used to compute an estimate of the autocorrelation function. The analog techniques are not usable for high-sensitivity spectral line analysis in radio astronomy because of lack of accuracy. (As stated in Section 1.5, if accuracy requirements allow analog instrumentation to be used, then the conventional bandpass-filter method of spectral analysis is preferable.)

Many-bit digital techniques are unwieldy for most radio astronomy applications because of the large number of operations which must be performed. In Section 1.5 it was shown that $16N^2/\Delta p^2$ is the total number of multiplications required for the estimation of N points on the spectrum with an accuracy of $100\Delta p$ per cent. For the deuterium line experiment, $\Delta p = 3 \times 10^{-5}$ and $N = 8$ which gives 10^{12} multiplications. A typical high-speed digital computer performs 10^4 many-bit multiplications per second and thus, about four years of computer time would be required. If one-bit multiplications

could be used, this computer time could be reduced by about a factor of 10. Of greater significance is the fact that a special purpose one-bit digital correlation computer can be built for about 1/10 the cost of a similar many-bit machine. The cost of a one-bit digital correlator is roughly \$1000 per point on the autocorrelation function (or, according to the discussion of Section 1.4, \$2000 per point on the spectrum). A one-bit digital correlator, capable of measuring 21 points on the autocorrelation function was built for the deuterium line experiment and experimental results will be discussed in later chapters.

The term, "many-bit autocorrelation", needs further explanation. By this, it is meant that the quantization levels are so small that the quantization error can be disregarded. This is usually the case in digital computers where the usual word lengths of 20 bits or more allow the quantization error to be 10^{-6} or less of the maximum value of the signal.

A general relationship between quantization error and the error in a spectral measurement does not appear to be known. At first thought, one might think that to measure the power spectrum with an accuracy of $X\%$, a quantization error of less than $X\%$ is required. This is not true because the spectral estimate is based on an average computed from many samples and the quantization error tends to average out. Kaiser and Angell⁷ have measured autocorrelation functions with 8, 3, and 1 bits per sample with surprisingly little difference in the results.

The main spectral analysis procedure to be discussed in this paper is one in which quantization is performed with one bit per sample and a correction is applied to the resulting autocorrelation function estimate; the procedure is illustrated in Figure 1.7. This method is based on a theorem by Van Vleck. The theorem is stated as follows:

Suppose $x(t)$ is a sample function of a Gaussian random process with zero mean and $y(t)$ is the function formed by infinite clipping of $x(t)$. That is,

$$\begin{aligned} y(t) &= 1 && \text{when } x(t) > 0 \\ y(t) &= -1 && \text{when } x(t) < 0 \end{aligned} \quad (3.1)$$

Then the normalized autocorrelation functions of $x(t)$ and $y(t)$ are related by

$$\rho_x(\tau) = \sin \left[\frac{\pi}{2} \rho_y(\tau) \right] \quad (3.2)$$

For completeness this equation will be derived in the next section; some of the steps in the derivation will also be useful for other work.

Equation (3.2) is valid for the true normalized autocorrelation functions, $\rho_x(\tau)$ and $\rho_y(\tau)$, which cannot be measured from a finite number of samples of $x(t)$ or $y(t)$. An estimate of $\rho_y(\tau)$ can be defined as $\hat{\rho}_y(\tau)$, where

$$\rho_y'(\tau) \equiv \frac{1}{K} \sum_{k=1}^K y(k\Delta t) y(k\Delta t + \tau) \quad (3.3)$$

Equation 3.3 describes the function performed by a one-bit digital correlator. An estimate of $\rho_x(\tau)$ is then defined as,

$$\rho_x'(\tau) \equiv \sin\left[\frac{\pi}{2} \rho_y'(\tau)\right] \quad (3.4)$$

The topic of Section 3.3 will be to find the mean and variance of $\rho_x'(\tau)$. This is not easily computed because of the complicated manner in which $\rho_x'(\tau)$ is related to $x(t)$ through Equations 3.1, 3.3, and 3.4. It has only been possible to calculate the mean and variance in the case where successive products, $y(k\Delta t) y(k\Delta t + \tau)$, in the summation of Equation 3.3 are statistically independent. In practice, this will be approximately the case. If Δt is chosen so small that successive products are dependent, then some of the data processing is redundant. The case of independent successive products is analogous to the special case examined in the previous chapter concerning many-bit samples (see Equations 2.27 and 2.28).

An estimate of the normalized power spectrum will be defined as a weighted Fourier transform of samples of $\rho_x'(\tau)$ in a manner similar to that used in Equation 2.3. This estimate will be discussed in the final section of this chapter.

It should be remembered that Equation 3.2 is true only for certain classes of functions. The Gaussian random process is the example of interest. The relation is also true for a single sine wave and McFadden¹⁵ has shown that it is approximately true for a weak sine wave in Gaussian noise.

3.2 THE VAN-VLECK RELATION

The derivation of Equation 3.2 is based on the definition of the autocorrelation function as a statistical average,

$$\rho_y(\tau) \equiv \frac{\overline{y(t) y(t + \tau)}}{\overline{y^2(t)}} \quad (3.5)$$

Due to the fact that $y(t)$ is defined to be $+1$ or -1 , the term, $\overline{y^2(t)}$, is equal to unity and the term, $\overline{y(t) y(t + \tau)}$, may be expressed as follows,

$$\overline{y(t) y(t + \tau)} = (1) (P_{++} + P_{--}) + (-1) (P_{+-} + P_{-+}) \quad (3.6)$$

where P_{++} is the joint probability that $y(t) = +1$ and $y(t + \tau) = +1$, and the other P 's are similarly defined. These probabilities can be written in terms of the joint Gaussian probability density of $x(t)$ by making use of the definition of $y(t)$. For example, P_{++} is equal to the joint probability that $x(t) > 0$ and $x(t + \tau) > 0$,

$$P_{++} = \int_0^{\infty} \int_0^{\infty} p[x(t), x(t + \tau)] dx(t) dx(t + \tau) \quad (3.7)$$

The term $p[x(t), x(t+\tau)]$ is the joint Gaussian probability density function and is given by Equation 1.8.

Equations entirely similar to Equation 3.7 exist for P_{--} , P_{+-} and P_{-+} and are identical except for the obvious changes in the limits of integration. Because of the evenness and symmetry of $p[x(t), x(t+\tau)]$ it can be seen that,

$$P_{--} = P_{++} \quad (3.8)$$

$$P_{+-} = P_{-+} \quad (3.9)$$

Additional inspection of $p[x(t), x(t+\tau)]$ reveals that P_{+-} or P_{-+} can be obtained from P_{++} by reversing the sign of $\rho_x(\tau)$ after Equation 3.7 has been integrated.

Equation 1.8 is substituted into Equation 3.7 and the remaining task is the integration of this equation. Fortunately this can be done and a simple result is obtained. The integration is performed by a transformation to cylindrical co-ordinates, i. e., $x(t) = r \cos \theta$ and $x(t+\tau) = r \sin \theta$, with θ going from 0 to $\pi/2$ and r going from 0 to infinity. The integral is thus transformed to,

$$P_{++} = \frac{1}{2\pi\sigma^2(1-\rho_x^2)} \int_0^{\pi/2} \int_0^{\infty} \exp\left[\frac{r^2(1-\rho_x \sin 2\theta)}{-2\sigma^2(1-\rho_x^2)}\right] r \, dr \, d\theta \quad (3.10)$$

The integral in r is of the form, $e^u du$, and the resulting integral in θ is tabulated (Dwight,¹⁶ p. 93, Integral #436.00). The result is,

$$\begin{aligned}
 P_{++} &= 1/4 + (1/2 \pi) \tan^{-1} \frac{\rho_x}{(1 - \rho_x^2)^{1/2}} \\
 &= 1/4 + (1/2 \pi) \sin^{-1} \rho_x
 \end{aligned}
 \tag{3.11}$$

and, according to the previous discussion, the other probabilities are given by,

$$P_{--} = P_{++} = 1/4 + (1/2 \pi) \sin^{-1} \rho_x \tag{3.12}$$

$$P_{+-} = P_{-+} = 1/4 - (1/2 \pi) \sin^{-1} \rho_x \tag{3.13}$$

Substitution of these terms into Equation 3.6 gives finally,

$$\rho_y(\tau) = (2/\pi) \sin^{-1} \rho_x(\tau) \tag{3.14}$$

which can be solved for $\rho_x(\tau)$ to give Equation 3.2

3.3 MEAN AND VARIANCE OF THE ONE-BIT AUTOCORRELATION FUNCTION ESTIMATE

In this section the mean and variance of the one-bit autocorrelation function estimate, $\rho'_x(\tau)$, will be calculated. The equations defining $\rho'_x(\tau)$ are repeated below,

$$\rho'_x(\tau) \equiv \sin \left[\frac{\pi}{2} \rho'_y(\tau) \right] \tag{3.15}$$

$$\rho'_y(\tau) \equiv \frac{1}{K} \sum_{k=1}^K y(k\Delta t) y(k\Delta t + \tau) \tag{3.16}$$

It will be necessary to assume that the terms, $y(k \Delta t) y(k \Delta t + \tau)$, in the summation of Equation 3.18 are independent of each other as was discussed in the introduction of this chapter. An approach utilizing characteristic functions (see Davenport and Root,¹ pp. 50-55) will be used.

The mean of $\rho_y^*(\tau)$ can be easily shown to be $\rho_y(\tau)$; however, the mean of $\rho_x^*(\tau)$ is not so easily found. (Since the sine is a non-linear operation, one cannot say in general, " $\overline{\sin x} = \sin \bar{x}$ ".) The mean and mean square of ρ_x^* can be expressed in terms of $p(\rho_y')$, the probability density function of ρ_y' ,

$$\overline{\rho_x} = \int_{-\infty}^{\infty} \sin(\pi \rho_y'/2) p(\rho_y') d\rho_y' \quad (3.17)$$

$$\overline{\rho_x^2} = \int_{-\infty}^{\infty} \sin^2(\pi \rho_y'/2) p(\rho_y') d\rho_y' \quad (3.18)$$

The probability density function, $p(\rho_y')$, is the Fourier transform of $M_y(v)$, the characteristic function of ρ_y' ,

$$p(\rho_y') = \frac{1}{2\pi} \int_{-\infty}^{\infty} M_y(v) e^{-jv\rho_y'} dv \quad (3.19)$$

Through application of Fourier transform properties (or directly by substitution of Equation 3.19 into Equations 3.17 and 3.18), the mean and mean square of ρ_x' can be simply expressed in terms of $M_y(v)$,

$$\overline{\rho_x} = (1/2j) [M_y(\pi/2) - M_y(-\pi/2)] \quad (3.20)$$

$$\overline{\rho_x^2} = 0.5 M_y(0) - 0.25 M_y(\pi) - 0.25 M_y(-\pi) \quad (3.21)$$

Since the characteristic function of a sum of statistically independent random variables is the product of the characteristic functions of the individual terms (see Davenport and Root, p. 54), $M_y(v)$ can be expressed as,

$$M_y(v) = \prod_{k=1}^K M_k(v) \quad (3.22)$$

where $M_k(v)$ is the characteristic function of a term, $(1/K) \cdot y(k\Delta t) \cdot y(k\Delta t + \tau)$, in the summation of Equation 3. 6.

Each of the terms, $(1/K) y(k\Delta t) y(k\Delta t + \tau)$, can assume either of two values, plus or minus $1/K$, with probabilities, $2P_{++}$ and $2P_{+-}$, respectively. The probability density function of $(1/K) y(k\Delta t) y(k\Delta t + \tau)$ then consists of an impulse of area $2P_{++}$ at $1/K$ and an impulse of area $2P_{+-}$ at $-1/K$. The probabilities, $2P_{++}$ and $2P_{+-}$, are given by Equations 3.12 and 3.13 of the previous section. A Fourier transformation gives the characteristic function, M_k ,

$$M_k = 2P_{++} e^{jv/K} + 2P_{+-} e^{-jv/K} \quad (3.23)$$

The mean and mean square of ρ_x are now given as follows by combining Equations 3.23, 3.22, 3.21, 3.20, 3.13 and 3.12,

$$\overline{\rho_x} = \frac{1}{2j} \left[\left(\cos \frac{\pi}{2K} + j \frac{2}{\pi} \sin^{-1} \rho_x \sin \frac{\pi}{2K} \right)^K - \left(\cos \frac{\pi}{2K} - j \frac{2}{\pi} \sin^{-1} \rho_x \sin \frac{\pi}{2K} \right)^K \right] \quad (3.24)$$

$$\begin{aligned} \overline{\rho_x^2} &= \frac{1}{2} - \frac{1}{4} \left[\left(\cos \frac{\pi}{K} + j \frac{2}{\pi} \sin^{-1} \rho_x \sin \frac{\pi}{K} \right)^K \right. \\ &\quad \left. + \left(\cos \frac{\pi}{K} - j \frac{2}{\pi} \sin^{-1} \rho_x \sin \frac{\pi}{K} \right)^K \right] \end{aligned} \quad (3.25)$$

Thus, expressions giving the mean and mean square of $\rho_x'(\tau)$ have been found in terms of $\rho_x(\tau)$, the true normalized autocorrelation function, and K , the number of statistically independent one-bit products used in the estimate.

Fortunately the case of interest is for K very large compared to π ; in this case Equations 3.24 and 3.25 are greatly simplified. Terms of higher order than π/K are dropped in the final result. The approximations used, in order of their application, are (a and b are constants of the order of π):

$$1) \quad \cos a/k \sim 1 - \frac{a^2}{2K^2}$$

$$2) \quad \sin a/k \sim a/k$$

$$3) \quad \left(1 + \frac{a}{K} + \frac{b}{K^2} \right)^K \sim e^a \left(1 - \frac{a^2}{2K} + \frac{b}{K} \right)$$

The validity of approximation 3) can be demonstrated by taking the logarithm of both sides of the equation and then expanding the logarithm.

Through the use of these approximations the following results are obtained for the mean and variance, $\overline{\sigma_{\rho 1}^2} = \overline{\rho_x'^2} - \overline{\rho_x^2}$,

$$\overline{\rho_x'} = \rho_x \left[1 + \frac{\pi^2}{8K} (\rho_y^2 - 1) \right] \quad (3.26)$$

$$\sigma_{\rho 1}^2 = \frac{\pi^2}{4K} (1 - \rho_x^2)(1 - \rho_y^2) \quad (3.27)$$

Equation 3.26 reveals that the mean of the estimate is biased by an amount, $\rho_x \pi^2 (1 - \rho_y^2)/8K$, from the desired value, ρ_x . This bias will be of the order of \sqrt{K} times smaller than the RMS deviation, $\sigma_{\rho 1}$, and hence can be neglected in most cases.

The variance, given by Equation 3.27, should be compared with the variance, $\sigma_{\rho m}^2$, given by Equation 2.52 for an estimate of the normalized autocorrelation function computed from unquantized or many-bit samples. This variance relation also contains the assumption of independent successive products and is repeated below,

$$\sigma_{\rho m}^2 = \frac{1 - \rho_x^2}{K} \quad (3.28)$$

Our conclusion, then, is that the RMS deviation of an autocorrelation function estimate based on K statistically independent products is increased by $(\pi/2) [1 - \rho_y^2(\tau)] \leq \pi/2$ when the samples are quantized to one-bit. In the unquantized case we were able to show that decreasing the time between samples so that successive products become dependent did not decrease the RMS deviation. We have not shown that this is true in the one-bit case. It may be possible to reduce the RMS deviation by increasing the sampling rate. However, this is doubtful and seems hardly worth the factor of $\pi/2$ which might be gained.

A comparison of one-bit and many-bit autocorrelation function estimates performed as a simulation experiment on a digital computer is given in Section 6.2.

3.4 MEAN AND VARIANCE OF THE ONE-BIT POWER SPECTRUM ESTIMATE

An estimate, $\hat{p}(f)$, of the power spectrum can be determined from the one-bit autocorrelation function estimate, $\hat{\rho}_x(\tau)$, in a manner similar to that used in the previous chapter, Equation 2.3. This relation is,

$$\hat{p}(f) = 2 \Delta\tau \sum_{n=-\infty}^{\infty} \hat{\rho}_x(n \Delta\tau) w(n \Delta\tau) e^{-j 2\pi f n \Delta\tau} \quad (3.29)$$

It is assumed that $\rho'_x(n \Delta\tau) = \rho'_x(-n \Delta\tau)$ defines $\rho'_x(n \Delta\tau)$ for negative n and that the weighting function, $w(n \Delta\tau)$, is zero for $|n| \geq N$. Thus $p'(f)$ requires that $\rho'_x(\tau)$ be computed for N equally spaced values of τ going from $\tau = 0$ to $\tau = (N - 1) \Delta\tau$. The estimate, $p'(f)$, is a normalized spectral estimate; that is Equation 2.17 may be used to show,

$$\int_0^{f_s/2} p'(f) df = \rho'_x(0) = 1 \quad (3.30)$$

where $f_s = 1/\Delta\tau$.

In the previous section it was shown that the mean of $\rho'_x(n \Delta\tau)$ is equal to the true normalized autocorrelation function plus a small bias term. This bias term will be neglected since it is of the order of \sqrt{K} times smaller than the RMS deviation of $\rho'_x(n \Delta\tau)$. Thus, by taking the mean of both sides of Equation 3.29, we find

$$\overline{p'(f)} = 2 \Delta\tau \sum_{n=-\infty}^{\infty} \rho(n \Delta\tau) w(n \Delta\tau) e^{-j 2\pi f n \Delta\tau} \quad (3.31)$$

The right-hand side of Equation 3.31 can be recognized as $p^*(f)$, the smoothed and normalized power spectrum defined by Equation 2.53,

$$\overline{p'(f)} = p^*(f) \quad (3.32)$$

The properties of $p^*(f)$ are fully discussed in Section 2.2 and at the beginning of Section 2.4-2; they will not be discussed further in this chapter.

A calculation of the variance of $p'(f)$ is quite difficult and has not been performed. The spectral variance calculation requires that the covariance of the autocorrelation function estimate be known (see Section 2.3-1). In the previous section the autocorrelation variance was computed through the characteristic function method. An attempt to extend this method to computation of the autocorrelation covariance leads to difficulty because integrals similar to that for P_{++} in Equation 3.10 must be carried out over the trivariate or quadvariate Gaussian probability density functions. The trivariate integral arises if statistically independent products are assumed and the quadvariate integral arises if this assumption is not made. In either case a closed form evaluation of the integrals has not been found.

It is possible, of course, to evaluate the above integrals numerically on a computer for a specific autocorrelation function or power spectrum. Some expansions of the quadvariate normal integral by McFadden¹⁷ may be helpful in this regard. However, in lieu of doing this, it was decided to simulate one-bit spectral analysis on a computer and hence "experimentally" determine the spectral variance. This work is presented in Section 6.2. An experimental value of the spectral variance as computed from data taken in the deuterium line experiment is given in Section 6.5.

A value for the spectral variance integrated over frequency can be obtained from only a knowledge of the autocorrelation variance.

The following relation is easily derived from the Parseval relation, Equation 2.19,

$$\int_0^{f_s/2} \sigma_{p1}^2(f) df = 2\Delta\tau \sum_{n=-\infty}^{\infty} \sigma_{\rho1}^2(n) w^2(n\Delta\tau) \quad (3.33)$$

where $\sigma_{p1}^2(f)$ and $\sigma_{\rho1}^2(n)$ are the spectral and autocorrelation variances respectively. The results of the previous section show that, in the case of statistically independent products, $\sigma_{\rho1}$ is increased by less than $\pi/2$ due to the one-bit quantization. We can thus say that the integrated spectral variance is increased by less than $\pi^2/4$ due to one-bit quantization. If it was known that the frequency distribution of the one-bit spectral variance was the same as that of the many-bit spectral variance (this is approximately the case), then it could be said that the spectral variance is increased by less than $\pi/2$ due to one-bit quantization.

It appears safe to postulate that $\sigma_{p1}(f)$ will have the same dependence on the observation time, T , and resolution, Δf , as in the many-bit case. We thus will express $\sigma_{p1}(f)$ in the form of the many-bit spectral RMS deviation, $\sigma_{pm}(f)$ given by Equation 2.56, multiplied by a numerical factor, β ,

$$\sigma_{p1}(f) = \frac{\alpha\beta}{\sqrt{T\Delta f}} \cdot p(f) \cdot \sqrt{1 - \Delta f/b} \quad (3.34)$$

where α is a dimensionless parameter discussed in Section 2.3-3, $p(f)$ is the true normalized power spectrum, and b is the total bandwidth of the spectrum being analyzed.

The numerical factor, β , depends somewhat on the particular $p(f)$ that is being analyzed. However, the experimental results of Sections 6.2 and 6.5 indicate that β is equal to 1.39 in the constant bandpass region of a spectrum similar to that shown in Figure 6.3. Most spectra analyzed in radio astronomy will have the same gross appearance as the spectrum shown in Figure 6.3. This is true because the input spectrum is nearly constant and, thus, the gross shape of the measured spectrum is determined primarily by the receiver bandpass function. At the edges of the receiver bandpass, β increases (see Figure 6.3 and Equation 6.10) and measurements at frequencies beyond the half-power points have markedly increased statistical uncertainty.

CHAPTER 4

THE RADIO ASTRONOMY SYSTEM

4.1 THE SYSTEM INPUT-OUTPUT EQUATION

In the previous chapters a technique for the measurement of the power spectrum, $P(f)$, of a time function, $x(t)$, has been presented; the procedure is described by Figure 1.7. A spectral estimate, $p'(f)$, is produced. The mean and variance of this estimate are discussed in Section 3.4 which refers back to Sections 2.2 and 2.4-2; these results will be briefly summarized in this section.

It has been assumed that $x(t)$ is a signal in the video-frequency portion of the spectrum; $P(f)$, is zero for f above an upper cutoff frequency, B_{20} . Thus, the spectra we wish to measure in radio astronomy must be restricted (by filtering) to a bandwidth, B_{20} , and then must be shifted (by heterodyning) down to the frequency range between 0 and B_{20} . For practical reasons the heterodyning and filtering will usually be performed in a few steps with the utilization of intermediate frequencies.

The spectrum we wish to measure in radio astronomy is $T_a(f)$, the power spectrum, expressed in degrees Kelvin, available at the antenna terminals. A receiver noise term, $T_r(f)$, must unavoidably

be added to $T_a(f)$. According to this statement and the preceding paragraph, the function of the radio frequency portion of the receiver (that is, everything between the antenna and the clipper input) is described by the following equation:

$$P(f) = [T_a(f+f_0) + T_r(f+f_0)] G(f+f_0) \quad f > 0 \quad (4.1)$$

[$P(f) = P(-f)$ defines $P(f)$ for $f < 0$].

In the above equation, f is a frequency in the video frequency range, f_0 is a frequency which is $B_{20}/2$ below the center frequency of the observed frequency range, and $G(f+f_0)$ is the power transfer function of the receiver. $G(f+f_0)$ should be zero outside of the band extending from f_0 to f_0+B_{20} . The frequency, f_0 , is determined by local oscillator frequencies. These may be chosen so that f_0 lies above f ; in this case f_0-f should replace $f+f_0$ wherever it occurs.

Equation 4.1 describes the modifications of the antenna temperature spectrum, $T_a(f)$, by the radio frequency portion of the receiver. These modifications can be removed since $T_r(f+f_0)$ and $G(f+f_0)$ can be measured; this topic will be discussed in the next section. The modifications resulting from further operations indicated in Figure 1.7 are as follows:

- 1) The clipping of the time function removes the amplitude scale from the measured spectrum; only the shape of the spectrum is

determined. All of the measured spectra are necessarily normalized to have unit area. A scale factor can be determined by some other means if it is needed. The measured spectra are, thus, independent of receiver gain to a high degree.

2) The fact that the autocorrelation function is determined only at discrete points spaced $\Delta\tau$ apart, limits the bandwidth that may be analyzed to $1/2\Delta\tau = f_s/2 = B_{20}$. The power spectrum must be forced (by filtering) to be zero outside of this band or else spurious results will occur. The sampling frequency, f_s , must be at least twice the bandwidth analyzed.

3) The truncation of the autocorrelation function to N points [$(N-1)\Delta\tau$ is the maximum lag time] limits the frequency resolution, Δf , of the spectral measurement to approximately $1/(N\Delta\tau) = f_s/N = 2B_{20}/N$. The parameter, N , is the number of correlation channels provided in the digital correlator. The number of significant points determined on the spectrum, $B_{20}/\Delta f$, is thus equal to $N/2$.

4) The power spectrum of a random time function cannot be exactly measured by any means since an infinite duration of data is required; this topic was discussed in Section 1.3. The quantity we measure, $p'(f)$, is a statistical estimate of the power spectrum. Its properties are described, for our purposes, by its mean or expected value, $\overline{p'(f)}$, and its variance, $\sigma_{p1}^2(f)$.

The modifications stated above are contained in the equations given below which, together with Equation 4.1, relate the measured quantity, $\overline{p}(f)$, to the antenna power spectrum, $T_a(f)$:

$$\overline{p}(f) = \frac{P^*(f)}{\int_0^{f_s/2} P^*(f) df} \quad (4.2)$$

$$P^*(f) = \sum_{i=-\infty}^{\infty} \int_{-\infty}^{\infty} P(\alpha) W(f - \alpha - if_s) d\alpha \quad (4.3)$$

Equation 4.2 expresses the normalization of the spectral estimate; $\overline{p}(f)$ [and also $p'(f)$] has unit area between 0 and $f_s/2$.

Equation 4.3 expresses the effects of sampling and truncation of the autocorrelation function. The quantity, $P^*(f)$, is related to the true power spectrum, $P(f)$, by Equation 4.3. This equation is discussed in Section 2.2-1 and is described by Figure 2.1. If sampling is performed at a fast enough rate, all terms in the summation of Equation 4.3 are zero except for the $i=0$ term, and $P^*(f)$ becomes simply the convolution (or smoothing) of $P(f)$ by $W(f)$. The function, $W(f)$ is determined by the choice of the weighting function, $w(\tau)$; this topic is discussed in Section 2.2-2. In general $W(f)$ is a narrow, spike-type function of bandwidth $\Delta f \sim f_s/N$. Thus, features in the spectrum narrower than Δf are smoothed out. If $P(f)$ does not change appreciably over bands of width, Δf , then $P^*(f) \sim P(f)$, for $0 < f < f_s/2$.

Equation 4.3 should also be considered as the definition of the star (*) operator which will be used further. A starred quantity is related to the unstarred quantity in the same manner as $P^*(f)$ and $P(f)$ are related. For example,

$$[T(f+f_o) G(f+f_o)]^* = \sum_{i=-\infty}^{\infty} \int_{-\infty}^{\infty} T(\alpha+f_o) G(\alpha+f_o) W(f-\alpha-if_s) d\alpha \quad (4.4)$$

Through the use of the star operator, it is possible to combine Equations 4.1, 4.2, and 4.3 into one compact equation relating the measured quantity, $p'(f)$, to the true power spectrum referred to the receiver input, $T(f) = T_a(f) + T_r(f)$,

$$\overline{p'(f)} = \frac{[T(f+f_o) G(f+f_o)]^*}{\int_0^{f_s/2} [T(f+f_o) G(f+f_o)]^* df} \quad (4.5)$$

4.2 SPECIFICATION OF ANTENNA TEMPERATURE

The noise power spectrum available at the antenna terminals, $T_a(f+f_o)$, can be estimated if some auxiliary calibration measurements are made in addition to the measurement of $p'(f)$. These auxiliary measurements are of the receiver bandpass, $G(f+f_o)$; the average (over frequency) noise temperature referred to the receiver input, T_{av} ; and the receiver noise power spectrum, $T_r(f+f_o)$.

4.2-1 Correction of Effect of Receiver Bandpass

The receiver bandpass can be accurately measured by observing the system output, $p'_o(f)$, when the input $T(f+f_o)$, is white noise (uniform spectrum over the frequency range $G(f+f_o)$ is non-zero). In this case, Equation 4.5 gives the system output as,

$$\overline{p'_o(f)} = \frac{G^*(f+f_o)}{\int_0^{f_s/2} G^*(f+f_o) df} \quad (4.6)$$

Before discussing how $p'_o(f)$ is applied, the problem of obtaining a white $T(f+f_o) = T_a(f+f_o) + T_r(f+f_o)$ will be discussed. This problem is simplified if $T_r(f+f_o)$ is white as is often the case when the receiver front-end is broadband compared to B_{20} . If this is the case, a white $T(f+f_o)$ can be produced by either of three methods:

- 1) Pointing the antenna at a region where no spectral line is expected.
- 2) Connecting a white noise generator (such as a matched load at 300°K) to the receiver input in place of the antenna.
- 3) If the receiver is broadband between the input and the first converter, by detuning the first local oscillator.

Each of the above methods has special problems which must be considered. It should be pointed out that the receiver bandpass

need not be determined too accurately once the large receiver noise term is subtracted off as will be discussed in Section 4.2-3.

In the case that the receiver noise is not white, a $T(f+f_o)$ which is nearly white can still be obtained by application of a white T_a which is much greater than $T_r(f+f_o)$. This may be accomplished with method 2) or with method 1) if a large enough T_a can be obtained from a strong radio source. Attenuation should be inserted into the receiver so that the clippers are operating at approximately the normal signal level.

The measurements of $p'_o(f)$ is applied by dividing $p'(f)$ by $p'_o(f)$ to give,

$$\left[\frac{p'(f)}{p'_o(f)} \right] = \frac{[T(f+f_o) G(f+f_o)]^*}{T_{av} \cdot G^*(f+f_o)} \quad (4.7)$$

where T_{av} is a measured quantity to be discussed in the next section and is given by,

$$T_{av} = \frac{\int_0^{f_s/2} [T(f+f_o) G(f+f_o)]^* df}{\int_0^{f_s/2} G^*(f+f_o) df} \quad (4.8)$$

An approximation has been used in Equation 4.7 in that $\overline{p'(f)/p'_0(f)}$ has been assumed equal to $\overline{p'(f)} / \overline{p'_0(f)}$. This is quite valid since the random part of $p'_0(f)$ is small compared to its mean.

The quantity, $[T(f+f_0) G(f+f_0)]^* / G^*(f+f_0)$, has an important interpretation and it is therefore convenient to assign a special symbol, \dagger , for this operation on $T(f+f_0)$. Thus $T^\dagger(f+f_0)$ is defined as,

$$T^\dagger(f+f_0) \equiv \frac{T(f+f_0) G(f+f_0)^*}{G^*(f+f_0)} \quad (4.9)$$

with identical relations between $T_a^\dagger(f+f_0)$ and $T_a(f+f_0)$ and between $T_r^\dagger(f+f_0)$ and $T_r(f+f_0)$. The mathematical relationship between $T^\dagger(f+f_0)$ and $T(f+f_0)$ is quite complicated; however, the relationship greatly simplifies when a restriction is applied to the shape of $G(f+f_0)$. The restriction is that $G(f+f_0)$ must be smooth over frequency bands of width, Δf , for values of f in the passband region (say between 1 db points). Stated another way,

$$G^*(f+f_0) \sim G(f+f_0) \quad (4.10)$$

for f in the passband region. This condition is easily met in practice.

Under this condition, $T^\dagger(f+f_0)$, becomes simply the convolution or smoothing of $T(f+f_0)$ by $W(f)$; that is,

$$T^{\dagger}(f+f_0) = \int_{-\infty}^{\infty} T(\alpha+f_0) W(f-\alpha) d\alpha \quad (4.11)$$

for values of f in the bandpass region. (The requirement that $G(f+f_0)$ is bandlimited to half the sampling frequency has also been used in Equation 4.11). Thus a dagger (\dagger) superscript on $T(f+f_0)$, $T_a(f+f_0)$, or $T_r(f+f_0)$ should be considered as a smoothing operation on these spectra. If f is outside of the 1 db receiver bandwidth or if the condition of Equation 4.10 is not true, then the dagger (\dagger) operator must be interpreted by Equation 4.9. Note that one cannot say, " $[G(f+f_0) T(f+f_0)]^* = G^*(f+f_0) T^*(f+f_0)$ ".

Through the use of the dagger operator, then, Equation 4.7 becomes,

$$\left[\frac{p'(f)}{p_0'(f)} \right] = \frac{T^{\dagger}(f+f_0)}{T_{av}} \quad (4.12)$$

$$= \frac{T_a^{\dagger}(f+f_0) + T_r^{\dagger}(f+f_0)}{T_{av}} \quad (4.13)$$

The smoothed antenna temperature, $T_a^{\dagger}(f+f_0)$ is thus expressed in terms of measurable quantities by Equation 4.13.

4.2-2 Measurement of T_{av}

The quantity, T_{av} , defined by Equation 4.8, can be expressed in a more usable form through the use of a property of the star

operator given by Equations 2.17 and 2.18. These equations show that the integral of a starred variable between limits 0 and $f_s/2$ is equal to the integral of the unstarred variable between limits of 0 and ∞ . Thus, T_{av} becomes,

$$T_{av} = \frac{\int_0^{\infty} T(f+f_0) G(f+f_0) df}{\int_0^{\infty} G(f+f_0) df} \quad (4.14)$$

and is recognized to be the average input noise temperature weighted by the receiver bandpass. It is the temperature that is determined if the receiver is used for continuum (broadband) measurements.

T_{av} is proportional to the power in the signal at the clipper input and is easily determined by conventional means. Note that T_{av} includes both the antenna temperature and the receiver noise temperature, $T_{av} = T_{a\ av} + T_{r\ av}$. All temperature measurements performed with the one-bit autocorrelation system are normalized to T_{av} as is expressed in Equation 4.13.

4.2-3 Measurement of $T_r^\dagger(f+f_0)$

The spectral measurement system determines the sum, $T^\dagger(f+f_0)$, of the smoothed antenna-temperature spectrum, $T_a^\dagger(f+f_0)$,

and the smoothed receiver noise-temperature spectrum, $T_r^\dagger(f+f_o)$. Thus, we wish to determine $T_r^\dagger(f+f_o)$ and subtract this from $T^\dagger(f+f_o)$. The measurement of $T_r^\dagger(f+f_o)$ is accomplished by applying a signal with a known, white, comparison spectrum, T_c , to the antenna terminals. The system output, $p_c'(f)$, divided by $p_o'(f)$, then gives

$$\left[\frac{p_c'(f)}{p_o'(f)} \right] = \frac{T_c + T_r^\dagger(f+f_o)}{T_{cav}} \quad (4.15)$$

where $T_{cav} = T_c + T_{rav}$ is the measured average input temperature with the comparison source connected. Equation 4.15 thus determines $T_r^\dagger(f+f_o)$ in terms of measured quantities.

It should be noted that if T_r is white, the measurements of $p_c'(f)$ and $p_o'(f)$ are identical and $p_c'(f) = p_o'(f)$. In this case, T_r is completely determined by the measurement of T_{cav} .

4.2-4 Summary

The smoothed antenna temperature spectrum, $T_a^\dagger(f+f_o)$, is specified by the measurement of two frequency-averaged antenna temperatures, T_{av} and T_{cav} , and three normalized power spectra, $p'(f)$, $p_c'(f)$, and $p_o'(f)$. Both T_{av} and $p'(f)$ are signal measurements; they are performed with the antenna connected to the receiver input and pointed in the desired direction. The other three quantities are auxiliary measurements used to specify the receiver noise

temperature spectrum, $T_r(f+f_o)$, and the receiver response, $G(f+f_o)$. They are determined with a known comparison spectrum applied to the receiver input at some time before or after the signal measurements are performed. Equations 4.13 and 4.15 can be combined to specify $T_a^\dagger(f+f_o)$ in terms of these five measured quantities,

$$T_a^\dagger(f+f_o) = T_{av} \left[\frac{p'(f)}{p_o(f)} \right] - T_{cav} \left[\frac{p'_c(f)}{p_o(f)} \right] + T_c \quad (4.16)$$

T_c is the temperature of a known, white comparison spectrum and f_o is known from the local oscillator frequencies.

If the receiver noise temperature spectrum is equal to a constant value, T_r , over the frequency band under observation, B_{20} , then $p'_c(f) = p'_o(f)$, and Equation 4.16 reduces to,

$$T_a^\dagger(f+f_o) = T_{av} \left[\frac{p'(f)}{p_o(f)} \right] - (T_{cav} - T_c) \quad (4.17)$$

where $T_{cav} - T_c = T_r$.

4.3 THE SWITCHED MODE OF OPERATION

4.3-1 Motivation and Description

In the preceding section we have seen that the measurement of the antenna temperature depends on auxiliary measurements performed before or after the actual observation. The problem of

error due to changes in the receiver characteristics $[T_r(f+f_o)$ and $G(f+f_o)]$ between the time the observation is made and the time the auxiliary measurements are made then arises. These changes may be made small (of the order of a few tenths of a percent in a 10 minute interval) by careful circuitry but are important in view of the high accuracy needed in spectral measurements in radio astronomy. The high accuracy is required because the spectrum we wish to measure, $T_a(f+f_o)$, is superimposed on a receiver noise spectrum, $T_r(f+f_o)$, which may be many times $T_a(f+f_o)$. The problem is aggravated by the fact that the time duration, T , required for a spectral measurement increases as higher accuracy is desired (Equation 1.20).

An approach to this problem is to periodically switch between the actual signal measurement and the calibration measurement. The switching is accomplished with a mechanical, ferrite, or diode switch which alternately connects the receiver input to the antenna terminals or to a noise source generating a uniform, comparison spectrum, T_c . Switching rates between 10 cps and 400 cps are common. While the switch is at the antenna position, the signal measurements, $p'(f)$ and T_{av} , are being performed (that is, a segment of integration time is accumulated); with the switch at the noise source position, the comparison measurements, $p'_c(f)$ and T_{cav} , are performed. At the output end of the receiver, a second

switch (usually of the diode type) is used to either separately totalize signal and comparison variables or, more commonly, to totalize the difference between signal and comparison variables. The switching technique has been extensively used in radio astronomy; the Dicke radiometer is based on this principle.

The switching technique, as it is used with the digital autocorrelation system, is diagrammed in Figures 4.1 and 4.2. The digital correlator is gated in phase with the front-end switch to add the products, $y(k\Delta t) y(k\Delta t + n\Delta\tau)$, which occur when the switch is at the antenna position and subtract the products which occur when the switch is at the noise source position. The quantity that is determined by the digital correlator is $\delta \rho'_y(n\Delta\tau) = \rho'_y(n\Delta\tau) - \rho'_{yc}(n\Delta\tau)$, the difference between the estimates of the one-bit autocorrelation functions of the antenna signal (plus receiver noise) and the noise source signal (plus receiver noise). When $\delta \rho'_y(n\Delta\tau)$ is properly corrected and Fourier transformed, the difference spectrum, $\delta p'(f) = p'(f) - p'_c(f)$, is determined.

The correction of $\delta \rho'_y(n\Delta\tau)$ to give the difference of the unclipped autocorrelation function estimates, $\delta \rho'_x(n\Delta\tau) = \rho'_x(n\Delta\tau) - \rho'_{xc}(n\Delta\tau)$, is not quite straight-forward. Application of the usual correction, Equation 3.15, gives

$$\delta \rho'_x(n\Delta\tau) = \sin [\pi \rho'_y(n\Delta\tau)/2] - \sin [\pi \rho'_{yc}(n\Delta\tau)/2] \quad (4.18)$$

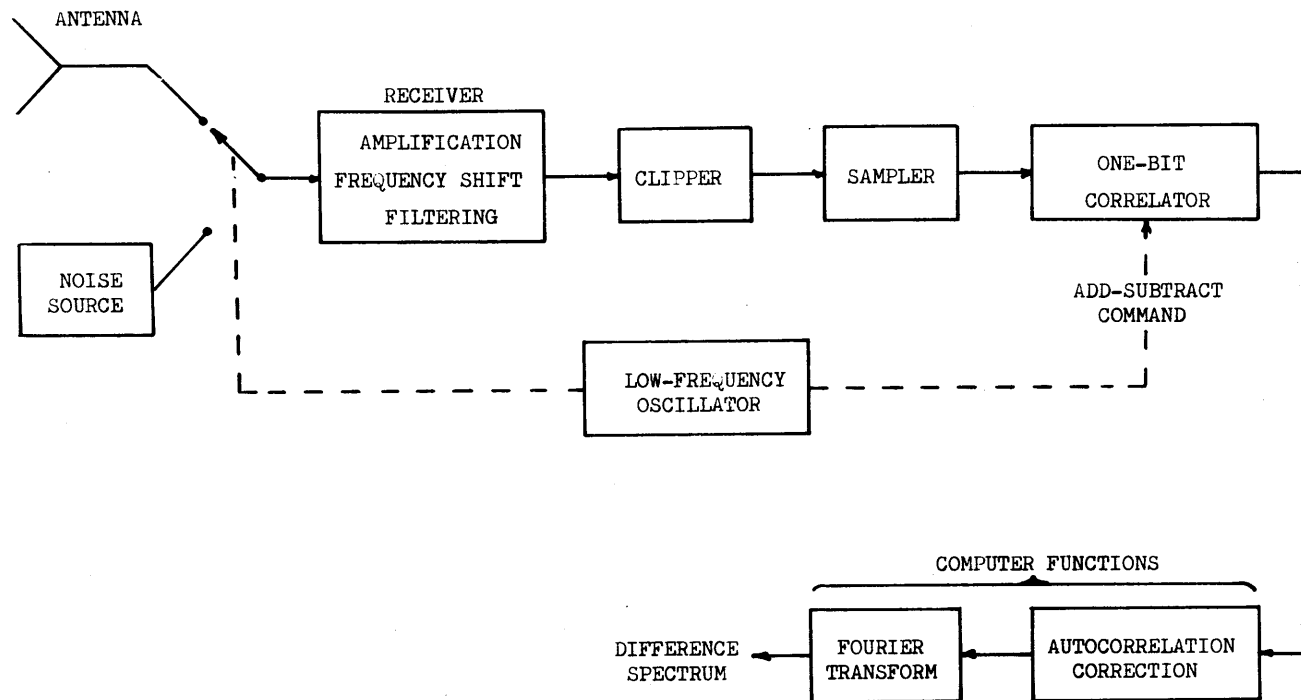


FIG. 4.1 - The switched one-bit autocorrelation radiometer system. Detailed receiver and correlator block diagrams are given in Figures 5.1 and 5.5.

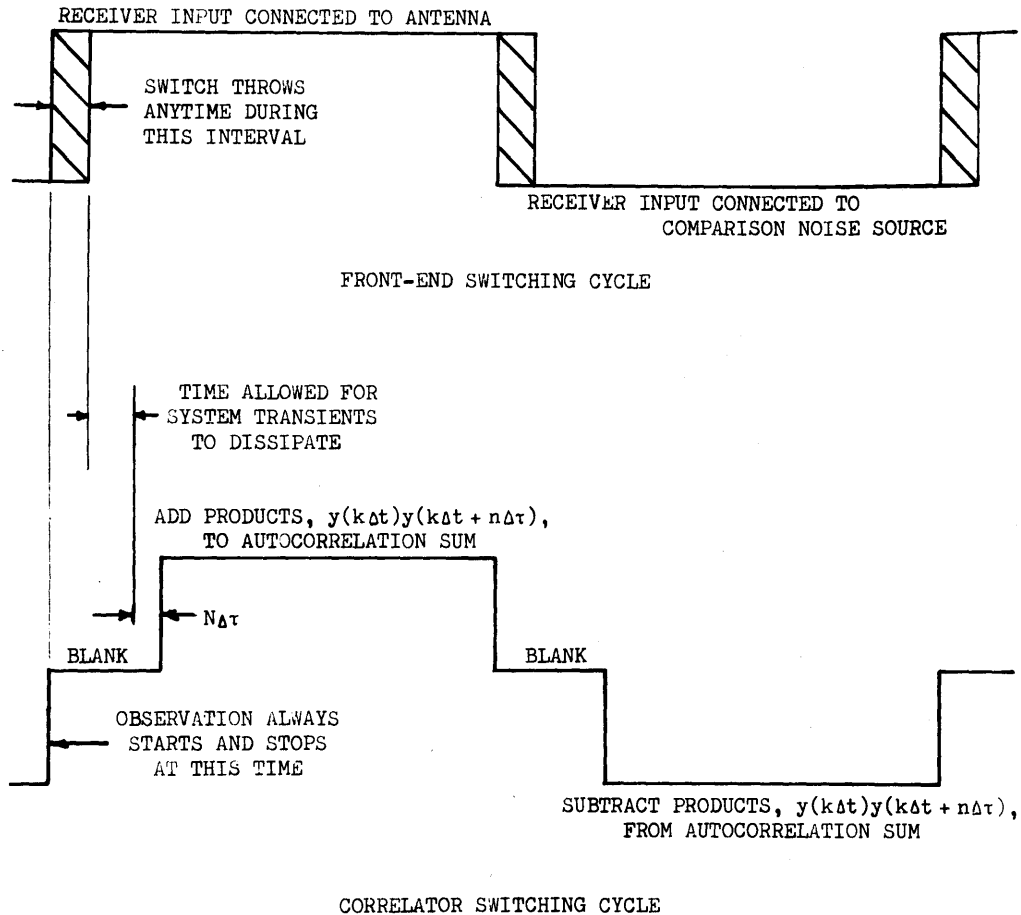


FIG. 4.2 - The timing of the front-end switch and correlator operations in a switched autocorrelation radiometer is indicated above. The timing of operations is best controlled by precise counts of the correlator sampling pulses. For example, in the deuterium-line correlator the blanking interval is 256 counts long and the add and subtract intervals are each 768 counts long. This gives 2048 counts for a complete cycle and thus the switching rate is 37.4 cps for the 75 kc sampling rate.

This relation is not usable as it stands because $\rho'_y(n\Delta\tau)$ and $\rho'_{yc}(n\Delta\tau)$ are not separately determined in the digital correlator; only their difference, $\delta\rho'_y(n\Delta\tau)$, is available. This is due to an economic consideration in the design of the digital correlator. However, $\rho'_{yc}(n\Delta\tau)$, can be determined at some time, before or after the actual observation time, and the correction equation can be put in the usable form,

$$\delta\rho'_x(n\Delta\tau) = 2 \sin \frac{\pi\delta\rho'_y(n\Delta\tau)}{4} \cdot \cos \frac{\pi[2\rho'_{yc}(n\Delta\tau) + \delta\rho'_y(n\Delta\tau)]}{4} \quad (4.19)$$

Small errors in the measurement of $\rho'_{yc}(n\Delta\tau)$ are not important since $\rho'_{yc}(n\Delta\tau)$ is used here only to modify a difference of autocorrelation functions.

It should be noted that the analysis of the switched system is being treated on a static basis. We are neglecting the fact that the system "remembers" the signal from the previous switch position. If the system time constants (the longest is of the order of $1/\Delta f$) are short compared to the switching period, the static approximation is good. However, if a blanking interval is inserted after each switch throw (see Figure 4.2), the static approximation is almost exact. During the blanking interval the correlator samples, delays, and multiplies as usual; however, the products, $y(k\Delta t) y(k\Delta t + n\Delta\tau)$, that occur are not added into the sum which forms the autocorrelation function estimate. The blanking interval simplifies the analysis,

eliminates possible error due to the switching transient, and removes the problem of fluctuations in switch dwell time or "jitter" in a mechanical switch.

4.3-2 The Antenna Temperature Equation

The antenna temperature can be expressed in terms of the difference quantities, $\delta p'(f)$ and δT_{av} , by substitution of $p'(f) = p'_c(f) + \delta p'(f)$ and $T_{av} = T_{cav} + \delta T_{av}$ into Equation 4.16. The result is,

$$T_a^\dagger(f+f_o) = (T_{cav} + \delta T_{av}) \left[\frac{\delta p'(f)}{p'_o(f)} \right] + \delta T_{av} \left[\frac{p'_c(f)}{p'_o(f)} \right] + T_c \quad (4.20)$$

The quantities, T_{cav} , $p'_o(f)$, and $p'_c(f)$ must still be measured at some time before or after the signal measurements. However, they have only a weak effect upon the spectral measurement since they only modify the difference quantities, $\delta p'(f)$ and δT_{av} .

If the receiver noise spectrum is white, $p'_c = p'_o$, and Equation 4.20 can be put in the convenient form,

$$\frac{T_a^\dagger(f+f_o) - T_{aav}}{T_{av}} = \left[\frac{\delta p'(f)}{p'_o(f)} \right] \quad (4.21)$$

where the relations, $T_{av} = T_{cav} + \delta T_{av}$ and $T_{aav} = T_c + \delta T_{av}$, have been used. This same result arises, even if T_r is not white, if the radiometer is balanced so that $\delta T_{av} = 0$ and $T_c = T_{aav}$.

The antenna temperature equation can be put in many other forms which may have special value or interpretation for specific experiments. A form that was used in the deuterium-line and Zeeman experiments is,

$$\frac{T(f+f_0) - T_{av}}{T_{av}} = \left[\frac{\delta p'(f)}{p_0(f)} \right] \quad (4.22)$$

which is easily derived from Equation 4.20 under the assumption of a white receiver noise spectrum.

4.4 SYSTEM SENSITIVITY

The sensitivity of a radiometer is specified by the RMS deviation, $\Delta T(f+f_0)$, of the antenna temperature measurement from its mean value, $T(f+f_0)$. The minimum detectable antenna temperature depends on the desired confidence limits; a value of a few times $\Delta T(f+f_0)$ is usually adopted.

The RMS deviation, $\sigma_{p_1}(f)$, of a normalized spectral estimate, $p'(f)$, obtained by the one-bit autocorrelation method is given by Equation 3.34 as,

$$\frac{\sigma_{p_1}(f)}{p(f)} = \frac{\alpha\beta}{\sqrt{\tau\Delta f}} \cdot \sqrt{1 - \Delta f/b} \quad (4.23)$$

where:

τ is the duration that the signal is observed

- Δf is the frequency resolution; it is the half-power bandwidth of $W(f)$
- α is a dimensionless parameter of the order of unity; it depends on the exact shape of $W(f)$ and is given in Section 2.2-3
- β is the increase in RMS deviation due to the clipping or one-bit operation; it is discussed in Sections 3.4, 6.2, and 6.5. It has a value of 1.39 in the midband region (say between 1 db points) of the receiver bandpass and increases according to Equation 6.8 on the edges of the receiver bandpass.
- b is the total noise bandwidth of the measured spectrum; it is approximately equal to the half power receiver bandwidth.

The specification of the antenna temperature depends, through Equation 4.16, on three normalized spectral measurements, $p'(f)$, $p'_c(f)$, and $p'_o(f)$, and two frequency-averaged antenna temperature measurements, T_{av} and T_{cav} . The RMS deviation of the antenna temperature can be expressed in terms of the RMS deviations of each of these measurements. This is accomplished by expanding each of these quantities in Equation 4.16 as its mean plus a small random part. The random part is then squared, a statistical average is taken, and higher order terms are dropped. The result of these operations is that $\Delta T(f+f_o)$ is equal to the square root of the sum of the squares of the following terms:

$$T_{av} \frac{(\sigma_{pl})_s}{p_o}, \quad T_{cav} \frac{(\sigma_{pl})_c}{p_o}, \quad \frac{p_1}{p_o} \Delta T_{av}$$

$$\frac{p_c}{p_o} \Delta T_{cav}, \quad \text{and} \quad (T_a^\dagger - T_c) \frac{(\sigma_{pl})_o}{p_o}$$

where $(\sigma_{pl})_s$, $(\sigma_{pl})_c$, and $(\sigma_{pl})_o$ refer to the RMS deviations of $p'(f)$, $p'_c(f)$, and $p'_o(f)$, respectively.

We now assume that: 1) The radiometer is near balance so that, $T_{av} \sim T_{cav}$. 2) The amplitude of the observed spectral line is small compared to white receiver noise so that, $p(f) \sim p_c(f) \sim p_o(f)$. The expression for the RMS deviation then becomes,

$$\frac{\Delta T^2}{T_{av}^2} = \frac{(\sigma_{pl})_s^2}{p^2} + \frac{(\sigma_{pl})_c^2}{p^2} + \frac{\Delta T_{av}^2}{T_{av}^2} + \frac{\Delta T_{cav}^2}{T_{cav}^2} + \frac{(T_a^\dagger - T_c)^2}{T_{av}^2} \frac{(\sigma_{pl})_o^2}{p^2}$$

(4.24)

The first two terms of Equation 4.24 are the largest and represent the variances of the measurements of the normalized signal and comparison spectra, $p'(f)$ and $p'_c(f)$, respectively. These variances are given by Equation 4.23 with the observation time, τ , equal to τ_s in the signal case and τ_c in the comparison case. The third and fourth terms represent the variance of the measurements of T_{av} and T_{cav} . Their exact values depend on the manner in which T_{av} and T_{cav} are measured. However, since they are of the order

of $b/\Delta f$ times smaller than the first two terms, they are given with sufficient accuracy by,

$$\frac{\Delta T_{av}^2}{T_{av}^2} = \frac{\alpha^2 \beta^2}{\tau_s b^2} \quad (4.25)$$

and

$$\frac{\Delta T_{cav}^2}{T_{cav}^2} = \frac{\alpha^2 \beta^2}{\tau_c b^2} \quad (4.26)$$

The final term in Equation 4.24 is very small if the radiometer is near balance, or equivalently if $(T_a^\dagger - T_c)/T_{av} \ll 1$. If $(T_a^\dagger - T_c)/T_{av}$ is equal to ϵ , then the observation time for the measurement of $p_o'(f)$ can be as short as $10\epsilon^2 \tau_s$ before the final term becomes 0.1 of the first term. This final term will be neglected in further equations.

According to the previous two paragraphs, then, the RMS deviation can be expressed as,

$$\frac{\Delta T}{T_{av}} = \alpha\beta \sqrt{\frac{1}{\tau_s \Delta f} + \frac{1}{\tau_c \Delta f}} \quad (4.27)$$

where τ_s and τ_c are the signal and comparison observation times. If τ is the total observation time (not including time spent in blanking), $\tau_s = 0.5\tau$, and $\tau_c = 0.5\tau$, so that Equation 4.27 becomes,

$$\frac{\Delta T}{T_{av}} = \frac{2\alpha\beta}{\sqrt{\tau\Delta f}} \quad (4.28)$$

CHAPTER 5

SYSTEM COMPONENTS

A brief discussion of the design parameters and design approaches of the major components of a switched one-bit autocorrelation radiometer (as in Figure 4.1) will be presented in this chapter. The deuterium-line detection system will be used as an example. The chapter is divided into sections concerning the radio-frequency portion of the system, the clipping and sampling operation, and the one-bit digital correlator.

5.1 RADIO-FREQUENCY PORTION OF THE SYSTEM

This section is concerned with the portion of the system which lies between the antenna terminals and the input to the clipper. The material of Chapter 4 is drawn upon heavily in this section. The block diagram of the radio-frequency portion of the deuterium-line detection system is shown in Figure 5.1 and will be referred to by the text.

5.1-1 Front-End Switch and Noise Source

Two highly important components in any switched radiometer are the switch and the comparison noise source. The quantity that is directly measured by the radiometer is the difference between

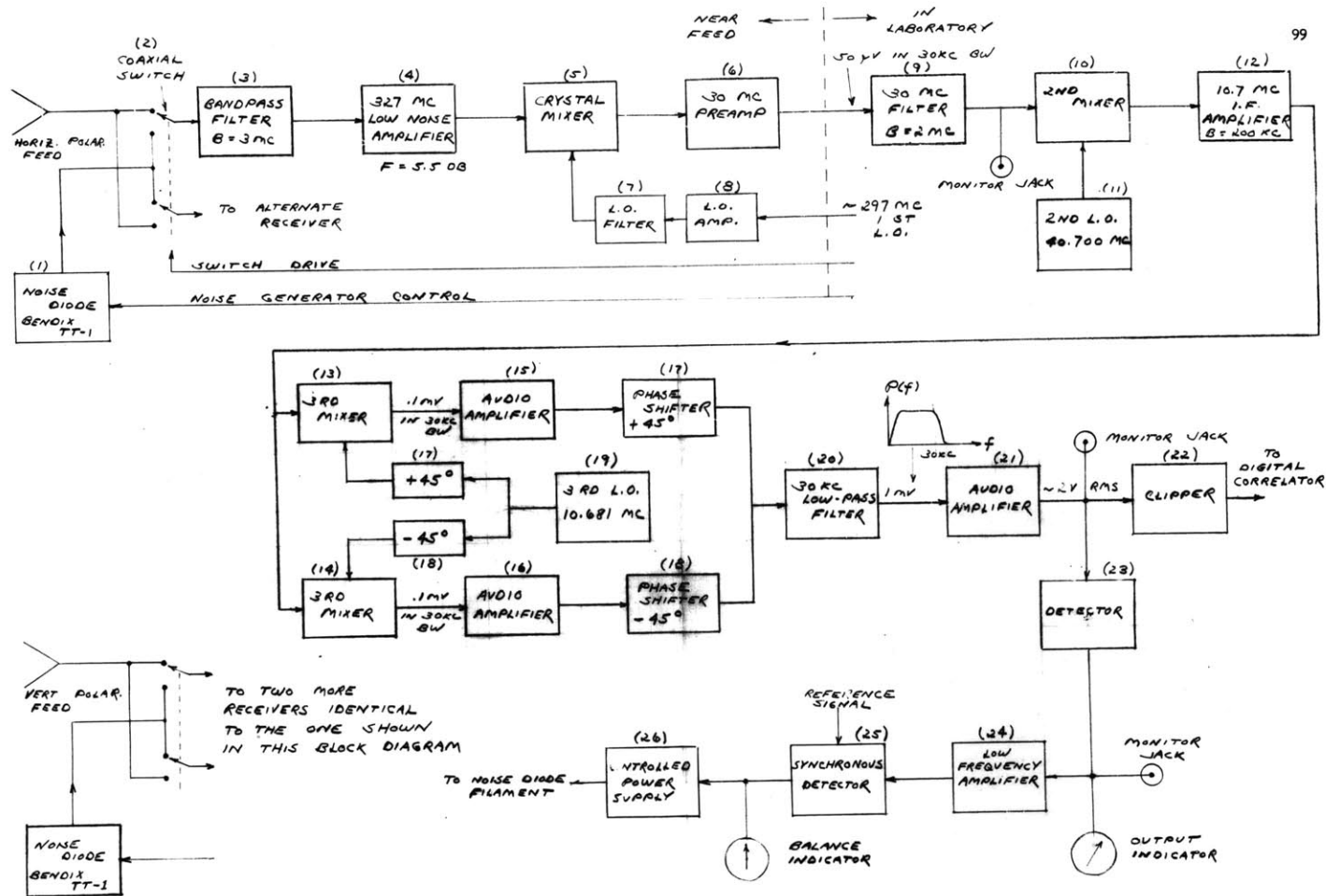


FIG. 5.1 - Radio-frequency portion of the deuterium-line detection system.

the comparison noise-source spectrum, T_c , transferred through the switch, and the antenna temperature spectrum, T_a , transferred through the other arm of the switch. The comparison spectrum and switch transfer characteristics must either be measured or assumed to be linear functions of frequency. The first of these alternatives can be achieved by using a celestial radio source of known spectrum as a "primary" standard to measure T_c , which then becomes a "secondary" standard.

The frequency variations of the switch and noise source have little effect if they can be assumed to be linear with frequency and if the linear component of the true spectrum is known or is not needed. The linear-with-frequency assumption is justified when the bandwidth analyzed, B_1 , is narrow compared with the frequency scale of changes in the characteristics of the switch and noise source. The linear component of the true spectrum is known when the bandwidth analyzed is somewhat greater than the bandwidth of the spectral line so that the background spectrum at frequencies above and below the spectral line can be established.

In the deuterium-line experiment $B_1 = 30$ kc at a center frequency of 327 mc. The switch and noise source are by no means high Q devices; and thus, their characteristics change appreciably only over a scale of tens of megacycles. The measured spectra had slopes of the order of 0.05%/30 kc which were removed in a computer so that the final result had zero slope. This slope correction

did not disturb the results of the experiment because the spectrum should have nearly zero slope whether the deuterium line is present or not.

5.1-2 Balance Requirements

The antenna temperature equation (4.20) contains a term, $\delta T_{av} \overline{p'_c(f)/p'_o(f)}$, which represents the effect of unbalance ($\delta T_{av} \neq 0$) in the radiometer. This term should be kept small in order to avoid errors due to time variations in the receiver noise spectrum, $T_r(f+f_o)$. The magnitude of this term is placed in evidence by application of Equation 4.15 and expansion of $T_r^\dagger(f+f_o)$ as $T_{rav} + \delta T_r^\dagger(f+f_o)$ and $T_c^\dagger(f+f_o)$ as $(T_{cav} + \delta T_c^\dagger(f+f_o))$. The terms, $\delta T_r^\dagger(f+f_o)$ and $\delta T_c^\dagger(f+f_o)$, thus represent the frequency variations of the receiver noise spectrum about their frequency-averaged values. The result is,

$$\delta T_{av} \overline{\left[\frac{p'_c(f)}{p'_o(f)} \right]} = \frac{\delta T_{av}}{T_{cav}} [T_{cav} + \delta T_r^\dagger(f+f_o) + \delta T_c^\dagger(f+f_o)] \quad (5.1)$$

which is small if the radiometer is near balance; and, in addition, is nearly constant if the receiver noise spectrum and the comparison spectrum are nearly constant with frequency.

In the deuterium line experiment a servo loop was used to hold $\delta T_{av}/T_{cav}$ to less than 0.3%, and $\delta T_r^\dagger(f+f_o)$ and $\delta T_c^\dagger(f+f_o)$ were each estimated to be less than 1° (they are small because of the

narrow bandwidth, B_1). The term given by Equation 5.1 is thus equal to a constant ($< 6^\circ$) and a frequency-varying component which is less than 0.006° . The constant term has negligible effect and the small frequency-varying term will be linear to first order and will be removed by the previously-mentioned linear correction. Therefore, in the deuterium line experiment, the unbalance term, $\delta T_{av} \overline{p'_c(f)/p'_o(f)}$, could be neglected. In other applications it may be necessary to determine $p'_c(f)$ and δT_{av} [$p'_o(f)$ is needed anyway] and include the unbalance term in the antenna temperature equation.

There are two more reasons for operating the radiometer near balance. The first is due to the clippers having different characteristics when operated at different signal levels (see Section 5.2 and Figure 5.2). If the signal and comparison power levels differ appreciably, an error due to this cause may occur in the difference spectrum, $\delta p'(f)$. This error should be negligible with proper clipper design and if $\delta T_{av}/T_{av}$ is kept to below a few per cent. A final reason for operating the radiometer near the balanced condition is that T_{av} must be measured by conventional Dicke radiometer techniques. It is well known that the error due to gain fluctuations in this measurement will be small if the radiometer is near balance.

5.1.3 Shape of the Receiver Bandpass, $G(f+f_0)$

The function of the radio-frequency portion of the system is described by the equation,

$$P(f) = G(f+f_0) T(f+f_0) \quad f > 0 \quad (5.2)$$

where $P(f)$ is the power spectrum at the input of the clipper, $G(f+f_0)$ is the power transfer function of the receiver, $T(f+f_0)$ is the power spectrum referred to the receiver input, and f_0 is determined by local oscillator frequencies [$P(f) = P(-f)$ defines $P(f)$ for $f < 0$]. In this section the requirements concerning the shape of $G(f+f_0)$ will be presented; in the next section the frequency conversion problem will be discussed.

A major requirement of $G(f+f_0)$ is that it be very small for f greater than half the sampling frequency, f_s . This is necessary in order to avoid spurious responses due to sampling (see Figures 1.3 and 2.1). For the deuterium line receiver, $G(f+f_0)$ was designed to be 20 db down at half the sampling frequency.

A second requirement of $G(f+f_0)$ is that it have a fairly uniform passband. This is necessary because the statistical uncertainty (RMS deviation divided by the mean) of the spectral measurement increases at frequencies where $G(f+f_0)$ decreases (see Figure 6.3 and Equation 6.10). Experimental results presented in Section

6.2 indicate that the statistical uncertainty will increase by less than 10% in regions where $G(f+f_0)$ is within 1 db (26%) of its maximum value. A criterion of a passband flat within ± 0.5 db was chosen for the deuterium-line receiver.

A third requirement on $G(f+f_0)$ is that it become very small for f near zero frequency. This requirement arises because of several practical considerations such as difficulty in constructing DC coupled amplifiers and clippers, difficulty in obtaining image rejection in the final frequency converter for frequencies near 0, and errors due to DC offset in the clipping operation. If a spectrum containing low frequency components is fed into AC coupled clipper stages, the spectral measurement at higher frequencies may be upset. Thus, these low-frequency components should be removed by high-pass filtering previous to the clipping operation. The spectrum that is within 1 or 2 Δf of zero-frequency should be disregarded, as it may contain an error due to DC offset in the clippers (although, the switching technique removes most of this error).

Assuming that the 20 db bandwidth, B_{20} , is set equal to half the sampling frequency and that the 1 db bandwidth, B_1 , is the region where a good spectral measurement is obtained, the ratio, $r = B_1/B_{20}$, becomes an important parameter describing $G(f+f_0)$. The frequency resolution, Δf , is proportional to the sampling frequency ($\Delta f \sim f_s/N \sim 2B_{20}/N$); and thus, the ratio of the usable bandwidth

analyzed, B_1 , to the frequency resolution, Δf , is proportional to r ($B_1/\Delta f \sim rN/2$). For efficient use of N , the number of correlator channels, r should be as close to unity as possible with practical filter designs. A value of $r = 0.67$ was used in the deuterium line receiver; other parameters were $f_s = 75$ kc, $B_{20} = 37.5$ kc, $B_1 = 25$ kc, $N = 21$, and $\Delta f = 3.75$ kc.

5.1-4 Frequency Conversion and Filtering

There are a few approaches to the frequency conversion problem. If a crystal filter with the desired bandwidth is available, it may be used in the I.F. amplifier (usually 10.7 MC or 30 MC center frequency) to give the desired response. A second mixer then shifts the spectrum down to between 0 and B_{20} cps. This technique was not used in the deuterium line experiment because it was feared that the ripples in the crystal filter bandpass might cause a false deuterium line result. Of course, a correction is made for the receiver response (by division by $p'_0(f)$, see Section 4.2-1) but some error may result in this correction. This is another reason why it is desirable to have a uniform passband.

In the deuterium line receiver, a phase-shift technique used in single-sideband receivers¹⁸ was applied to give a $G(f+f_0)$ with a sharp cutoff and a uniform passband. By conventional means, a wide-band portion of the input spectrum is converted to a center frequency

of 10,700 kc. This signal is then heterodyned with a 10,681 kc local oscillator and passed through a low-pass filter having $B_{20} = 37.5$ kc. The output of the low-pass filter contains the desired spectrum (which was between 10,681 kc and 10,718.5 kc) but also contains the image spectrum (which was between 10,643.5 kc and 10,681 kc). A method utilizing 90° phase-shift networks (see Figure 5.1) is utilized to cancel this image.

The advantage of the phase-shift method is that the bandpass is primarily determined by a stable low-pass filter which is more easily realized (requiring lower Q elements, less affected by variations in the elements, little or no adjustments necessary) than a bandpass filter. The disadvantage is that it is difficult to obtain constant phase-shift over a wide range of frequencies; a phase-shift error results in incomplete cancellation of the image. In the deuterium line receiver phase-shift networks giving 25 db image rejection for frequencies between 3.75 kc and 37.5 kc were designed according to information given by Luck.¹⁹ The band of frequencies below 3.75 kc was eliminated with a high-pass filter. The final result was a usable, uniform pass-band between 5 kc and 30 kc.

A third method of performing the filtering and frequency conversion is to utilize L-C bandpass filters with multiple-stage frequency conversion to reduce Q problems and image-rejection problems. (It is difficult to realize bandpass filters having good skirt selectivity

unless the center frequency to bandwidth ratio is not too large, say less than 15. Furthermore, if this ratio is large, the shape of the response is very critical to small changes in the L and C values.) For example, suppose it was desired to select a 30 kc band out of a 2 mc wide I.F. bandpass centered at 30 mc. A reasonable conversion process would be to place a second I.F., 200 kc wide, centered at 2000 kc and a third I.F., 30 kc wide, centered at 200 kc. A fourth mixer would then shift this band down to between 0 and 30 kc. The obvious disadvantage of this method is the complexity.

5.2 CLIPPERS AND SAMPLERS

It is quite easy to describe the ideal clipper and ideal sampler: The clipper output, $y(t)$, equals 1 when the input, $x(t)$, is greater than 0 and $y(t) = -1$ when $x(t) < 0$. The sampler output, $y(k\Delta t)$, is the instantaneous value of $y(t)$ at $t = k\Delta t$. [The clipper output is not actually 1 or -1, but is either of two voltage levels which are interpreted to mean 1 and -1 by the sampler and digital correlator.]

Real clippers and samplers can come close to this ideal behavior. However, they are very difficult to describe and analyze and, most important, it is difficult to calculate the error in the spectral measurement that is caused by non-ideal sampling and clipping. The areas where this non-ideal behavior exists and the approaches used in the deuterium line receiver are as follows:

1) Real clippers are more accurately characterized by an output, $y(t)$, which is equal to +1 when $x(t)$ is greater than a small voltage, ϵ_+ , and $y(t) = -1$ when $x(t)$ is smaller than ϵ_- . When $x(t)$ is between ϵ_- and ϵ_+ , the output may be +1 or -1 or some value in between. Furthermore, ϵ_- and ϵ_+ may depend on the past history of $x(t)$ and may themselves be functions of time (as caused by noise fluctuations, 60 cps hum, or slow drifts due to temperature changes).

Fortunately, the effect of non-zero clipping levels can be reduced to any degree by simply increasing the amplitude of the signal before clipping. The clippers used in the deuterium line receiver (see Figure 5.2) had values of ϵ_+ and ϵ_- of less than 20 mv. A signal level 40 db above this (2 volts RMS) was used with satisfactory results.

2) The ideal clipper response is independent of the frequency of the input signal. The real clipper is affected at high frequencies by stray capacities and at low frequencies by coupling capacitors (if successive stages are AC coupled). In the deuterium line receiver, the time constants were arranged so each stage had half-power points of 50 cps and 2 mc while the spectrum under analysis extended from 5 kc to 30 kc.

3) In the deuterium line experiment, sampling was accomplished by the arrangement shown in Figure 5.3. The flip-flop is

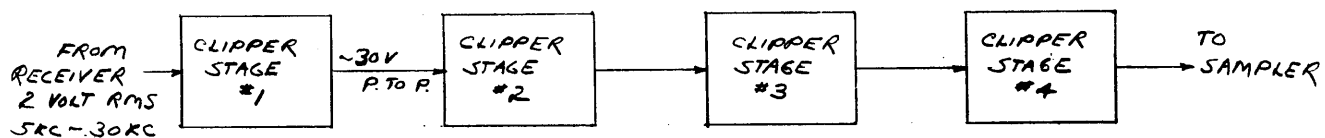
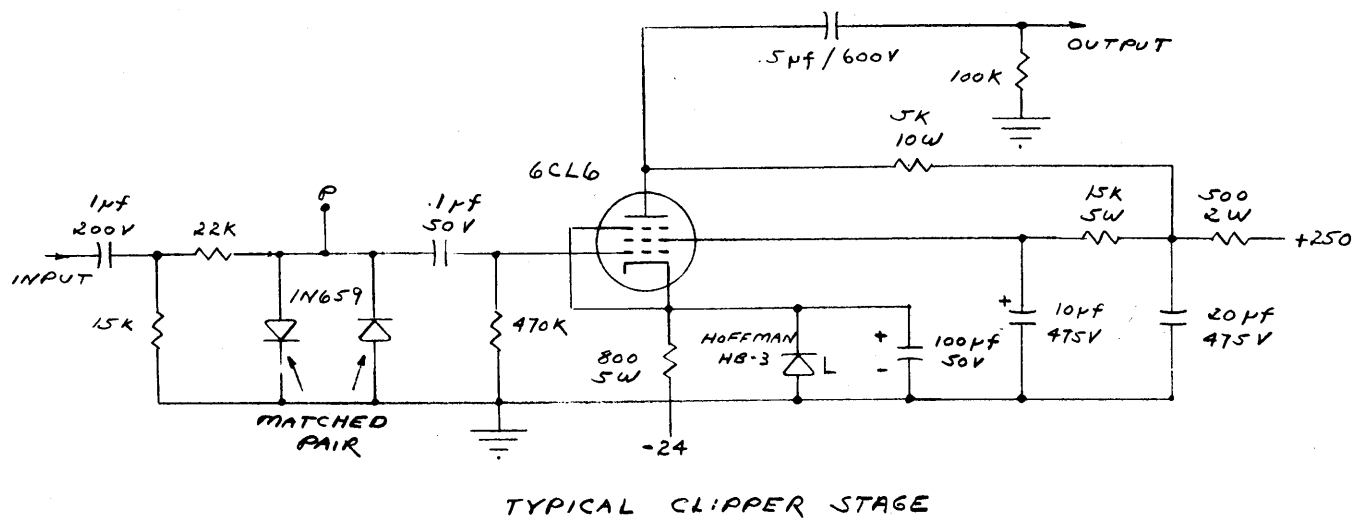


FIG. 5.2 - Clipping circuitry used in the deuterium-line receiver. The 1N659 silicon diodes conduct heavily when their forward bias voltage exceeds .5 volt; thus the voltage at point P is approximately a 1 volt peak to peak square wave. The gain of the amplifier stage is approximately 30.

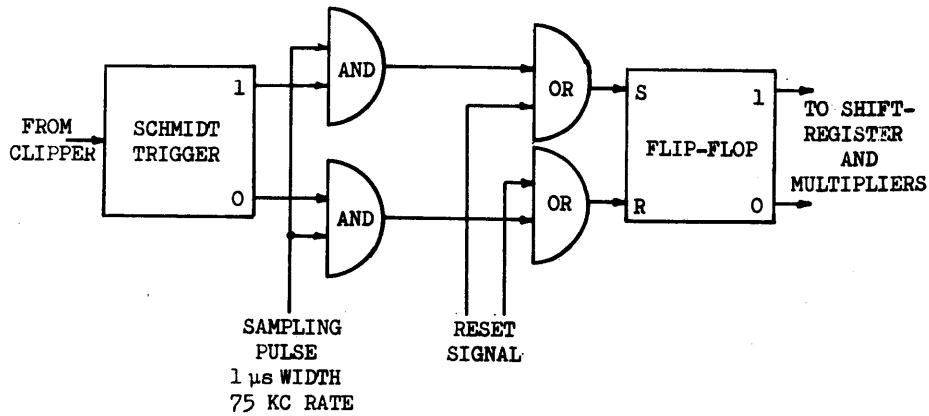


FIG. 5.3 - Sampling configuration used in the deuterium-line receiver.

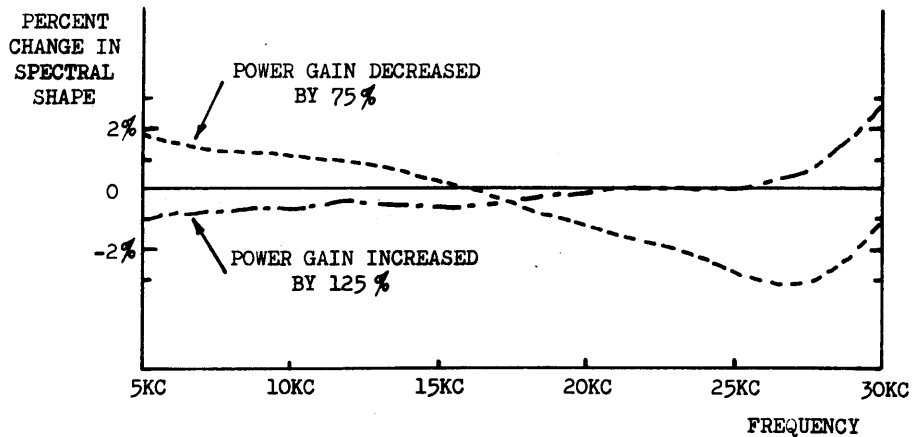


FIG. 5.4 - The effect of large gain changes upon a spectral measurement performed with the one-bit autocorrelation system is shown; the effect is due to non-ideal clipper operation. These measurements were repeated with the gain varied by a different means and identical results were obtained. In actual operation these large gain changes would not occur and the switched mode of operation greatly reduces the effect of the small gain changes which do occur.

set [$y(k\Delta t) = 1$] or reset [$y(k\Delta t) = -1$] according to whether the input signal was 1 or -1 during the duration, t_s , of the sampling pulse. If the signal is making a transition during t_s , the flip-flop will be set, reset, or will stay in its previous state according to the result of a weighted average of the signal during t_s . The flip-flop is randomly set or reset between samples so that the error is random if the flip-flop refers to its previous state. This precaution was taken (it is not known if it is necessary) in order to prevent a false high correlation between successive samples; this would lead to false features in the spectrum (again, the switching technique would cancel most of these errors, anyway).

The duration, t_s , of the sampling pulse was $1 \mu s$ which is $1/30$ of the period of the highest frequency component of the signal. This gave satisfactory performance. In the case of many-bit or unquantized samples, it is possible to show that if the sampling pulse has shape, $p(t)$, the effect is to multiply the spectrum by the square of the magnitude of the Fourier transform of $p(t)$. Thus, if $1/t_s$ is much larger than the highest component in the power spectrum, little change occurs.

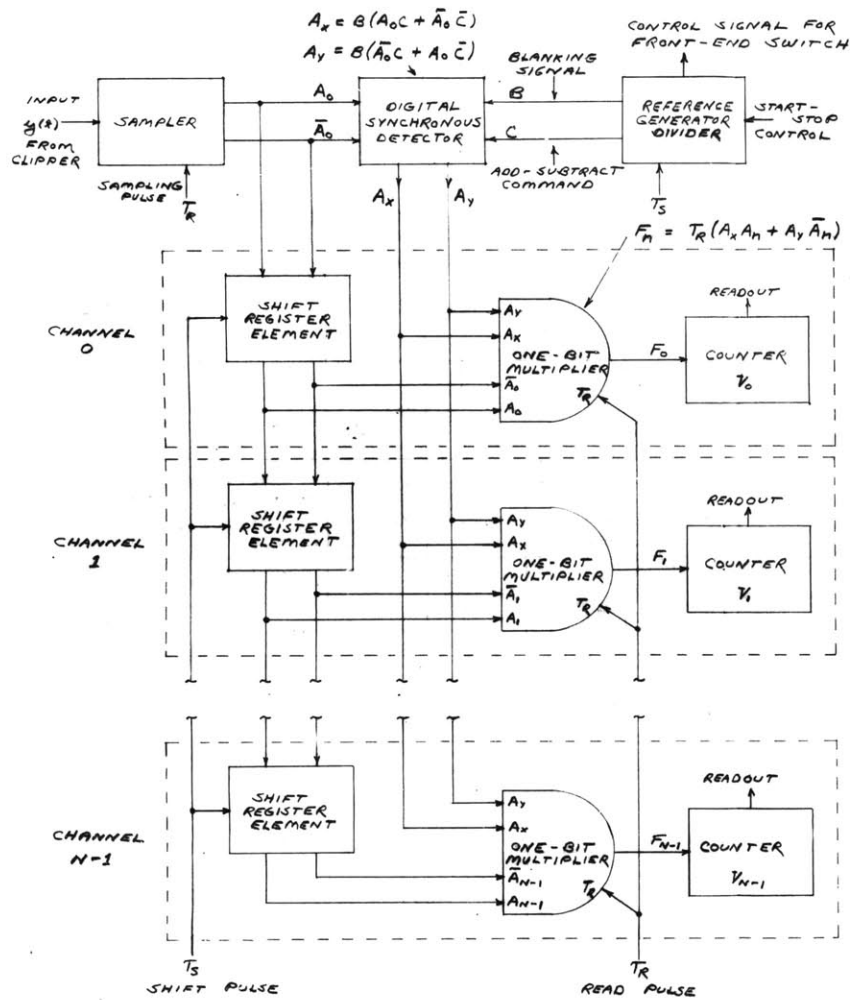
The experimental results of the next chapter indicate satisfactory performance of the clippers and samplers used in the deuterium-line receiver. Of particular importance towards evaluating the samplers and clippers was the comparison of a spectrum measured by the

system (not using switched operation) with that measured by another means (see Section 6.3). The agreement was within 1.5% and the error is most likely due to the error of the "other" measurement method.

The results of another test which is useful for evaluating the clipping circuitry in the deuterium line receiver are presented in Figure 5.4. A spectrum is measured (not using switched operation) and then, the signal level is changed by large amounts. If the clipper was ideal, no change would occur in the measured spectrum. The results indicate that gain changes of the order of 100% cause a few percent change in the measured spectrum. The spectral error probably decreases more than linear with the gain change; in other words, a 1% gain change would cause less than a few hundredths of a percent change in the measured spectrum. Of course, in actual operation the switching technique cancels most of this error.

5.3 DIGITAL CORRELATOR

The basic block diagram of a one-bit digital correlator is presented in Figure 5.5. The function of each block should be understood from its title, the logical equations on the diagram, and the definition of symbols given to the right of the diagram. Although the individual blocks can be realized in many ways, only two major variations of the block diagram come to mind. These are:



A_n represents the input sample which occurred n units back in time. $A_n = 1$ if this sample was 1 and $A_n = 0$ if this sample was -1. A_n is stored in the n 'th shift-register element. A_0 is the value of the current sample.

\bar{A}_n is the complement of A_n .

B equals 0 when blanking is applied or the correlator is stopped, $B = 1$ otherwise.

C equals 1 when the front-end switch is in the antenna position. $C = 0$ when the front-end switch is in the comparison position.

A_x , A_y are the variables which multiply each A_n (see definition of F_n). When $B = 1$ and $C = 1$, $A_x = A_0$ and $A_y = A_0$; when $B = 1$ and $C = 0$, $A_x = \bar{A}_0$ and $A_y = A_0$; and when $B = 0$, $A_x = 0$ and $A_y = 0$. In Boolean equations:

$$A_x = B(A_0C + \bar{A}_0\bar{C})$$

$$A_y = B(\bar{A}_0C + A_0\bar{C})$$

T_R is a timing pulse. $T_R = 1$ when it is time to interrogate the one-bit multipliers $T_R = 0$, otherwise. T_R occurs periodically at a rate, f_n . It is also used to sample the signal.

T_S is another timing pulse. $T_S = 1$ when it is time to shift the shift register; $T_S = 0$, otherwise. T_S is shifted by $1/2$ clock period from T_R . All changes in B and C should occur during the time T_S occurs.

F_n is the output pulse of the n 'th one-bit multiplier. If $B = 0$, then $F_n = 0$ (no pulse occurs); if $B = 1$ and $C = 1$, then $F_n = 1$ if A_n and A_0 are alike; and if $B = 1$ and $C = 0$, then $F_n = 1$ if A_n and A_0 are not alike. If the pulse occurs ($F_n = 1$), it occurs at the same time as T_R . Expressed in a Boolean equation:

$$F_n = T_R(A_x A_n + A_y \bar{A}_n)$$

v_n is the contents of the n 'th counter which counts the number of F_n pulses.

FIG. 5.5 - Basic block diagram of a one-bit digital correlator.

1) The set of N counters, each having a capacity of M bits (usually, $M > 20$), may be replaced by an $N \cdot M$ bit memory (ferrite core, delay line, or other) and a high-speed serial adder. The sums, v_n , of the F_n pulses would be stored in memory and would be periodically brought out to be increased by the new F_n pulse. The $N \cdot M$ bit memory will be cheaper and have less components than the $N \cdot M$ flip-flops required by the counters; however, speed will be a problem. A combination of counters and memory may be optimum. If a computer is available, it may provide the memory and the adder. A straight counter system was used in the deuterium line correlator.

2) The sum of K simultaneously-computed autocorrelation functions can be calculated by providing K sets of all elements in the block diagram except the counters, where only one set, capable of counting K times faster, is needed. The outputs of K one-bit multipliers are OR'ed (with proper timing) into a common counter. Since the cost of counters is an appreciable portion of the total cost, the cost of the correlator is not proportional to K . One cost study has indicated that the cost increases by 1.25 for $K = 2$ and 1.75 for $K = 4$. This technique is useful if one wishes to gain factors of 2 or 4 in effective observation time by simultaneously observing the orthogonal component of polarization and/or using an additional receiver switched

180° out of phase with the first. Both of these steps were taken in the deuterium line attempt so that $K = 4$ for the deuterium line correlator.

The correlator, as it is shown in the block diagram, is connected for the switched mode of operation. The difference autocorrelation function, $\delta \rho'_y(n\Delta\tau)$, is computed and after proper correction (Equation 4.19) and Fourier transformation (Equation 3.29), the difference, $\delta p'(f)$, between the signal spectrum, $p'(f)$, and comparison spectrum, $p'_c(f)$, is computed. These spectra [and also $p'_o(f)$] may be individually measured by locking the control signal, C , at 1 and locking the front-end switch in the antenna position or comparison position. The correlator is stopped (that is, counting stops; the counters may be read out and cleared) by locking the blanking control signal, B , at 0.

An interesting test of the correlator is provided by locking the front-end switch in one position or the other and operating the correlator in switched mode so that products are added ($C = 1$) during half the switching cycle and subtracted ($C = 0$) during the other half cycle. The resulting autocorrelation function and power spectrum should be zero within a few RMS deviations. A more sensitive and easily interpreted test is provided by feeding a periodic square wave (derived from the reference-generator divider) into the sampler input and locking C at 1. The resulting autocorrelation function

should be an exactly known triangular function. A single error in millions of operations can be detected in this way. A constant can also be fed into the sampler input; the resulting autocorrelation function should be exactly constant. Controls for inserting these test signals, along with controls for B, C, and the front-end switch, should be provided on the correlator front panel.

The contents of the N counters, v_n , $n = 0$ to $N - 1$, must be either visually or electronically read out, recorded, and prepared for entry into a computer. In the deuterium line experiment the counter contents were visually indicated, written down, and then manually punched on cards. Automatic readout and recording on a medium suitable for computer entry is obviously desirable. The counters' contents are not directly equal to values of points on the autocorrelation function, as this would require more costly add-subtract type counters. The autocorrelation function is given in terms of the counters' contents by

$$\delta \rho'_y(n\Delta\tau) = \frac{2v_n - 2v_0}{v_0} \quad n = 0, N-1 \quad (5.3)$$

for the switched mode of operation and,

$$\rho'_y(n\Delta\tau) = \frac{2v_n - v_0}{v_0} \quad n = 0, N-1 \quad (5.4)$$

for the unswitched ($C = 1$) mode of operation.

There are four major parameters which specify the capability of a one-bit digital correlator. The first and most obvious is N , the number of channels or points on the autocorrelation function. This determines the ratio of the bandwidth analyzed, B_1 , to the frequency resolution, Δf . The value of this ratio depends on the choice of the weighting function, $w(\tau)$, and the shape of the receiver bandpass, $G(f+f_0)$. In the practical case, $B_1/\Delta f$ will be between $N/1.5$ and $N/3$. The second parameter, K , the number of signals autocorrelated at one time, was discussed at the beginning of this section.

A third major parameter is the maximum sampling frequency, $(f_s)_{\max}$, which is limited by the repetition rate of the digital logic elements. The value of $(f_s)_{\max}$ determines the maximum bandwidth that can be analyzed, $(B_1)_{\max} \sim 0.4(f_s)_{\max}$. For present transistor logic circuits, the cost of the correlator will increase by about a factor of two if $(f_s)_{\max}$ is increased from 500 kc to 10 mc. Above 10 mc the price will rapidly increase, although future developments may change this picture.

The final parameter is M , the bit capacity of the counters. This determines the maximum time, T_{\max} , which may elapse before the counter is full and readout must occur. The maximum number of counts a counter may receive is one for each sample, thus T_{\max} is specified by $f_s T_{\max} = 2^M - 1$.

All M bits in the counters need not be read out as some bits at the input end will be insignificant and L bits at the slow end will always be zero if $f_s T < 2^{M-L}$. The number of insignificant bits is also a function of $f_s T$. The RMS deviation of v_n ($n \neq 0$) is approximately $\sqrt{f_s T}$ for either the switched or unswitched mode of operation. (This follows from application of Equation 3.27 which gives the RMS deviation of an autocorrelation function estimate.) Thus, a round-off error that is much less than $\sqrt{f_s T}$ can be neglected. If $f_s T = 2^{M_0}$, then it is safe to discard the $M_0/2 - 3$ most insignificant bits. Since $f_s T$ will rarely be less than $10^6 \sim 2^{20}$ in radio astronomy applications, the 7 bits at the high-speed end of the counter need not be read out.

The digital correlator that was used for the deuterium-line and Zeeman experiments is pictured in Figure 5.6. This machine has 21 channels, can simultaneously autocorrelate 4 signals, has a maximum sampling rate of 300 kc, and contains counters with a capacity of 36 bits. The slowest 20 bits of each counter are provided inexpensively by a 6 digit electromechanical counter with visual readout; the remaining 16 bits are transistorized counters with neon-bulb indicators. With the exception of the counters, the machine was built by Control Equipment Corporation at a cost of \$14,000. The counters were designed by the author and constructed by an outside vendor for an additional \$5,000. The machine uses 2100 transistors

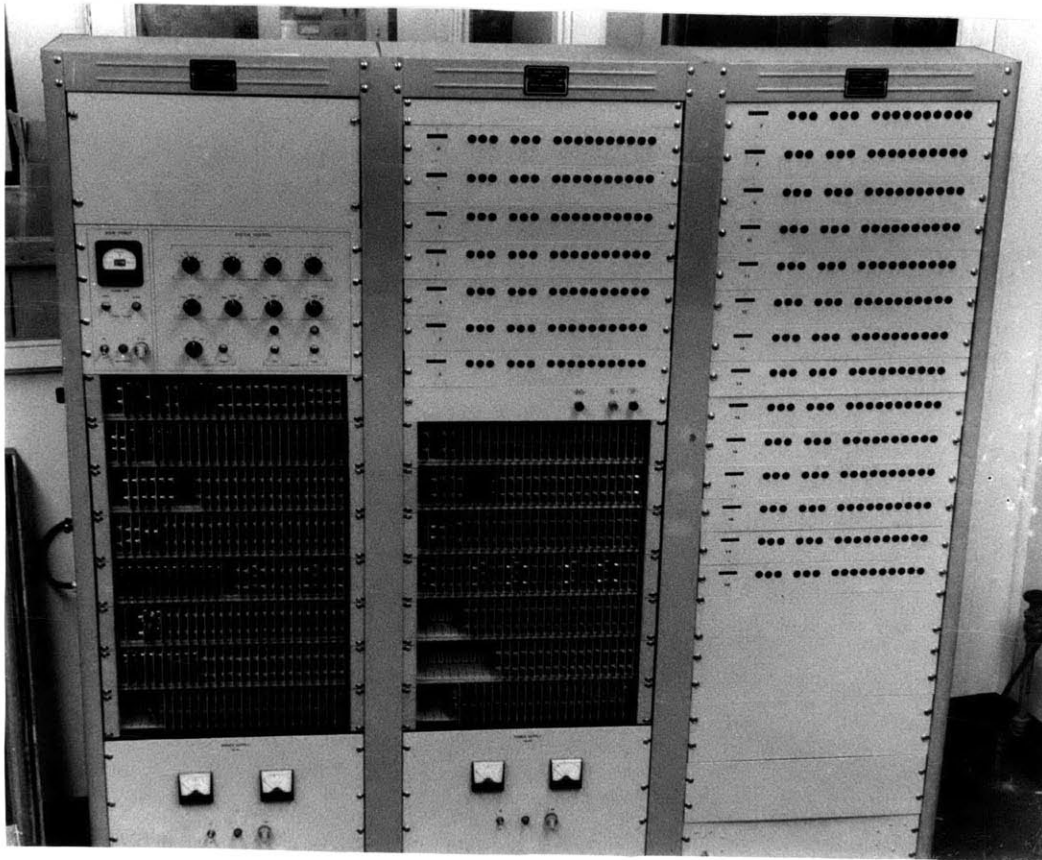


FIG. 5.6 - The one-bit digital correlator used for the deuterium-line and Zeeman experiments is shown at left while the receiver console is shown at right. The left and lower-middle bays of the correlator cabinet contain printed circuit cards which comprise four 21-bit shift registers and 84 1-bit multipliers. The right and upper-middle bays contain 21 sets of 16-bit binary counters with neon bulb readout plus 6-digit electromechanical counters. The receiver console contains, from top to bottom, the clippers, a noise-generator control unit, 2 receivers, local oscillators, a second noise-generator control unit, 2 more receivers, and power supplies. The receiver front-ends were in a box mounted on the radio-telescope.

and has operated for its first 4500 hours without failure except for some minor difficulties with the electromechanical counters.

A schematic diagram of shift-register and one-bit multiplier circuitry designed for a high-speed correlator channel is given in Figure 5.7. This circuitry was developed by Control Equipment Corporation for the National Radio Astronomy Observatory. The design parameters of this machine are: $N = 100$ channels, $K = 2$ receivers, $(f_s)_{\max} = 10$ mc, and a counter capacity, M , of 30 bits. Electronic readout (to a computer or paper tape punch) is provided on the slowest 24 bits of the counter. An expected cost of this machine is \$400 to \$700 per channel.

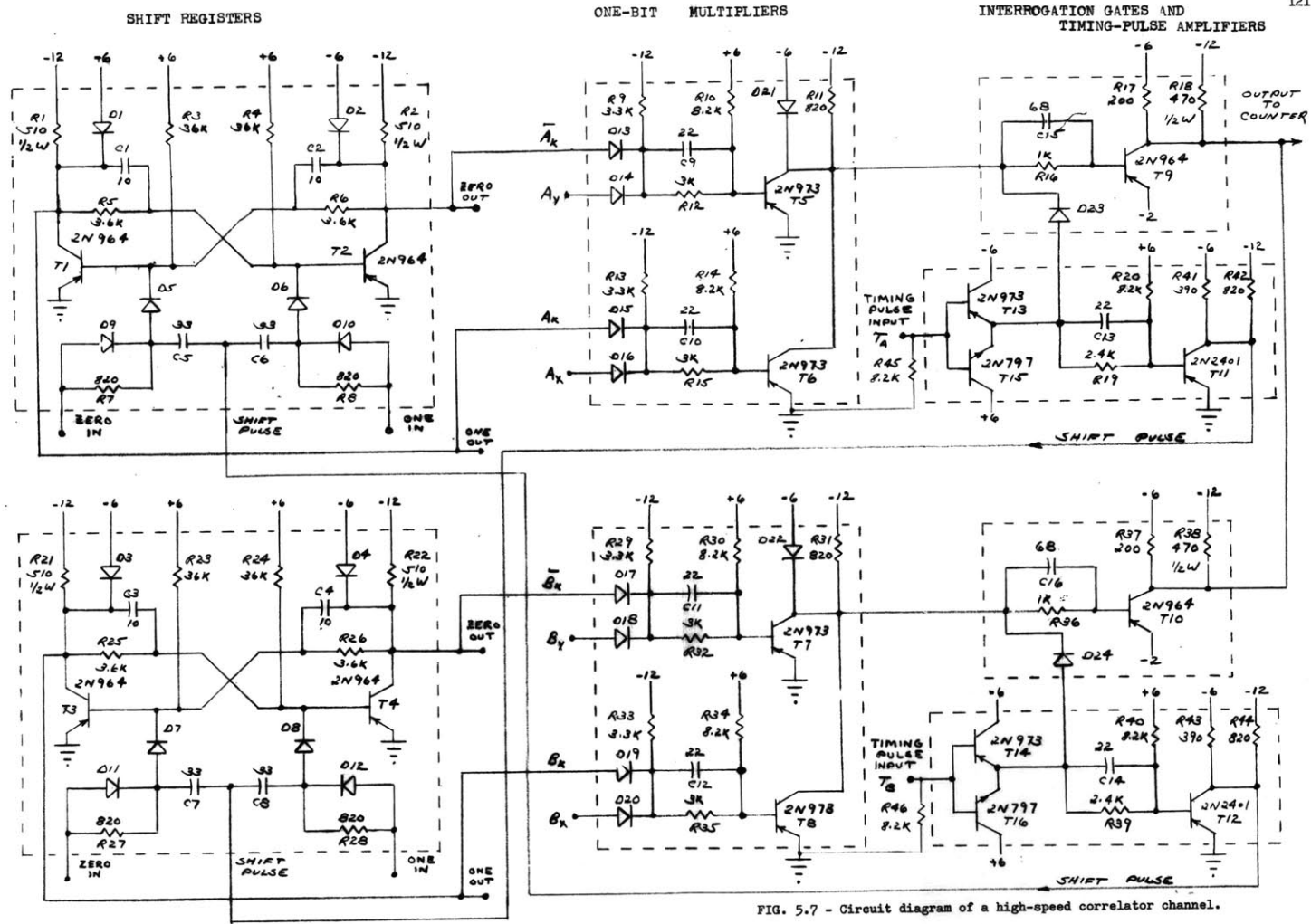


FIG. 5.7 - Circuit diagram of a high-speed correlator channel.

CHAPTER 6

SYSTEM TESTS

6.1 INTRODUCTION - SUMMARY

A series of experiments, designed to test various aspects of the digital autocorrelation spectral analysis system, are described in this chapter. These tests and their objectives are as follows:

1) Computer Simulation of the Signal and the Signal Processing System

Samples of a time function having Gaussian statistics and known power spectrum are generated in a computer. This time series is analyzed in the computer through the use of both many-bit and one-bit autocorrelation processing. One-hundred such time series (1050 samples each) were analyzed in order to give statistical information concerning the mean and variance of both one-bit and many-bit estimates of the autocorrelation function and power spectrum. The main objective was to find the variance of the one-bit power spectrum estimate; this is difficult to calculate theoretically and is needed to specify the sensitivity of the radio-astronomy system utilizing the one-bit autocorrelation function method.

2) Measurement of a Known Noise Power Spectrum

A noise power spectrum which is "known" to within 1% is produced by passing white noise through a filter whose power transfer function is measured by conventional sinusoidal techniques.

This signal is in the video frequency range and is analyzed using the same clippers, one-bit correlator, and computer program used in the deuterium line attempt. This was the first measurement performed with the system and served mainly as an equipment check.

3) Measurements of Artificial Deuterium Lines

A small signal having a spectrum similar to the deuterium line (except it is a "bump" instead of the deuterium absorption "dip") was produced and injected into the deuterium line receiver input (at 327 mc). A second large, broadband noise signal, simulating the radio source, Casseopeia, was also injected into the receiver input. A means of calibrating the artificial deuterium line signal in relation to the noise was provided. Artificial lines of various magnitudes were detected, the weakest being 37 db (0.02%) below the noise level.

4) Analysis of the RMS Deviation of the Deuterium Line Data

A major advantage that is expected of the digital autocorrelation system is that the theoretical sensitivity (which increases as the square root of the observation time) is achieved when observations are carried out for long periods of time. This is often not the case with analog equipment because of non-stationarity or drift in the apparatus. The realization of this advantage is

demonstrated by an analysis of the RMS deviation of 68 days of deuterium line data.

Before discussing these tests, it should be mentioned that the digital correlator itself can be checked by the application of a few simple test signals. Two such test signals are a constant, which gives a constant autocorrelation function, and a square wave (derived from the correlator clock circuitry) which gives a triangular autocorrelation function. These tests were built into the digital correlator used for the deuterium experiment and were periodically performed. The only errors which were ever found were missed counts in electromechanical counters used in this machine. The tests are very sensitive; with a 10 second run at 300 kc. sampling rate, a single error in 3×10^6 operations can be detected.

6.2 COMPUTER SIMULATION OF THE SIGNAL AND THE SIGNAL PROCESSING SYSTEM

The procedure and objective of this section was summarized in the introduction of this chapter. Computer-generated estimates of the mean and variance of both one-bit and many-bit estimates of the autocorrelation function and power spectrum will be discussed. (The reader should not be confused by the fact that we are considering statistical estimates of the mean and variance of another statistical estimate.) Many terms must be defined and this will be our first

(3)

task. After this has been done, a large portion of the experimental procedure and results can be understood by referring to Figures 6.1, 6.2, and 6.3. A discussion of the procedure and results will be given in the second and third sections, respectively.

6.2-1 Definitions and Terminology

The notation of this section is the same as that used in Chapters 2 and 3 with one minor exception. The time intervals, Δt and $\Delta \tau$, will be assumed equal and $k\Delta t$ and $n\Delta \tau$ will be replaced by simply k and n . As usual, ρ refers to normalized autocorrelation functions; p refers to normalized power spectra; a single prime, $'$, or a subscript, l , refers to one-bit samples; a double prime, $''$, or a subscript, m , refers to many-bit samples; and a σ with appropriate subscripts refers to RMS deviation of the variable indicated by the subscript.

An example is $\sigma_{pl}(f)$ which is the RMS deviation of the spectral estimate computed from one-bit samples. A statistical estimate of $\sigma_{pl}(f)$ is $\sigma'_p(f)$. In a similar manner, the meaning of $\sigma_{pm}(f)$ and $\sigma''_p(f)$, $\sigma_{\rho l}(n)$ and $\sigma'_\rho(n)$, and $\sigma_{\rho m}(n)$ and $\sigma''_\rho(n)$ should be clear. The many-bit RMS deviations, $\sigma_{\rho m}(n)$ and $\sigma_{pm}(f)$ have been discussed in Chapter 2 and, the one-bit RMS deviations, $\sigma_{\rho l}(n)$ and $\sigma_{pl}(f)$, have been computed in Chapter 3. The statistical estimates of these quantities will be defined later in this section.

The quantity, $x(k)$, will denote a sample of a time function having Gaussian statistics. These samples will be generated in the computer by a method described in the next section. As in earlier work, $y(k)$ is the one-bit sample corresponding to $x(k)$; $y(k) = 1$ when $x(k) > 0$ and $y(k) = -1$ when $x(k) < 0$. The time between samples, $\Delta t = \Delta \tau$, will always be assumed equal to $1/75$ kc so that the time and frequency scale of our computer-generated results will be the same in the deuterium-line results.

Following the procedure used in earlier chapters, the one-bit and many-bit autocorrelation function estimates will be defined as:

$$\rho_i'(n) = \sin \left[\frac{\pi}{2} \cdot \frac{1}{K} \sum_{k=1}^K y(k) y(k + |n|) \right] \quad (6.1)$$

and

$$\rho_i''(n) = \frac{\sum_{k=1}^K x(k) x(k + |n|)}{\sum_{k=1}^K x^2(k)} \quad (6.2)$$

The subscript, i , where i will go from 1 to 100, is used to denote each of 100 independent, but statistically alike, estimates of $\rho(n)$. Each $\rho_i'(n)$ is determined from a different group of $K+n$ randomly generated samples; however, each group is generated under the same conditions. The sample size, K , will be fixed at 1050.

The values of $\rho_1'(n)$ and $\rho_1''(n)$ will be calculated for $n = 0$ to 20 which is analogous to the deuterium-line processing.

The one-bit and many-bit estimates of the power spectrum, $p_1'(f)$ and $p_1''(f)$, respectively, will be computed from $\rho_1'(n)$ and $\rho_1''(n)$ in the same manner as previously used (Equation 2.3).

For example,

$$p_1'(f) = 2 \Delta\tau \sum_{n=-20}^{20} \rho_1'(n) w(n\Delta\tau) e^{-j 2\pi f n \Delta\tau} \quad (6.3)$$

where the cos weighting function will be used in analogy with the deuterium-line data processing. According to the theory presented in Chapters 2 and 3, the mean or expected value of $p_1'(f)$ and $p_1''(f)$ is the smoothed spectrum, $p^*(f)$, which is discussed in Sections 2.4-2 and 2.2,

$$\overline{p_1'(f)} = \overline{p_1''(f)} = p^*(f) \quad (6.4)$$

The arithmetic averages of $\rho_1'(n)$, $\rho_1''(n)$, $p_1'(f)$, and $p_1''(f)$ will be denoted by $\rho_{av}'(n)$, $\rho_{av}''(n)$, $p_{av}'(f)$, and p_{av}'' respectively, where, for example,

$$p_{av}'(f) = \frac{1}{100} \sum_{i=1}^{100} p_i'(f) \quad (6.5)$$

Similarly, estimates of the RMS deviations of $\rho_i'(n)$, $\rho_i''(n)$, $p_i'(f)$, and $p_i''(f)$, will be denoted as $\sigma_\rho'(n)$, $\sigma_\rho''(n)$, $\sigma_p'(f)$, and $\sigma_p''(f)$ respectively, where, for example,

$$\sigma_p'(f) = \sqrt{\frac{1}{100} \sum_{i=1}^{100} [p_i'(f) - p^*(f)]^2} \quad (6.6)$$

It can be shown (see Burington and May,²⁰ p. 149) that if I functions are used to estimate the RMS deviation of a function (as in Equation 6.6 where $I = 100$), then the RMS error of the estimate is $100/\sqrt{2I}$ percent. For example,

$$\frac{\sqrt{[\sigma_p'(f) - \sigma_{p1}(f)]^2}}{\sigma_{p1}(f)} \cong \frac{1}{\sqrt{2I}} \quad (6.7)$$

Since $I = 100$ in our case, the true RMS deviations, $\sigma_{p1}(f)$, $\sigma_{pm}(f)$, $\sigma_{\rho1}(n)$ and $\sigma_{\rho m}(n)$, are estimated by $\sigma_p'(f)$, $\sigma_p''(f)$, $\sigma_\rho'(n)$, and $\sigma_\rho''(n)$, respectively, with an RMS error of approximately 7%.

6.2-2 Computer Method

A block diagram of the computer program used to generate the one-bit and many-bit estimates of the autocorrelation function and power spectrum is shown in Figure 6.1. This program was run 100 times with a different (but statistically alike) sequence of random numbers each time. The results which will be presented are

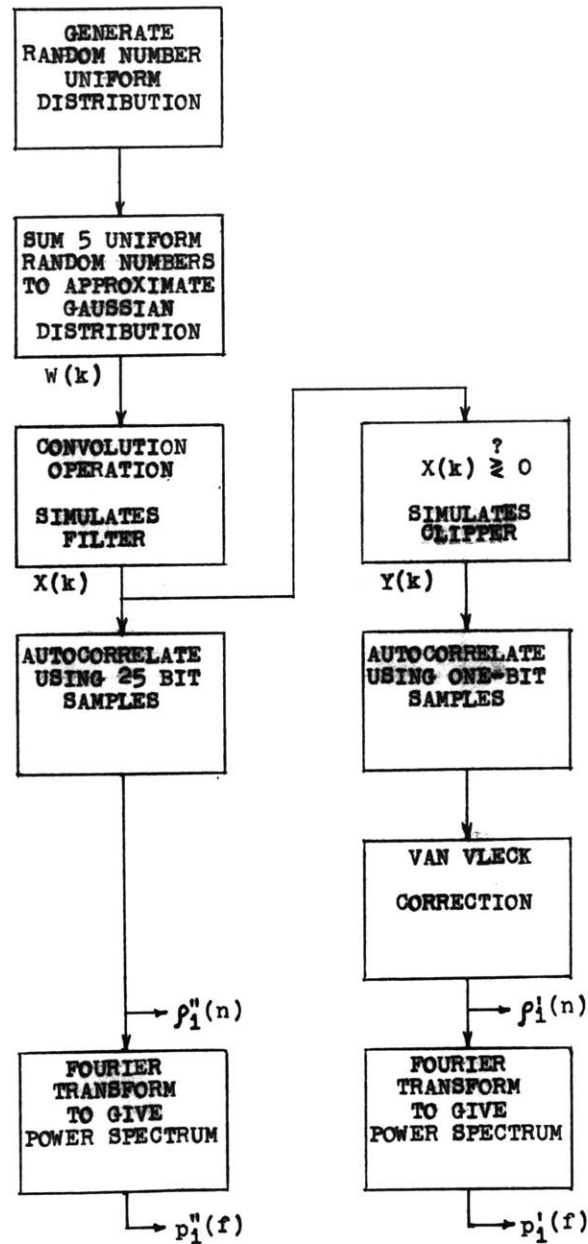


FIG. 6.1 - Block diagram of the computer program used to simulate the signal and the signal processing system.

the arithmetic averages and RMS deviation estimates defined in the previous section.

A complete listing of the computer program is given in Appendix D and should be referred to for details. The main steps in the program should be fairly obvious from Figure 6.1 and the previous definitions. However, the generation of the Gaussian time series, $x(k)$, with known spectrum will be briefly discussed in this section. The generation of this time series occurs in the following three steps:

- 1) Random numbers with uniform probability density are generated by taking the last 4 digits of a non-convergent, iterative, arithmetic operation (see program, statements 67 to 73).
- 2) A sum of 5 uniform random numbers is used to form a new random number which has an approximate Gaussian probability density function (see Davenport and Root,¹ pp. 81-84, The Central Limit Theorem). The probability density function of this sum consists of the uniform density function convolved with itself 5 times; this will closely approximate a Gaussian distribution.
- 3) The Gaussian distributed random numbers are statistically independent and thus, they have the character of samples of Gaussian noise with uniform spectrum (white noise). These samples must then be passed through a sampled-data filter to give the desired

spectrum. This is accomplished by convolving the white-noise samples with a filter impulse response. The output samples, $x(k)$, are then Gaussian with a spectrum equal to the square of the magnitude of the Fourier transform of the impulse response.

6.2-3 Results and Conclusions

All of the results of the computer simulation experiment are given in Tables 6.1 and 6.2; the more important results are also plotted in Figures 6.2 and 6.3.

The arithmetic averages, $\rho_{av}''(n)$, $\rho_{av}'(n)$, $p_{av}''(f)$, and $p_{av}'(f)$, should be within a few times $\sigma/\sqrt{100}$ of the true mean, where the respective σ of a single estimate is used. The $\sqrt{100}$ term arises because the arithmetic averages are taken over 100 independent estimates. The agreement of the averages of the estimates with the true mean is quite as expected and is not too illuminating since the theoretical work for this result is quite clear.

Our major interest is in the estimates of the RMS deviations, $\sigma_{\rho}''(n)$, $\sigma_{\rho}'(n)$, $\sigma_p''(f)$, and $\sigma_p'(f)$. It should be kept in mind that these quantities are statistical estimates of the true values, $\sigma_{\rho m}(n)$, $\sigma_{\rho 1}(n)$, $\sigma_{p m}(f)$, and $\sigma_{p 1}(f)$, and will have an RMS error of $1/\sqrt{200} \sim 7\%$ of the true value as is indicated by Equation 6.7.

The many-bit and one-bit RMS deviations, $\sigma_{\rho}''(n)$ and $\sigma_{\rho}'(n)$, respectively will be discussed first. Examination of $\sigma_{\rho}''(n)$ in

TABLE 6.1

RESULTS OF COMPUTER SIMULATION EXPERIMENT
AUTOCORRELATION FUNCTIONS

n	$\rho(n)$ x 10,000 True Function	$\rho''_{av}(n)$ x 10,000 Many-Bit Estimate	$\rho'_{av}(n)$ x 10,000 One-Bit Estimate	$\sigma''_{\rho}(n)$ x 10,000 Many-Bit RMS Dev.	$\sigma'_{\rho}(n)$ x 10,000 One-Bit RMS Dev.
0	10000.0	10000.0	10000.0	0.0	0.0
1	-0.3	24.7	43.6	269.8	393.5
2	-3094.2	-3177.1	-3185.3	273.5	389.7
3	-0.4	-9.2	-42.0	338.1	466.9
4	-1801.3	-1702.9	-1766.4	375.8	467.2
5	-0.7	-21.8	44.2	322.3	460.0
6	-501.7	-476.9	-462.3	349.9	502.9
7	-3.0	19.3	41.1	319.2	513.8
8	210.7	194.5	228.1	346.8	486.1
9	-5.8	-9.0	-28.7	350.4	517.8
10	242.8	233.9	285.4	345.8	531.3
11	16.4	-21.0	-36.7	317.7	498.5
12	29.2	31.5	-31.0	343.4	575.0
13	3.9	48.9	107.4	340.0	552.1
14	-74.5	-85.9	-42.4	314.1	493.8
15	-3.3	-40.5	-31.9	357.3	500.1
16	-50.7	-75.5	-92.8	383.8	533.3
17	-10.4	-16.6	-1.2	331.9	486.3
18	7.4	38.0	20.3	326.5	475.8
19	-8.8	26.8	34.3	324.6	462.7
20	9.1	-32.4	-55.0	372.3	570.7

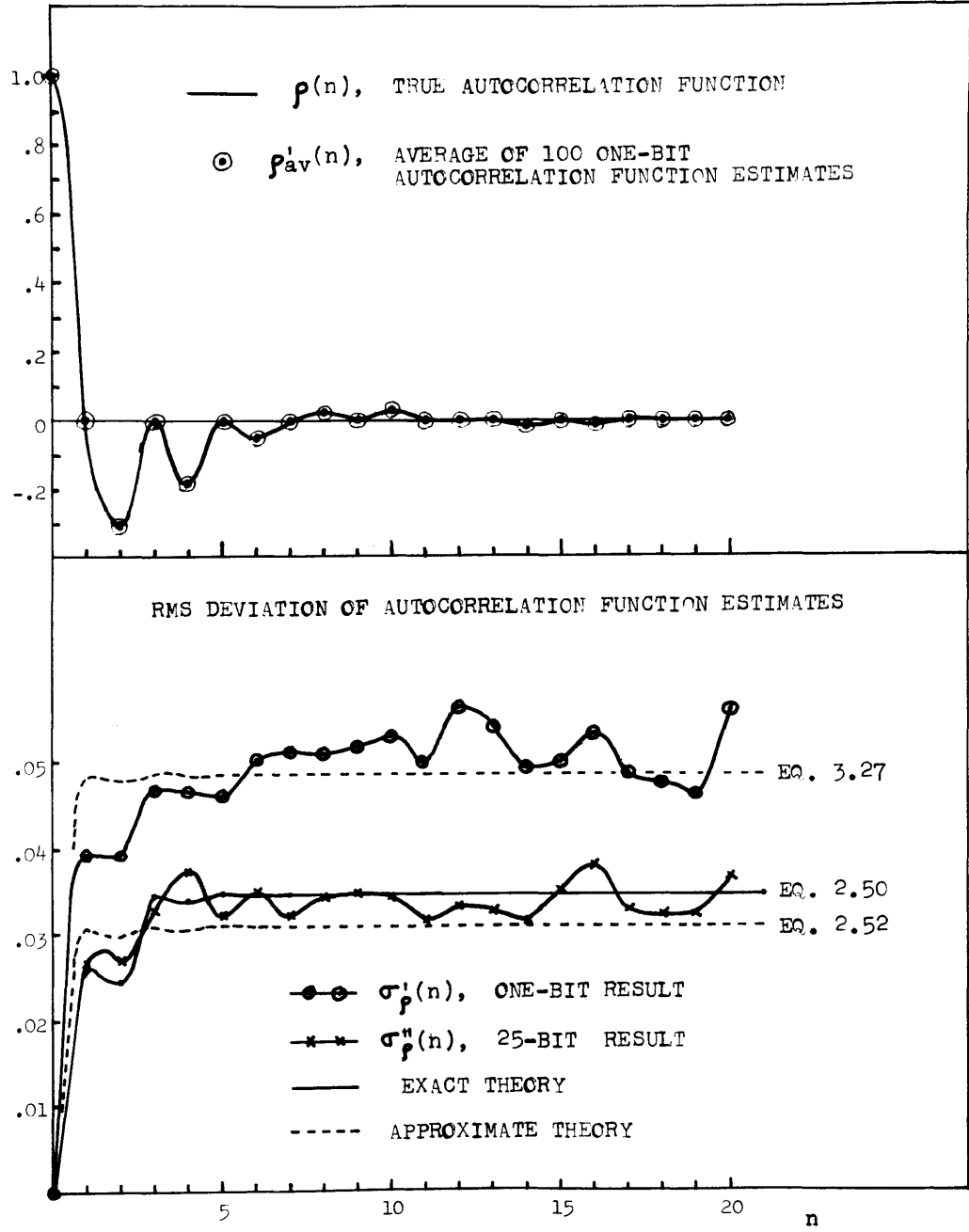


FIG. 6.2 - Results of computer simulated autocorrelation function measurements.

TABLE 6.2
RESULTS OF COMPUTER SIMULATION EXPERIMENT
POWER SPECTRA

f kc	$p^*(f)$ x 5000 True Mean	$p_{av}''(f)$ x 5000 Many-Bit Estimate	$p_{av}'(f)$ x 5000 One-Bit Estimate	$\frac{\sigma_p''(f)}{p^*(f)}$ Many-Bit RMS Dev.	$\frac{\sigma_p'(f)}{p^*(f)}$ One-Bit RMS Dev.
0	4.9	5.2	6.4	0.237	2.882
1	8.1	8.5	9.2	0.181	1.547
2	17.7	18.3	17.9	0.145	0.625
3	34.1	34.4	33.0	0.128	0.375
4	57.5	57.0	55.3	0.122	0.258
5	86.8	85.4	83.9	0.118	0.187
6	118.4	116.3	115.1	0.122	0.166
7	146.8	144.3	143.7	0.126	0.166
8	167.1	164.7	165.1	0.115	0.157
9	178.1	176.1	178.1	0.099	0.144
10	182.1	181.2	184.5	0.096	0.144
11	182.5	183.1	186.6	0.110	0.160
12	182.1	183.6	186.3	0.119	0.167
13	181.8	183.2	185.0	0.109	0.151
14	181.7	182.7	184.5	0.098	0.136
15	181.7	183.2	185.3	0.103	0.139
16	181.7	184.6	186.5	0.108	0.145
17	181.7	185.8	186.3	0.112	0.149
18	181.8	186.1	184.5	0.115	0.154
19	182.0	185.7	182.7	0.112	0.156
20	182.2	185.4	182.6	0.105	0.155
21	182.1	185.5	183.9	0.106	0.155
22	181.8	185.5	184.8	0.116	0.155
23	181.4	184.9	183.7	0.127	0.157
24	181.3	183.4	181.1	0.127	0.163
25	181.6	181.6	178.8	0.116	0.162
26	182.3	180.3	178.6	0.105	0.151
27	183.0	179.5	180.2	0.104	0.149
28	181.4	177.4	180.2	0.111	0.160
29	174.0	170.1	173.8	0.115	0.161
30	157.9	154.1	157.2	0.117	0.161
31	132.8	129.4	130.8	0.123	0.177
32	102.2	99.5	99.2	0.126	0.199
33	71.6	69.6	68.3	0.126	0.236
34	45.2	44.1	42.6	0.131	0.314
35	25.3	24.9	23.3	0.145	0.470
36	12.2	12.2	10.4	0.160	0.941
37	5.7	5.8	3.7	0.190	2.323

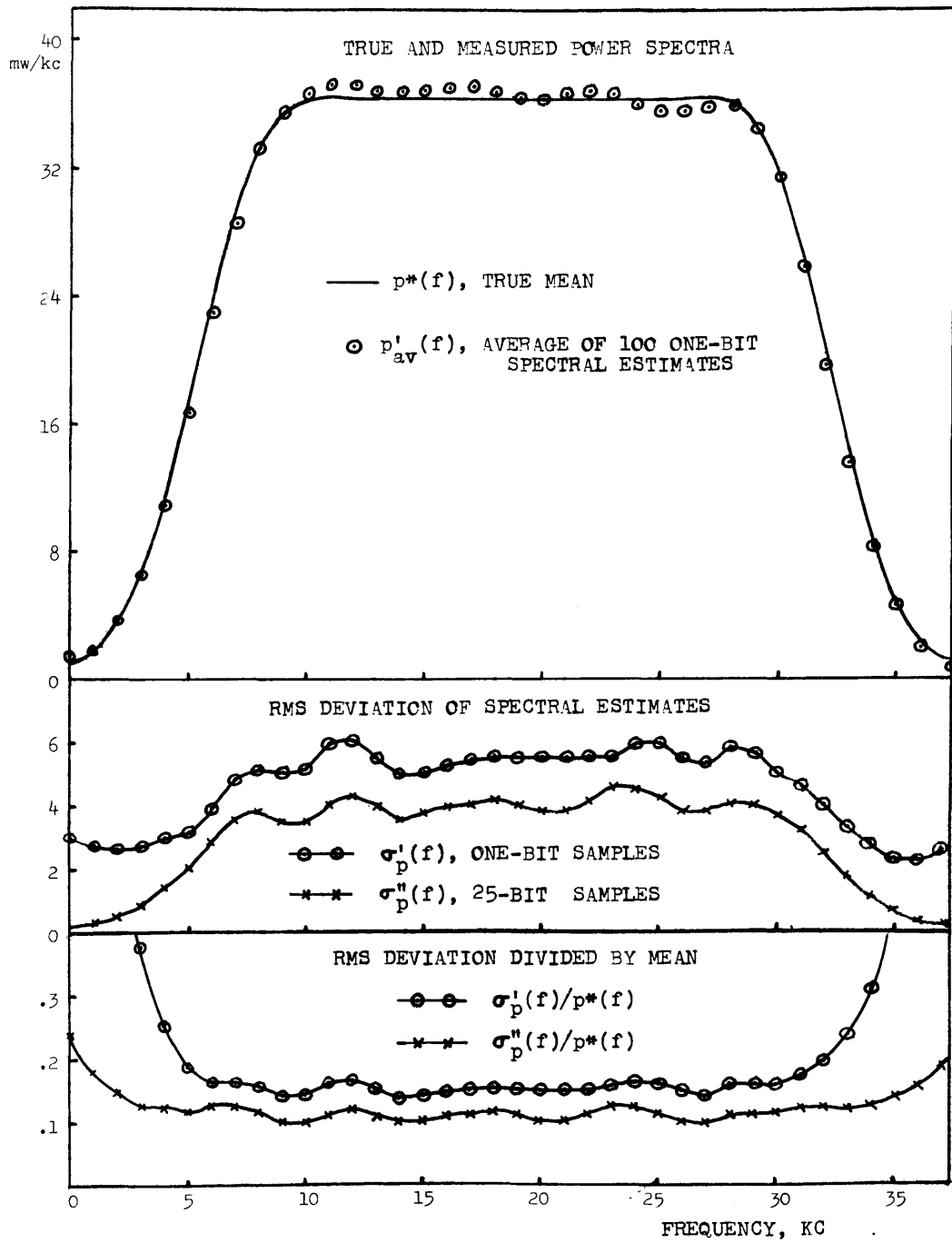


FIG. 6.3 - Results of computer simulated spectral measurements.

Figure 6.2 indicates that it is in good agreement with the "exact" theory (the approximations are well justified) given by Equation 2.50. Equation 2.52, which assumes linearly independent products of many-bit samples, gives a value for $\sigma_{\rho m}(n)$ which is somewhat low. Similarly, Equation 3.27, which assumes statistically independent products of one-bit samples, gives a $\sigma_{\rho 1}(n)$ which is somewhat lower than $\sigma_{\rho}'(n)$.

A closer and more compact comparison of the autocorrelation RMS deviations can be obtained by averaging along n , for example,

$$\sigma_{\rho}' = \frac{1}{18} \sum_{n=3}^{20} \sigma_{\rho}'(n) \quad (6.8)$$

Since σ_{ρ}' is the average of 18 approximately independent points, its RMS error is reduced by $\sqrt{18}$ to a value of 1.65%. The results concerning autocorrelation function RMS deviations are summarized in the following table.

TABLE 6.3 AUTOCORRELATION FUNCTION RMS DEVIATION
(average value in interval $3 \leq n \leq 20$)

ONE-BIT		MANY-BIT			RATIO
Results of Computer Simulation σ_{ρ}'	Approx. Theory Eq. 3.27 $\sigma_{\rho 1}$	Results of Computer Simulation σ_{ρ}''	Approx. Theory Eq. 2.52 $\sigma_{\rho m}$	Exact Theory Eq. 2.50 $\sigma_{\rho m}$	Increase Due to Clipping $\sigma_{\rho}'/\sigma_{\rho}''$
.0500 $\pm .0008$.0485	.0338 $\pm .0006$.0309	.0346	1.48 $\pm .04$

The results concerning the RMS deviations of the many-bit and one-bit spectral estimates, $\sigma_p''(f)$ and $\sigma_p'(f)$, are indicated in Figure 6.3. These results indicate that $\sigma_p'(f)$ is slightly greater than $\sigma_p''(f)$ in the constant passband region of $p^*(f)$. However, at the edges of the band, where $p^*(f)$ becomes small, $\sigma_p'(f)$ becomes much greater than $\sigma_p''(f)$. In the many-bit case, $\sigma_p''(f)/p^*(f)$, is fairly constant (except for small increases near $f=0$ and $f=f_s/2$) and hence, a measurement of $p^*(f)$ at a frequency where $p^*(f)$ is small is just as accurate as at a frequency where $p^*(f)$ is large. This is not true in the one-bit case; $\sigma_p'(f)/p^*(f)$ becomes large when $p^*(f)$ becomes small. This is the most valuable result of the computer-simulation experiment. Experimental results on actual spectra indicated the same phenomenon; however, it was thought that the increase of $\sigma_{p1}(f)/p^*(f)$ at the edge of the band may have been due to non-ideal operation of the sampler and clipper. In actual radio-astronomy measurements, the observations were confined to the constant passband region, such as between 5 kc and 30 kc in Figure 6.3.

It is convenient to define β as the ratio of the one-bit spectral RMS deviation to the many-bit spectral RMS deviation; β is estimated by $\sigma_p'(f)/\sigma_p''(f)$. Strictly speaking, β is some unknown function of f and depends on $p(f)$ and $W(f)$. However, since the spectra we will measure in most radio-astronomy applications have the same gross

shape as the spectrum of Figure 6.3, the estimate of β given by $\sigma_p'(f)/\sigma_p''(f)$ has more general application.

In the midband region where $p^*(f)$ is constant, β appears to be constant. An accurate value can be obtained by averaging the spectral RMS deviations in the interval, $10 \text{ kc} \leq f \leq 29 \text{ kc}$, i. e.,

$$\sigma_p' = \frac{1}{20} \sum_{f=10}^{29} \sigma_p'(f) \quad (6.9)$$

There are about 10 independent points in this interval, thus the RMS error is reduced by $\sqrt{10}$ to give a value of 2.4%. We then obtain the following table.

TABLE 6.4 SPECTRAL RMS DEVIATION
(average value in interval $10 \text{ kc} \leq f \leq 29 \text{ kc}$)

ONE-BIT	MANY-BIT		RATIO
Results of Computer Simulation	Results of Computer Simulation	Exact Theory Eq. 2.56	Increase Due to Clipping
σ_p'/p^*	σ_p''/p^*	σ_{pm}/p^*	$\beta = \sigma_p'/\sigma_p''$
.1534 $\pm .0036$.1107 $\pm .0025$.1150	1.39 ± 0.04

The most important result in this section is the value, $\beta = 1.39 \pm .04$, which applies in the constant region of a spectrum similar to that of

Figure 6.3. Examination of $\sigma_p'(f)$ and $\sigma_p''(f)$ indicates that the increase in β at the edges of the band follows an empirical law of the form,

$$\beta = 1.39 [p_0^*/p^*(f)]^{1/2} \quad (6.10)$$

where p_0^* is the value of $p^*(f)$ in the constant midband region. This equation holds only for $p_0^*/p^*(f) < 4$; the increase in β is greater for $p_0^*/p^*(f) > 4$. Thus, at 1 db points, $\beta = 1.56$; at 3 db points, $\beta = 1.95$; and at 6 db points, $\beta = 2.78$.

The increase of β for small $p^*(f)$ implies, in the case of radio-astronomy measurements, that the observed frequency band should be in the constant midband region of the receiver power transfer function, $G(f+f_0)$. A correction, is, of course, made for the multiplication of the receiver input spectrum, $T(f+f_0)$, by $G(f+f_0)$ (see Section 4.2-1). However, the uncertainty of the $T(f+f_0)$ measurement will increase at the edges of the band in a manner indicated by the previous paragraph.

The spectral RMS deviation results found in this section will be compared in Section 6.5 with the RMS deviation of the data taken in the deuterium-line experiment; the results are in excellent agreement.

6.3 MEASUREMENT OF A KNOWN NOISE POWER SPECTRUM

6.3-1 Procedure

The goal of this test was to compare, as accurately as possible, a spectral measurement made by the one-bit digital autocorrelation method with a spectral measurement performed by some other method. The limitation on the accuracy of the comparison lies in how accurately the spectrum can be determined by the "other method." The basic limitation on the accuracy of the autocorrelation method is the statistical uncertainty due to finite duration of data; this uncertainty can easily be made less than 0.1%.

A spectrum which is "known" to an accuracy of about 1% can be produced by passing white noise (uniform spectrum) through a filter whose power transfer function, $|H(f)|^2$, is measured (see Figures 6.4 and 6.5). The power spectrum, $P(f)$, at the output of the filter is given in terms of the input spectrum, $P_o(f)$, by

$$P(f) = |H(f)|^2 P_o(f) \quad (6.11)$$

Thus, if $P_o(f)$ is constant over the region $H(f)$ is non-zero, then $P(f)$ is proportional to $|H(f)|^2$.

The one-bit autocorrelation function method of spectral measurement produces a spectral estimate, $\hat{p}_1(f)$, whose mean is the smoothed

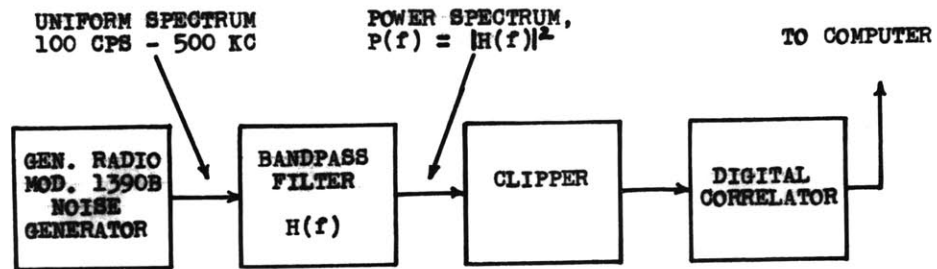


FIG. 6.4 - Procedure for producing the "known" power spectrum.

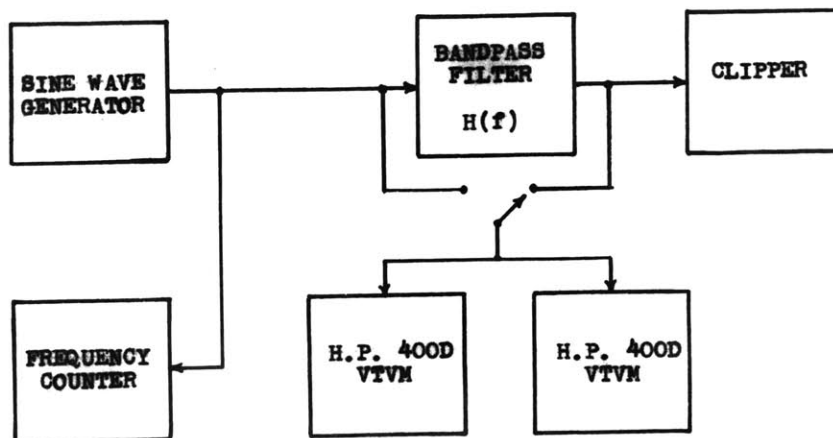


FIG. 6.5 - Procedure used to measure $|H(f)|$.

and normalized spectrum, $p^*(f)$. Ten such estimates ($i = 1$ to 10) were obtained with the same equipment utilized in the deuterium-line experiment, this was one of the early tests of the equipment. A 75 kc sampling rate and one hour integration time were used; 21 points on the autocorrelation were determined; and a uniform weighting function was applied in the Fourier transformation. According to Table 2.1 and Equation 3.34, the frequency resolution, Δf , is 2.16 kc, and the statistical uncertainty, $\sigma_{p1}/p(f)$ is 0.053%.

The arithmetic average of the ten estimates is defined as $p'_{av}(f)$, where

$$p'_{av}(f) = \frac{1}{10} \sum_{i=1}^{10} p'_i(f) \quad (6.12)$$

The RMS deviation of the spectral estimate, $\sigma_{p1}(f)$, is estimated by $\sigma'_p(f)$ which is defined as follows,

$$\sigma'_p(f) = \sqrt{\frac{1}{10} \sum_{i=1}^{10} [p'_i(f) - p'_{av}(f)]^2} \quad (6.13)$$

The object of the experiment, then, is to compare $p'_{av}(f)$ or a $p'_i(f)$ with the $|H(f)|^2$ measurement. We will also compare $\sigma'_p(f)$ with the theoretical value, $\sigma_{p1}(f)$.

The measured value of $|H(f)|^2$, which we will call $|H_m(f)|^2$, cannot be compared directly with $p_{av}^*(f)$ or a $p_i^*(f)$ since these spectra have been normalized and smoothed. Therefore, $|H_m(f)|^2$ was also smoothed and normalized to give $p_m(f)$, where

$$p_m(f) = \frac{|H_m(f)|^2 * W(f)}{\int_0^{f_s/2} |H_m(f)|^2 * W(f) df} \quad (6.14)$$

(The asterisk denotes convolution.) Note that even if $|H_m(f)|^2$ were perfectly measured, $p_m(f)$ would not quite be equal to $p^*(f)$. This is because $p^*(f)$ also contains a modification due to sampling (see Equation 2.10). As a result, a difference between $p^*(f)$ and $p_m(f)$ should occur for frequencies near half the sampling frequency.

6.3-2 Results

The results of the experiment are presented in Figure 6.6. In general, the agreement of the spectrum determined by the measurement of $|H(f)|$ and the spectrum measured by the one-bit autocorrelation system is excellent. Within the region (6 kc to 32 kc) between the filter half-power points, the largest error is 1.5% which is probably due to error in the measurement in $|H(f)|$. The large increase in error for $f > 32$ kc is due to spectral foldover (an effect of sampling). The increase in the error at very low frequencies may

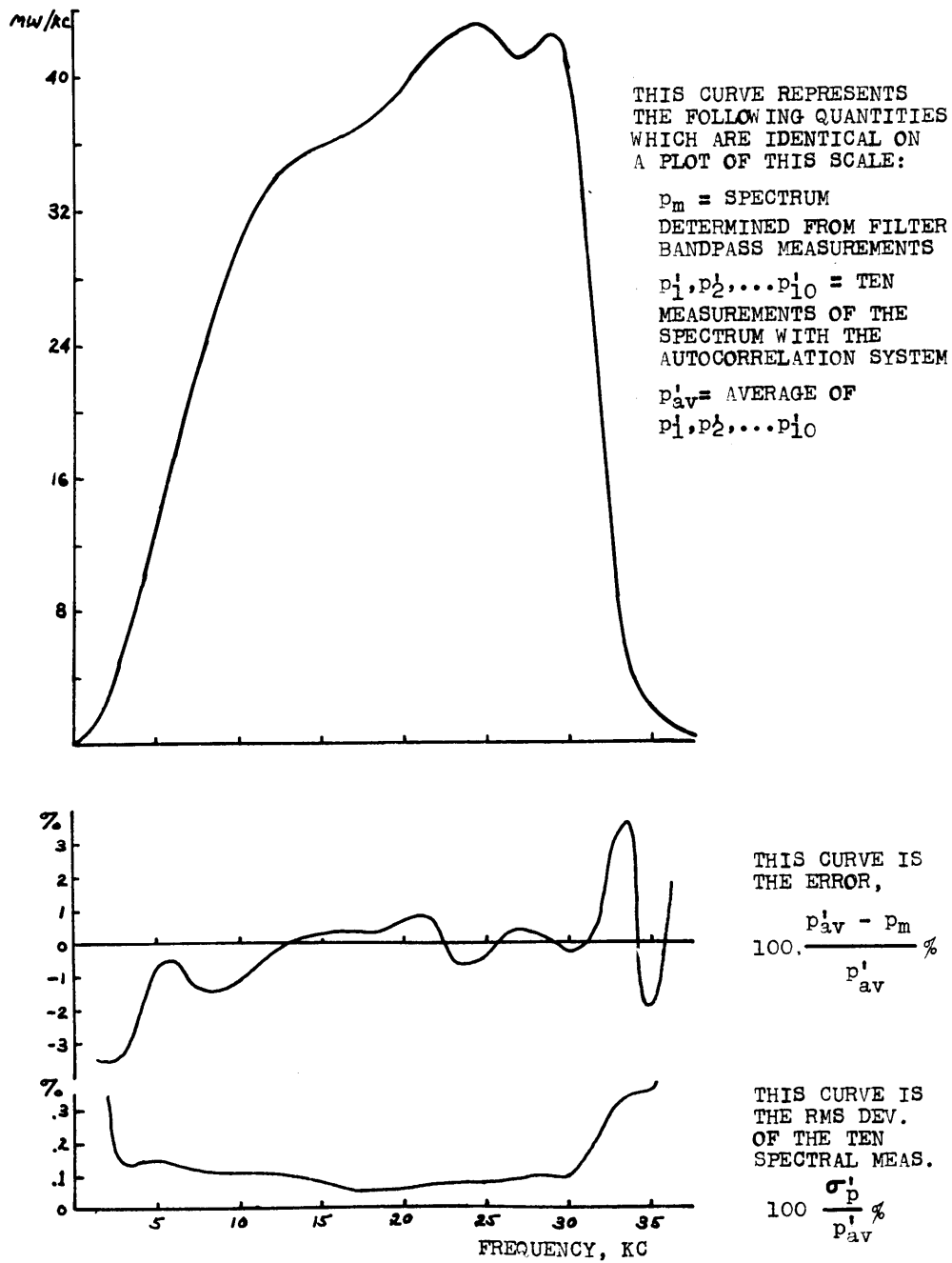


FIG. 6.6 - Results pertinent to Section 6.3.

be due to the noise generator not having a flat spectrum at these frequencies. The error may also be due to increased RMS deviation for small $p^*(f)$ as was discussed at the end of Section 6.2-3.

The estimate of the RMS deviation, $\sigma_p'(f)$, is also shown in Figure 6.6 and is of the order of a few tenths of a percent. This is higher than the theoretical value of 0.053% (which applies only in the midband region between 6 and 32 kc). The reason for the higher experimental value is apparently due to variations in the filter characteristics during the measurement time. The temperature coefficients of the capacitors and inductors used in the filter are of the order of 200 ppm per °C. The measurements of the ten spectra took two days and it is estimated that the temperature varied $\pm 5^\circ\text{C}$, thus causing a $\pm 0.1\%$ change in inductor and capacitor values. This would tend to shift the filter center frequency; an effect which can be observed upon examination of the ten spectra and is evident both in the shape and magnitude of the experimental RMS deviation curve. Subsequent experiments (next two sections) indicate that the system does realize the theoretical RMS deviation.

6.4 MEASUREMENT OF ARTIFICIAL DEUTERIUM LINES

The goal of the deuterium line experiment was to detect the 327 mc deuterium line if the galactic and terrestrial deuterium-to-hydrogen

ratios are equal. The search was made for the line in absorption from the Cassiopeia A radio source. The spectrum that is expected in this case can be predicted from hydrogen-line observations in this same direction and is shown in Figure 7.3. Essentially, a 3 kc-wide, 0.01% dip in the noise spectrum near 327 mc must be measured. The receiver noise temperature is approximately 1000°; the background source, Cassiopeia A, supplies another 1000°; and the peak deuterium absorption will be approximately 0.2° if the galactic and terrestrial abundance ratios are equal.

A spectrum which is similar to this (a "bump" is produced instead of a "dip") can be generated with the apparatus shown in Figure 6.7. A 3 kc-wide noise spectrum, centered at 18 kc, is generated by the noise generator - filter method used in the preceding section. This spectrum is heterodyned up to 327 mc through the use of the receiver local oscillators. Care was taken to prevent the generation of spurious signals. The signal is passed through a calibrated (± 0.5 db) high-frequency attenuator and then coupled through the -20 db parts of two-directional couplers to give two outputs. The radio source, Cassiopeia A, is simulated by high-frequency broad-band noise generators attenuated to a proper level.

Two sources of the signal are needed, since both polarizations are observed by the deuterium-line equipment. In the actual experiment,

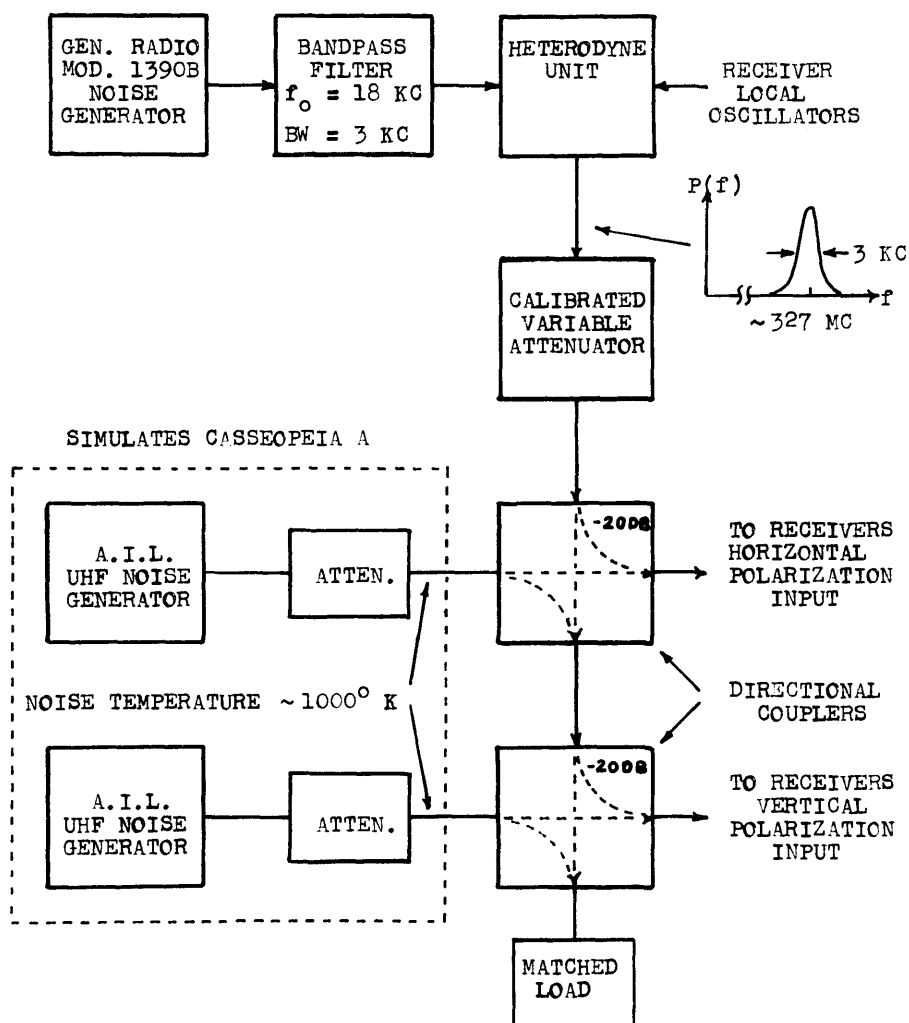


FIG. 6.7 - Artificial deuterium line generator.

each polarization gives an independent but statistically alike signal; this doubles the effective observation time and, hence, increases the sensitivity by $\sqrt{2}$. In our artificial experiment, two separate high-frequency noise generators (each simulating a component of the random polarization of Cassiopeia A) are used and, hence, the 1000° broad-band noise signals are independent. In contrast to this, the weak, 3 kc-wide, artificial deuterium-line signals arise in a common source and are, therefore, not independent. However, as long as these signals are small ($\ll 1000^\circ$), there will not be an increase in RMS fluctuation due to the coherence of the two artificial signals.

The ratio of the artificial signal power to the broadband noise power can be determined by observing (on a meter) the change in total receiver output power as the artificial signal is increased by varying the calibrated attenuator. By knowing the shape of the artificial line and the shape of the receiver bandpass, the peak artificial signal temperature is found. The attenuator then provides a means of adjusting the strength of the artificial deuterium line.

The results of some artificial deuterium-line observations are shown in Figure 6.8. Two observations of an artificial line, which is 1% of the total noise temperature 2000°, are shown in the top portion of the figure. The two observations were performed two weeks apart and illustrate the repeatability of the measurement.

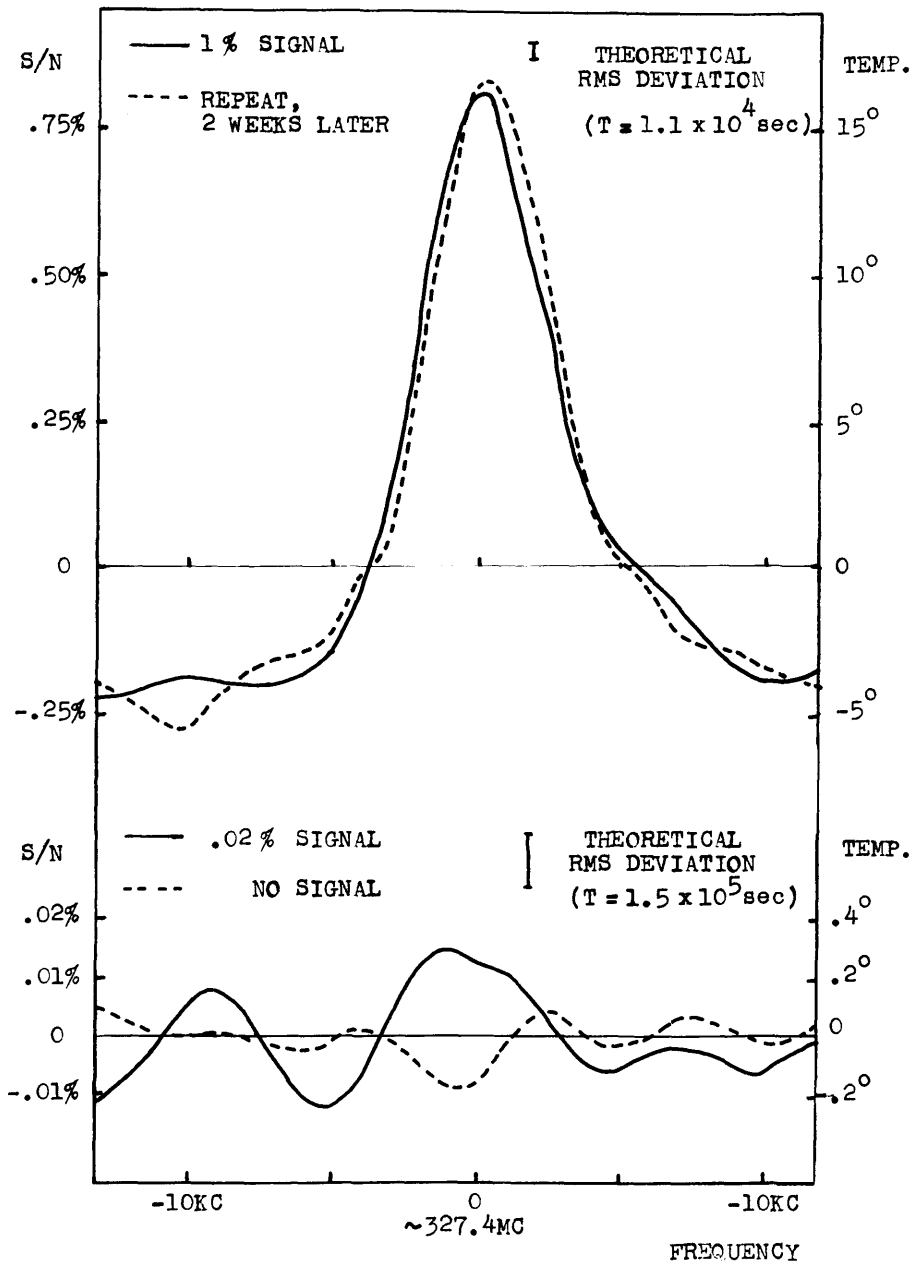


FIG. 6.8 - Artificial deuterium line results. The ordinates of the curves are expressed as a temperature difference from T_{av} , the total noise temperature ($\sim 2000^\circ$) averaged over the receiver bandpass.

The lower portion of Figure 6.8 shows the results of an observation of a 0.02%, 0.4°, artificial line and, for comparison, an observation with no line. The 0.02% line is just at the borderline of detectability, being just twice the theoretical RMS deviation for the integration time of 1.5×10^5 seconds.

6.5 ANALYSIS OF THE RMS DEVIATION OF THE DEUTERIUM-LINE DATA

6.5-1 Theoretical RMS Deviation

The deuterium-line data was processed slightly differently from the procedure to specify antenna temperature presented in Chapter 4 and, thus, an RMS deviation equation slightly different from that given by Equation 4.28 arises. The quantity that was examined is the measured difference spectrum, $\delta p'(f) = p'(f) - p'_c(f)$, divided by the measured receiver bandpass function, $p'_o(f)$. This dimensionless quantity, $\delta p'(f)/p'_o(f)$, will be designated as $s(f)$ and has physical significance in that it is simply related to the deuterium optical depth.

Under the assumption (discussed in Section 5.1-2) that the receiver is balanced ($\delta T_{av} = 0$), the mean of $s(f)$ is given by Equation 4.22 as,

$$\overline{s(f)} = \left[\frac{\delta p'(f)}{p'_o(f)} \right] = \frac{T^\dagger(f+f_o) - T_{av}}{T_{av}} \quad (6.15)$$

where $T^\dagger(f+f_0)$ is the smoothed input temperature spectrum and T_{av} is $T^\dagger(f+f_0)$ averaged in frequency over the receiver bandpass. $T^\dagger(f+f_0)$ is the sum of the smoothed antenna temperature spectrum, $T_a^\dagger(f+f_0)$, and the receiver noise temperature, T_r . (All of these terms have been defined and discussed in Chapter 4). If Equation 6.15 is solved for $T^\dagger(f+f_0)$, Equation 4.20 (with $\delta T_{av} = 0$) results. The RMS deviation of $T_a^\dagger(f+f_0)$ is then given by Equation 4.28.

The RMS deviation of $s(f)$ is found upon application of Equation 4.23, which gives the RMS deviation of a normalized spectral estimate such as $p^r(f)$, $p_c^r(f)$, or $p_o^r(f)$. As explained in Section 4.4, the RMS deviation of $p_o^r(f)$ can be neglected. The RMS deviation of $\delta p^r(f) = p^r(f) - p_c^r(f)$ is twice that of $p^r(f)$ or $p_c^r(f)$ [a factor of $\sqrt{2}$ arises because $\delta p^r(f)$ is the difference of two random quantities; another factor of $\sqrt{2}$ arises because only half the total observation time, τ , is spent on each measurement]. The result is,

$$\Delta s(f) = \frac{2\alpha\beta}{\sqrt{\tau\Delta f}} \cdot \sqrt{1 - \Delta f/b} \quad (6.16)$$

where α , β , Δf , and b are defined after Equation 4.23. The numerical values which apply in the deuterium-line experiment are $\alpha = 0.866$, $\beta = 1.39$, $\Delta f = 3.75$ kc, and $b = 30$ kc.

The time, τ , in Equation 6.16 is equal to the actual observation time only if a single switched receiver is used and if no blanking time

is allowed in the switching cycle. As previously explained, four switched receivers, each monitoring an independent signal, were used in the deuterium-line experiment. The time, τ , then becomes the observation time per receiver and, except for blanking, would be equal to 4 times the actual observation time. The blanking time is 1/4 of the total time; thus, τ is equal to 3 times the actual deuterium-line observation time, τ_a . In the course of the experiment, τ was recorded (it is proportional to the number of counts accumulated in the first counter of the correlator) and whenever observation times are quoted, τ (and not τ_a) is meant. In the deuterium-line experiment a τ of 76.5 days was achieved even though the antenna was in use only 68 days and the source was observable only 12 hours a day.

One further step was taken in the processing of the deuterium-line data. A linear (with frequency) correction was applied to the measured spectrum to remove any slope that was present (typical slope correction, $1.5 \times 10^{-5}/\text{kc}$). In other words, the slope-corrected function, $c(f)$, is given by,

$$c(f) = s(f) - (a + bf) \quad (6.17)$$

where a and b are chosen to minimize the mean square value of $c(f)$. The reason this correction is needed is due to imperfections in the front-end switch and noise source and is discussed in Section 5.1-1.

Some of the statistical error is removed by the slope correction and the theoretical RMS deviation of $c(f)$ is lower than that of $s(f)$. It can be shown (Kenney and Keeping,²¹ Section 8.7) that the reduction is by a factor of $\sqrt{1 - 2/N}$ where N is the number of independent points on the curve. Assuming that points $\Delta f/2 = 1.87$ kc apart are independent, $N = 13.4$ for the 25 kc bandwidth which was analyzed. Thus, the RMS deviation should be reduced by a factor of 0.92. The result of applying this correction and substituting numerical values for α , β , and b is,

$$\Delta c(f) = \frac{-2.05}{\sqrt{\tau \Delta f}} \quad (6.18)$$

It is convenient at times to give a temperature scale to $s(f)$ and $c(f)$ by multiplying them by T_{av} which was approximately 2000°. The quantity, $\Delta T \equiv T_{av} \Delta c(f)$ then has an interpretation as the RMS deviation of the measurement of $T^\dagger(f+f_0) - T_{av}$, and is given by,

$$\Delta T = \frac{2.05}{\sqrt{\tau \Delta f}} T_{av} \quad (6.19)$$

$$= \frac{1.1^\circ}{\sqrt{(\tau)_{\text{HRS}}}} \quad (6.20)$$

6.5-2 Experimental Results

The deuterium-line data consists of 169 spectral estimates, each accumulated with an average observation time, τ , of 10.8 hours.

These estimates will be labeled $c_i(f)$ where i goes from 1 to 169. The mean of each estimate is given by Equation 6.15 (with a slope correction) and the RMS deviation is given by Equation 6.18, 6.19, or 6.20. The computer program that was used to produce each $c_i(f)$ from the output of the digital correlator is listed in Appendix D.

Each spectral estimate was plotted and examined for interference. A few spectra were discarded due to unusual appearance. The remaining 169 spectra were averaged into weekly averages, tri-weekly averages, and a final, overall nine-week average. The results of the three week and nine week averages are shown in Figure 7.3.

An experimental estimate of the frequency-averaged RMS deviation of each $c_i(f)$ is given by Δc_i , computed as follows,

$$\Delta c_i = \sqrt{\frac{1}{26} \sum_{f=5}^{30} c_i^2(f)} \quad (6.21)$$

(It is assumed in this computation that the mean of each $c_i(f)$ is zero, meaning the deuterium line is not present. Unfortunately, this proved to be the case.) The RMS error of an estimate of the RMS deviation computed in this manner is equal to $100/\sqrt{2I}$ percent (Burington and May,²⁰ p. 149) where I is the number of independent points on the spectrum. Assuming points $\Delta f/2 = 1.87$ kc apart are independent,

$I = 13.4$, and the error is approximately 19%. If the Δc_i from L different records are averaged together, the RMS error will be $19/\sqrt{L}$ percent.

In addition to computing the Δc_i for each 10.8 hour record, the frequency-averaged RMS deviation was also computed for longer records formed by averaging the 10.8 hour records. The results are presented in the table below and, in somewhat different form, in Figure 6.9.

TABLE 6.5
ANALYSIS OF RMS DEVIATION OF THE
DEUTERIUM-LINE DATA

AVERAGE RECORD LENGTH τ	NUMBER OF RECORDS L	THEORETICAL RMS DEVIATION $T_{av} \Delta c$	EXPERIMENTAL RMS DEVIATION $T_{av} \Delta c_i$
10.8 hrs	169	0.340°	0.340°±0.010°
229 hrs	8	0.073°	0.087°±0.012°
612 hrs	3	0.045°	0.066°±0.014°
1835 hrs	1	0.026°	0.042°±0.016°

The results indicate that the departure from the theoretical sensitivity is not large, even for integration times of the order of

10^6 to 10^7 seconds. This should be compared with the conventional Dicke radiometer, where the theoretical RMS deviation is usually not achieved for integration times longer than 10^2 to 10^3 seconds. The stability advantage of the one-bit autocorrelation system is put clearly in evidence in Figure 6.9.

SPECTRAL RMS DEVIATION $\sim \frac{1}{2}$ MIN. DETECTABLE SIGNAL
 EXPRESSED AS % OF NOISE LEVEL
 (3.75 KC BANDWIDTH IS ASSUMED)

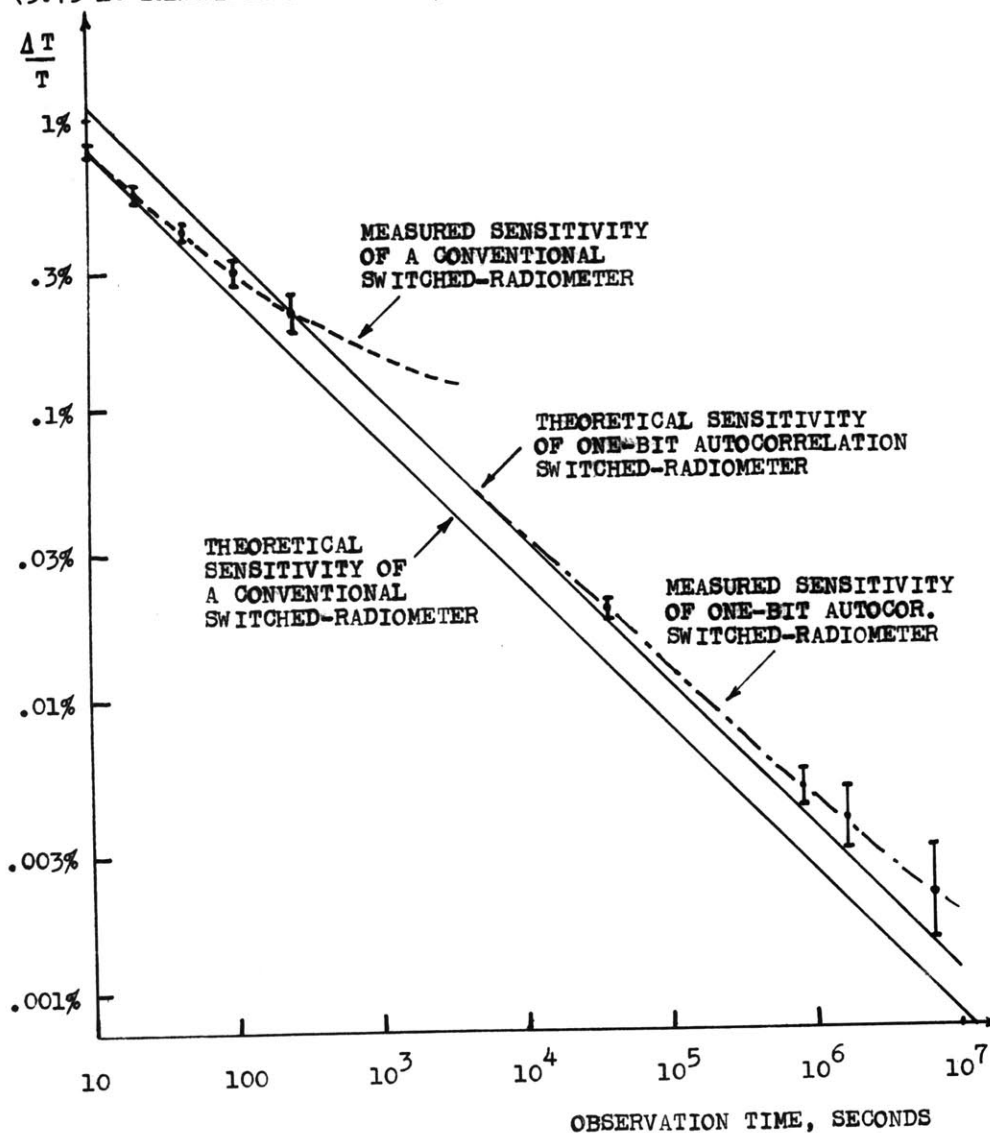


FIG. 6.9 - Experimental and theoretical sensitivity of a conventional Dicke radiometer compared with a one-bit autocorrelation radiometer. The measurements on the Dicke radiometer were performed by Cohen and Orhaug²².

CHAPTER 7

THE DEUTERIUM LINE EXPERIMENT

7.1 INTRODUCTION

At present, only one spectral line has been observed in radio astronomy. This is the 1420 mc (21 cm) hydrogen line, detected in 1951 by Ewen and Purcell. This line is due to hyperfine splitting of the ground state of cold, neutral, atomic hydrogen which exists in the interstellar regions of a galaxy. During the past 11 years, extensive studies of the hydrogen line have been made (see Shklovsky,²³ Chapter 4) and valuable physical characteristics (such as density, temperature, line-of-sight velocity) of the interstellar medium have been measured. Indeed, it has been found that a large fraction of the total mass of our galaxy consists of this neutral atomic hydrogen, which is presently not observable by any other means.

Deuterium, an isotope of hydrogen (sometimes called "heavy hydrogen") exhibits a similar hyperfine transition which occurs at approximately 327 mc. In 1952, Shklovsky²⁴ predicted that it might be possible to detect this line. Since 1952, there have been at least four attempts to detect the deuterium line and all have given negative results.^{25, 26, 27, 28} The most recent of these, by Adgie at Jodrell Bank, had a sensitivity which was not quite sufficient to detect the

line if the interstellar deuterium-to-hydrogen ratio, N_D/N_H , was equal to the terrestrial value of 1/6600. The goal, then, of our experiment was to detect the deuterium line if the interstellar and terrestrial deuterium-to-hydrogen ratios are equal.

The interstellar deuterium-to-hydrogen ratio is of astrophysical importance because it gives information concerning the nucleogenesis of the interstellar medium.^{29, 30} The role that N_D/N_H plays in nucleogenesis will be very briefly outlined in the following two paragraphs:

The relative abundances of elements formed by the nuclear burning in a star can be predicted by stellar nuclear theory. For most elements, these abundances agree remarkably well with the abundances found on earth and in meteorites. However, an outstanding anomaly exists in the case of deuterium. The predicted value of N_D/N_H is 10^{-17} , which is approximately 10^{13} times less than the measured terrestrial ratio.

Fowler, Greenstein, and Hoyle³¹ have attempted to explain the high terrestrial N_D/N_H ratio in terms of nuclear processes which occurred on the primordial earth. According to this theory, the N_D/N_H ratio of 1/6600 would appear to be purely a terrestrial phenomenon and there would be no reason to expect this value to be true in the interstellar regions. If the interstellar medium primarily

consists of the ashes of stars, an interstellar N_D/N_H of 10^{-17} would be expected. An interstellar N_D/N_H of $1/6600$ would tend to say that both the earth and the interstellar medium were formed from material which had never been through the stellar burning process.

Some background material concerning the deuterium line experiment is presented in the author's B.S. Thesis.³² The major topics that are discussed are:

- 1) The bandwidth and magnitude of the expected deuterium line are derived in terms of N_D/N_H . This will be discussed in the next section.

- 2) The choice of a direction of observation is discussed. Assuming that N_D/N_H is constant in the interstellar medium, the best signal-to-noise ratio is predicted for an attempt to detect the line in absorption from the Cas A radio source.

The deuterium-line observations were performed with the 85-ft Howard Tatel Radio Telescope at the National Radio Astronomy Observatory, Green Bank, West Virginia. The receiving system has been discussed, of course, in the earlier chapters of this paper. The basic steps in the signal processing system are given by Figures 4.1 and 1.7. A detailed block diagram of the deuterium line receiver is given in Figure 5.1 and components of the system are discussed

in Chapter 5. The treatment of the data and the theoretical and experimental sensitivities are discussed in Section 6.5.

7.2 PHYSICAL THEORY AND ASSUMPTIONS

The relation between the antenna temperature spectrum, $T_a(f)$, and the interstellar deuterium-to-hydrogen ratio, N_D/N_H , will be discussed in this section. This relationship can be written down very simply if some very important assumptions are made. These assumptions have been made, but not stated, by past researchers looking for the deuterium line. Indeed, these same assumptions are included in the basic statement of the results of our work. — The galactic deuterium-to-hydrogen ratio is less than 1/2 the terrestrial value. A few of these assumptions are not well justified and a reinterpretation of our measurements may be necessary based upon future theoretical and experimental work in astrophysics.

In light of the above statements, the three basic steps relating the antenna temperature to N_D/N_H will be briefly reviewed. The simple relation between $T_a(f)$ and N_D/N_H will then be stated and the important assumptions that are contained in this statement will be listed. The three basic steps are as follows:

1) The antenna temperature, $T_a(f)$, is equal to a weighted spatial average of the sky brightness temperature, $T_b(f, \theta, \phi)$,

$$T_a(f) = \frac{1}{4\pi} \int_{4\pi} T_b(f, \theta, \phi) g(\theta, \phi) d\Omega \quad (7.1)$$

where $g(\theta, \phi)$ is the antenna gain function and $d\Omega = \sin\theta d\theta d\phi$ is the solid angle increment.

2) The sky brightness temperature, $T_b(f, \theta, \phi)$, is related by the classical equation of transfer (see Chandrasekhar³³) to the optical depth of the gas (deuterium or hydrogen), $\tau(f, \theta, \phi)$; the spin temperature of the gas, T_g (assumed constant in space and frequency) and the background brightness temperature, $T_{bg}(\theta, \phi)$ (assumed independent of frequency). The relation is,

$$T_b(f, \theta, \phi) = T_{bg}(\theta, \phi) e^{-\tau(f, \theta, \phi)} + T_g [1 - e^{-\tau(f, \theta, \phi)}] \quad (7.2)$$

3) The optical depth of the gas is related to $n(\theta, \phi)$, the number of gas atoms (in both of the hyperfine states) in a column of unit cross section extending from the observer to infinity in the direction of θ and ϕ . The relation is the following,³²

$$\tau(f, \theta, \phi) = \frac{hc^2}{8\pi k} \cdot \frac{A}{T_g f_o \Delta f} \cdot \frac{g_1}{g_1 + g_o} \cdot u(f) \cdot n(\theta, \phi) \quad (7.3)$$

where $hc^2/8\pi k$ is a constant, A is the spontaneous emission probability, T_g is the spin temperature, f_o is the line frequency,

Δf is the Doppler-broadened linewidth, g_1 and g_0 are the statistical weights of the upper and lower states, and $u(f)$ is the line shape function [$u(f_0) = 1$].

The problem is now to apply these equations to the physical situation shown in Figure 7.1 and to interpret a deuterium-to-hydrogen ratio from our deuterium results, previous hydrogen line observations in this same direction, and measurements and calculations of the physical properties of deuterium and hydrogen.

In the configuration of Figure 7.1, the background brightness temperature distribution, $T_{bg}(\theta, \phi)$ consists of a term, T_0 , which is constant within the antenna beam and a term, $T_p(\theta, \phi)$, representing the contribution of the discrete source. It is convenient to describe the antenna temperature in terms of measurable, spatial averages of $T_p(\theta, \phi)$ and $e^{-\tau(f, \theta, \phi)}$. These spatial averages are T'_p , $e^{-\tau'(f)}$, and $e^{-\tau''(f)}$, defined as follows:

$$T'_p \equiv \frac{1}{4\pi} \int_{4\pi} T_p(\theta, \phi) g(\theta, \phi) d\Omega \quad (7.4)$$

$$e^{-\tau'(f)} \equiv \frac{1}{4\pi} \int_{4\pi} e^{-\tau(f, \theta, \phi)} \cdot \frac{T_p(\theta, \phi)}{T'_p} \cdot g(\theta, \phi) d\Omega \quad (7.5)$$

$$e^{-\tau''(f)} \equiv \frac{1}{4\pi} \int_{4\pi} e^{-\tau(f, \theta, \phi)} \cdot g(\theta, \phi) d\Omega \quad (7.6)$$

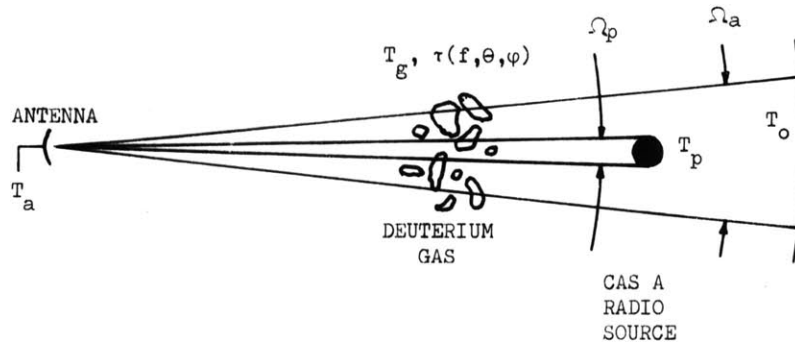


FIG. 7.1 - Configuration for the deuterium-line experiment.

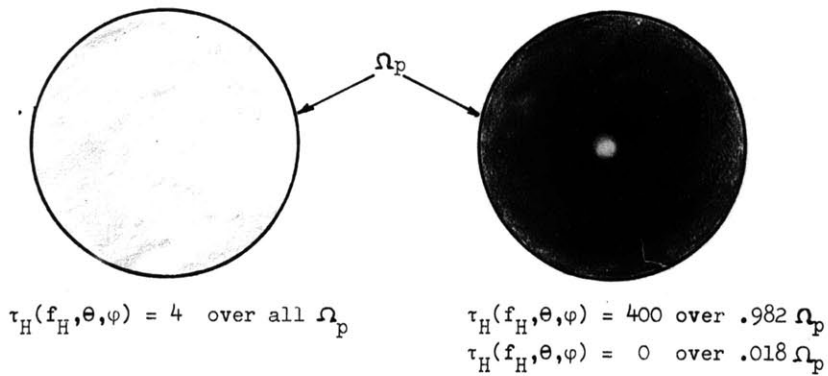


FIG. 7.2 - Two extremes of the possible distributions of hydrogen optical depth in front of the Cas A radio source are shown. Both configurations would give the same measured, spatially-averaged, hydrogen optical-depth, $\tau_H(f_H)$, defined by Equation 7.5. However, the distribution at right would give a measured, spatially-averaged, deuterium optical-depth, $\tau_D(f_D)$, which would be 100 times greater than that given by the uniform distribution with the same N_D/N_H ratio. The major point is that the assumption of uniform hydrogen optical-depth is the most conservative distribution that can be chosen as far as setting an upper limit on the N_D/N_H ratio.

In words: T_p' is the contribution to antenna temperature from the discrete source; $\tau'(f)$ is minus the logarithm of the average of $e^{-\tau(f, \theta, \phi)}$ taken over the solid angle subtended by the discrete source; and $\tau''(f)$ is minus the logarithm of the average of $e^{-\tau(f, \theta, \phi)}$ taken over the entire antenna beam. It is important to note that $\tau'(f)$ and $\tau''(f)$ are not just simple averages of $\tau(f)$.

Equations 7.1 and 7.2 can be combined to specify the antenna temperature in terms of the quantities defined above,

$$T_a(f) = T_p' e^{-\tau'(f)} + T_o e^{-\tau''(f)} + T_g [1 - e^{-\tau''(f)}] \quad (7.7)$$

The first term in the above equation represents the contribution to antenna temperature from the discrete source attenuated by the gas, the second terms represent the background contribution attenuated by the gas; and the last term represents emission by the gas.

In the case of the deuterium line, $\tau'(f) = \tau_D'(f)$ and $\tau''(f) = \tau_D''(f)$, are much less than one. The exponentials can be expanded to give,

$$T_a(f) = T_p' - \tau_D'(f) T_p' + T_o + \tau_D''(f) [T_s - T_o] \quad (7.8)$$

In the direction of the Cas A radio source, the last term can be neglected since $\tau_D''(f)$ will be of the same order as $\tau_D'(f)$ and $T_p' \sim 1000^\circ$ (with an 84-ft telescope) is much larger than $T_g - T_o \sim 45^\circ$

(this assumes that T_g for deuterium is the same as T_g for hydrogen $\sim 125^\circ\text{K}$). Thus, the final result for the antenna temperature is,

$$T_a(f) = T_p' + T_o - \tau_D'(f) T_p' \quad (7.9)$$

The relation between the peak optical depth, $\tau_D'(f_D)$ and N_D/N_H can be calculated with the aid of Equation 7.3 evaluated for both deuterium and hydrogen. We find,

$$\frac{\tau_D'(f_D)}{\tau_H'(f_H)} = 0.30 \frac{N_D}{N_H} \quad (7.10)$$

The following assumptions, listed in order of increasing degree of justification, are contained in Equation 7.10:

1) The value of N_D/N_H that is interpreted from the measurement of $\tau_D'(f_D)/\tau_H'(f_H)$ really depends on the angular distribution of hydrogen, $n_H(\theta, \phi)$, within the solid angle, Ω_p , subtended by the discrete source. It also depends on the discrete source temperature distribution, $T_p(\theta, \phi)$. These statements are illustrated in Figure 7.2 and are explained in the next paragraph.

The ratio, $\tau_D(f_D, \theta, \phi)/\tau_H(f_H, \theta, \phi)$, does not depend on $n_H(\theta, \phi)$ if the deuterium spatial distribution is the same as that of hydrogen; i. e., $n_D(\theta, \phi) = (N_D/N_H) n_H(\theta, \phi)$. However, even if the distributions are the same, the ratio that is measured, $\tau_D'(f_D)/\tau_H'(f_H)$,

depends on $n_H(\theta, \phi)$. This arises because of the peculiar way $\tau'_H(f_H)$ depends on $\tau_H(f_H, \theta, \phi)$ in Equation 7.5. If $\tau'_H(f_H)$ was a simple spatial average of $\tau_H(f_H, \theta, \phi)$, then $\tau'_D(f_D)/\tau'_H(f_H)$ would be directly related to N_D/N_H in a manner independent of $n_H(\theta, \phi)$ [assumed proportional to $n_D(\theta, \phi)$].

Due to the high resolution that is required, neither $n_H(\theta, \phi)$ nor $T_p(\theta, \phi)$ have been measured. It is assumed in Equation 7.10 that both $n_H(\theta, \phi)$ [and, hence $\tau_H(f_H, \theta, \phi)$] and $T_p(\theta, \phi)$ are constant over Ω_p . It appears (see Figure 7.2) that this is the most conservative distribution that can be assumed. In other words, any other distribution would allow a lower upper-limit of N_D/N_H to be interpreted from our results. Future measurements of $n_H(\theta, \phi)$ and $T_p(\theta, \phi)$ for the Cas A radio source will allow a more sensitive interpretation of our results.

2) The spin temperatures for deuterium and hydrogen are assumed equal. Justification of this assumption is uncertain, since it depends on estimates of the intensity and detailed profile of the interstellar radiation field at the frequency of deuterium Lyman α radiation. This problem has been discussed by Field.³⁴

3) The ratio of the Doppler-broadened linewidths of deuterium and hydrogen, $\Delta f_D/\Delta f_H$, would be equal to the ratio of the line frequencies, f_D/f_H , if the atoms had the same RMS velocity.

However, a portion of the RMS velocity is due to thermal motion in which the deuterium atoms, having twice the mass, would have $1/\sqrt{2}$ of the RMS thermal velocity of the hydrogen atoms. The other component of RMS velocity is believed due to random cloud motion which would give the same velocity to deuterium and hydrogen atoms. These velocities are independent and, hence, the total RMS velocity is the square root of the sum of the squares of the RMS thermal and random velocities. Approximately $0.5 \Delta f_H$ is due to thermal motion and, thus, $0.866 \Delta f_H$ must be due to random cloud motion. These numbers give $\Delta f_D / \Delta f_H = 0.935 f_D / f_H$.

4) The value of the deuterium transition probability, $A_D = 4.65 \times 10^{-17} \text{ sec}^{-1}$, given by Field³⁴ is correct (this same value was independently computed by Professor A. H. Barrett of M.I.T.). The value, $A_D = 6.6 \times 10^{-17}$, given by Shklovsky²³ is incorrect (Equations 14-6, 15-4, 18-3, and 18-4 appear to be incorrect). The value of $A_H = 2.85 \times 10^{-15} \text{ sec}^{-1}$ is not in doubt.

5) The value of the peak hydrogen optical depth, $\tau'_H(f_H)$, in the Cas A radio source is also the subject of some controversy, its large value being difficult to measure. The first observers, Hagen, Lilley, and McClain,³⁵ using a 50-ft paraboloid, report $\tau'_H(f_H) = 2.6$. Muller,³⁶ using an 83-ft reflector, gives 4.0, and observers at California Institute of Technology,³⁷ using a single 90-ft telescope, report $\tau'_H(f_H) > 4.7$, and 3.4 ± 0.4 when using two 90-ft

telescopes as an interferometer. We will assume that a value,

$\tau_{\text{H}}^{\prime}(f_{\text{H}}) = 4.0$, is correct and, thus Equation 7.10 gives,

$$\tau_{\text{D}}^{\prime}(f_{\text{D}}) = 1.8 \times 10^{-4} \quad (7.11)$$

for $N_{\text{D}}/N_{\text{H}} = 1/6600$.

7.3 RESULTS AND CONCLUSION

The final result of the deuterium-line data analysis described in Section 6.5 is the normalized spectral function, $c(f)$. The mean or expected value of this function is given by,

$$\overline{c(f)} = \frac{T_{\text{a}}^{\dagger}(f+f_{\text{o}}) + T_{\text{r}} - T_{\text{av}}}{T_{\text{av}}} \quad (7.12)$$

where $T_{\text{a}}^{\dagger}(f+f_{\text{o}})$ is the smoothed (by an equivalent scanning filter of 3.75 kc bandwidth) antenna temperature spectrum, T_{r} is the receiver noise temperature, and T_{av} is the frequency-averaged value of $T_{\text{a}}^{\dagger}(f+f_{\text{o}}) + T_{\text{r}}$ (see Equation 4.14).

The antenna temperature spectrum is specified by Equation 7.9 in terms of the deuterium optical depth, $\tau_{\text{D}}^{\prime}(f)$, the sky background temperature, T_{o} , and the contribution to antenna temperature from the discrete source, T_{p}^{\prime} . The substitution of Equation 7.9 into Equation 7.12 gives,

$$c(f) = \frac{T_{\text{p}}^{\prime}}{T_{\text{p}}^{\prime} + T_{\text{o}} + T_{\text{r}}} \cdot [\tau_{\text{av}} - \tau_{\text{D}}^{\dagger}(f)] \quad (7.13)$$

where τ_{av} is the frequency averaged value of $\tau_D'(f)$ and $\tau_D^*(f)$ is the smoothed version of $\tau_D'(f)$. (A term, $-\tau_{av} T_p'$, has been neglected in the denominator of Equation 7.13.) The ratio, $T_p'/(T_p' + T_o + T_r)$, was measured directly each day by noting the change in total power as the antenna was moved on and off Cas A; its value is 0.46 ± 0.02 . (The individual temperatures were, $T_p' \sim 920^\circ$, $T_o \sim 80^\circ$, and $T_r \sim 1000^\circ$.)

The value of $\overline{c(f)}$ that is expected if $N_D/N_H = 1/6600$ is shown at the top of Figure 7.3 and the measured results are shown beneath it. The shape of $\tau_D'(f)$ can be predicted from the measured hydrogen profile,³² $\tau_H'(f)$. The value of the peak deuterium absorption dip, $\tau_D'(f_D)$, is given by Equation 7.11. A reduction by a factor of 0.9 was allowed because of the smoothing effect of the spectral measurement system; i. e., $\tau_D^*(f_D) = 0.9 \tau_D'(f_D)$.

The theoretical RMS deviations of the measurement are given by Equation 6.18, 6.19, or 6.20, and are indicated on Figure 7.3. The theoretical RMS deviation of the average of all the data equals the peak spectral dip expected from an N_D/N_H of 1/36,000. If a detection criterion of twice the theoretical RMS deviation (97.7% confidence) is used, the minimum detectable N_D/N_H is 1/18,000. Examination of the data in Section 6.5-2 indicates that the experimental RMS deviation is approximately 1.4 times the theoretical value; and, thus, the minimum detectable N_D/N_H should be raised to 1/13,000.

Our conclusion, then, is that the deuterium-to-hydrogen ratio in the region examined is, with probability 0.977 and within the stated assumptions, less than half the terrestrial value.

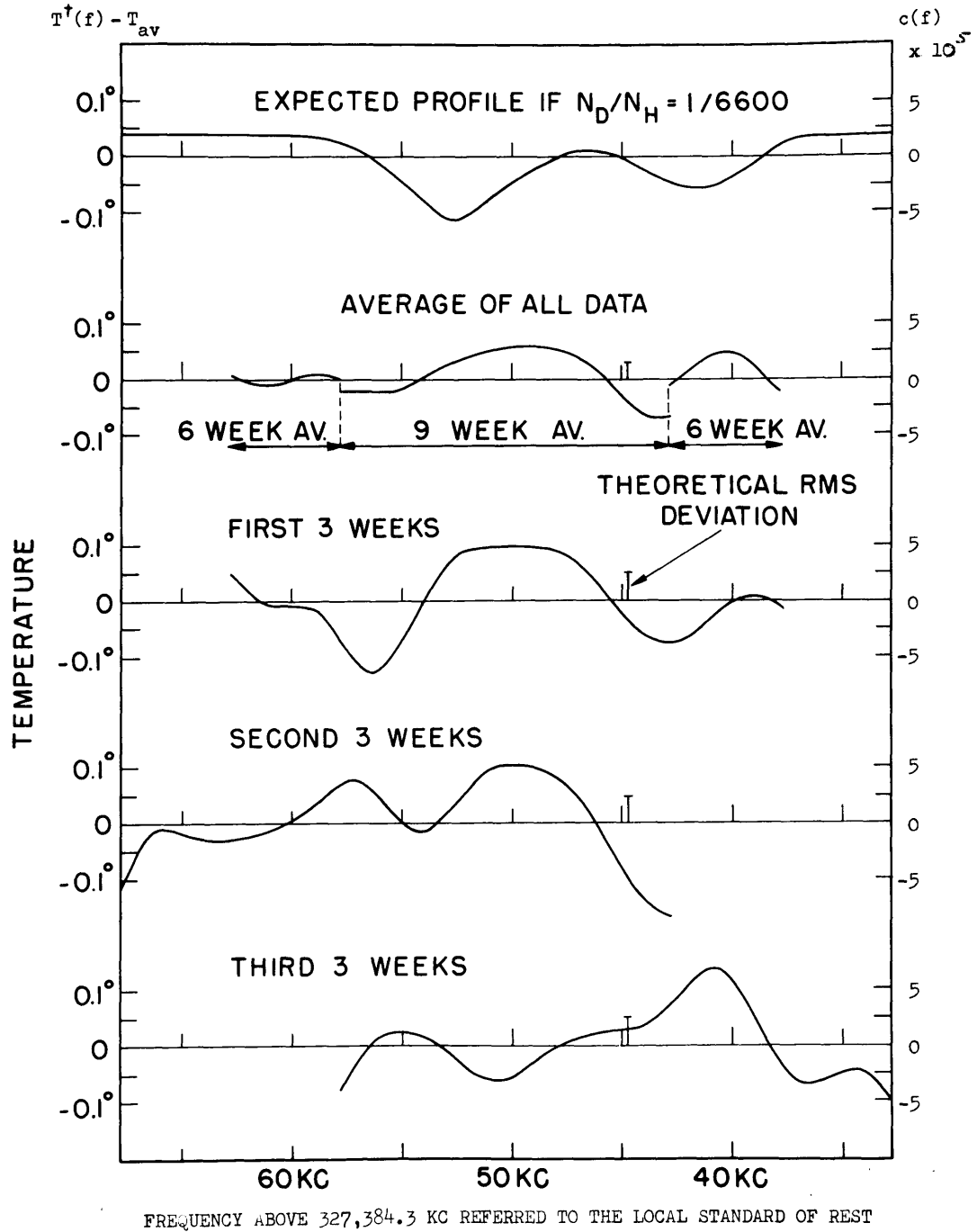


FIG. 7.3 - Results of the deuterium-line search in the Cas A radio source. The temperatures indicated on the left-hand margin are with respect to the total noise temperature ($\sim 2000^\circ$) averaged over the receiver bandpass. The quantity, $c(f)$, is defined by Equation 7.12.

CHAPTER 8
AN ATTEMPT TO MEASURE ZEEMAN SPLITTING OF THE
21-CM HYDROGEN LINE

8.1 INTRODUCTION

The existence of a galactic magnetic field is presupposed by theories describing the polarization of starlight, the emission of galactic radio noise, and the behavior of cosmic rays. The magnitude of the field cannot be measured directly from these effects, although estimates of from 10^{-5} gauss to 10^{-6} gauss are common. These facts are discussed and referenced by Shklovsky,²³ and also in two papers^{38, 39} that describe previous attempts to measure the field by measuring the Zeeman splitting of the 21-cm hydrogen line. The experiment was first suggested by Bolton and Wild.⁴⁰

A brief description of the Zeeman effect on hydrogen line radiation may be given as follows. The line-of-sight component of the galactic magnetic field causes a splitting of the radiation into left-hand and right-hand circularly polarized waves with a difference in frequency of 2.8 cps per 10^{-6} gauss. The sharpest hydrogen lines found in absorption of the strong discrete sources are $\sim 10 - 20$ kc wide, and thus the expected splitting of 3 - 30 cps is quite difficult to measure. The procedure consists of alternately measuring the hydrogen profile with feeds that are receptive to circular polarization of opposite sense

and recording the difference profile. This difference profile, $\Delta T(f)$, is related to the observed (either polarization) profile, $T(f)$, by the following relation which holds if the frequency splitting, Δf , is small compared with the width of the observed line:

$$\Delta T(f) = \Delta f \cdot T'(f) \approx 2.8 \times 10^6 \text{ H} \cdot T'(f) \quad (8.1)$$

where H is the magnetic field, and the prime denotes derivative with respect to frequency. The observed profile and the expected difference profile for the two observed sources, Cas A and Taurus A, are shown in Figures 8.1 and 8.2.

8.2 EXPERIMENTAL PROCEDURE

Observations of Cas A and Taurus A were performed with the use of the 85-ft Howard Tatel Radio Telescope at the National Radio Astronomy Observatory, Green Bank, West Virginia, in conjunction with a dual circular polarization feed built by Jasik Laboratories. The receiving system and the treatment of data were the same as used in the deuterium-line experiment except for the following changes:

- 1) Instead of switching between the antenna feed and a comparison noise source, switching was performed between an antenna feed receptive to right-hand circular polarization and another feed receptive to left-hand circular polarization. Thus, a measure of the difference spectrum, $\Delta T(f)$, given by Equation 8.1, is obtained.

Switching between polarizations was done at a 1/14 cps rate by using a mechanical coaxial switch. Double stub tuners were inserted between each arm of the switch and the feed, and were adjusted so that the standing-wave ratio of each polarization feed was less than 1.01 when measured through the switch.

2) Of course, it was necessary to change the receiver front-end and first local-oscillator. An electron-beam, traveling wave, parametric amplifier was used for all observations except for those of Taurus, Data B, for which a crystal mixer was used. The single-channel noise temperature, including switch and stub losses, was 600° for the parametric amplifier, and 1080° for the crystal mixer.

3) The filter and phase shift networks (items 20, 18, and 17 in the block diagram of Figure 5.1) were changed so that the receiver bandwidth was doubled. The 1 db bandwidth became 50 kc and the 20 db bandwidth became 75 kc. The correlator clock frequency was changed so that the sampling frequency became 150 kc. The frequency resolution, Δf , is therefore 7.5 kc.

The observational procedure consisted, first, of making a ten-minute observation of the absorption profile, with the use of the right-hand circular polarization feed. Typical results are the top curves in Figures 8.1 and 8.2. A loss in sensitivity or a frequency

error could be found in this manner. Next, after this run, a five-hour run for measuring the difference profile was made. The local oscillator was reset every half hour to correct for Doppler shift resulting from the earth's motion. One or two 5-hour runs were made on Cas A and Taurus A each day for approximately 35 days.

8.3 RESULTS AND CONCLUSION

A difficulty that arises in performing the Zeeman experiment is due to small differences in gain between the right-hand and left-hand circular polarization feeds. If the gain of one feed is $1 + \alpha$ times the gain of the other feed, then the difference profile, $\Delta T(f)$, will contain a term $\alpha \cdot T(f)$; the absorption profile will appear in the data. Since the absorption profile is known, it may be removed from the difference profile. However, care must be taken that the correction is not shifted in frequency, for this would cause a false Zeeman effect. It is easily seen that if an unbalance signal, $\alpha \cdot T(f)$, is corrected by subtraction of a profile, $\alpha \cdot T(f + \delta f)$, then the result is the same as that which would be found for a Zeeman splitting of value $\alpha \cdot \delta f$.

Approximately 20 percent of the data that were taken showed values of α less than 0.003 (Data A); 40 percent had α between 0.003 and 0.03 (Data B); and the rest had α greater than 0.03 and were not used. The variations in α are probably due to temperature

effects on the feed, stubs, and switch, and to tracking errors and flexure of the telescope. The largest error in the local oscillators was less than 100 cps; thus, even with $\alpha = 0.03$, the largest spurious Zeeman effect would be 3 cps, or $\sim 10^{-6}$ gauss.

The average of the Data A and Data B runs for Cas A and Taurus A are plotted in the figures. The Data A runs require no correction for feed unbalance, while the Data B runs have been corrected as indicated in Table 8.1. Our conclusion is that the line-of-sight component of the magnetic field is less than 3×10^{-6} gauss in Cas A and less than 5×10^{-6} in Taurus A. This conclusion contains the important assumption that the line-of-sight component of the magnetic field is constant within the absorbing hydrogen gas.

TABLE 8.1 ZEEMAN RESULTS

	Theoretical RMS Fluctuation*	Actual RMS Fluctuation	Total Noise Temperature T	Profile Depth	Observ. Time τ (sec)	Treatment of Data
Cas Data A	0.073° 1.4	0.099° 1.9	1060°	180°	1.2×10^5	No correction to data
Cas Data B	0.053° 1.0	0.12° 2.3	1060°	180°	2.1×10^5	Absorption profile of 1.37° peak subtracted from raw data
Taurus Data A	0.044° 2.2	0.04° 2.0	850°	60°	2.2×10^5	Small slope correction of 0.12°/10 kc
Taurus Data B	0.08° 4.0	0.05° 2.5	1330°	60°	1.6×10^5	Absorption profile of 1.15° peak subtracted from raw data

* $\Delta T = 2.1 T / \sqrt{B\tau}$, where T = Antenna † Receiver Noise Temperature, $B = 7.5 \times 10^3$, and τ is the Observation Time. (The quantity below ΔT is the magnetic field in units of 10^{-6} gauss which will give a peak signal = ΔT .)

$\Delta T'$ = RMS value of data, with the mean taken over frequency.

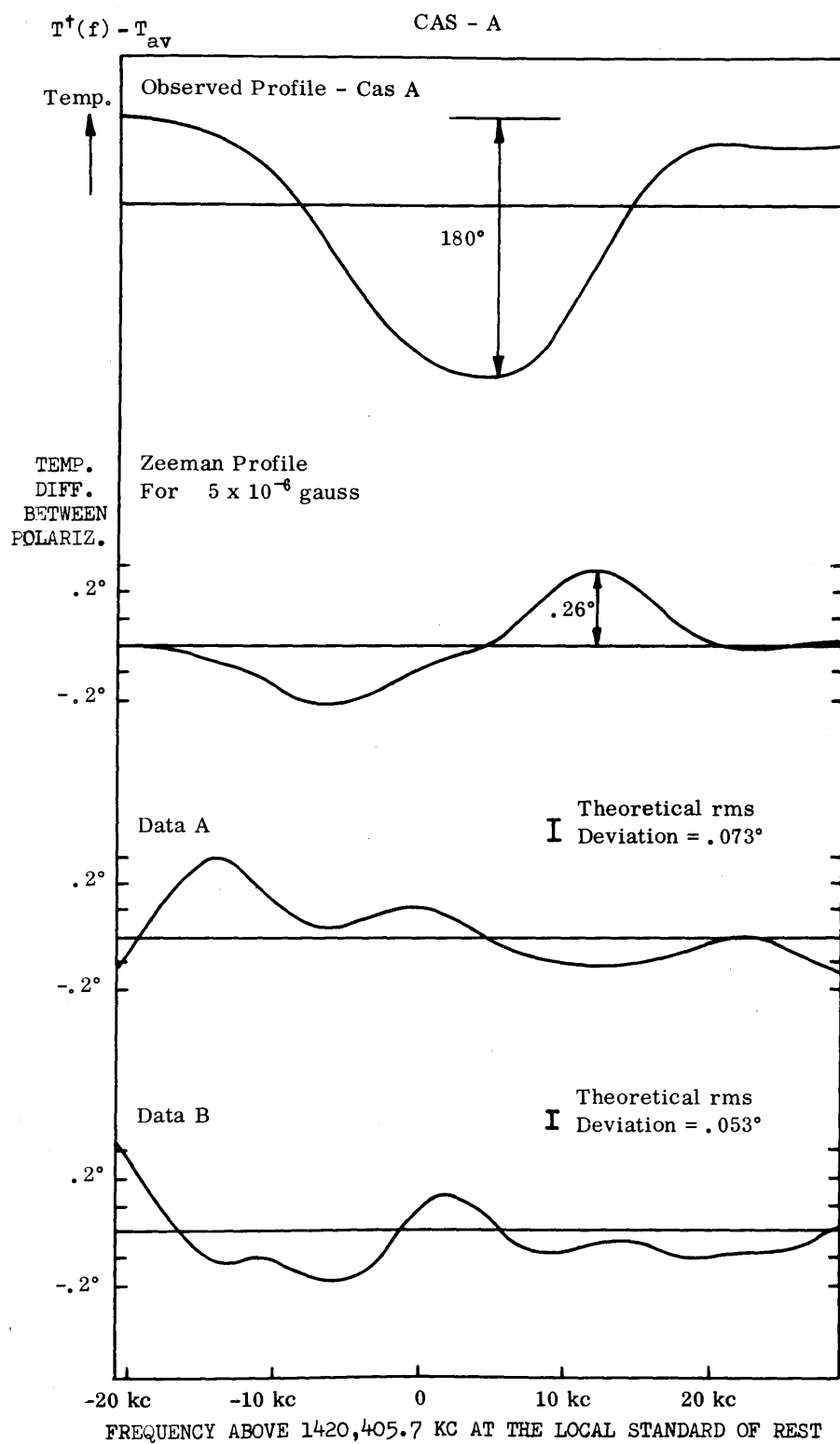


FIG. 8.1 - Results of attempt to measure Zeeman splitting of the 21-CM galactic hydrogen line observed in absorption of the Cas A radio source.

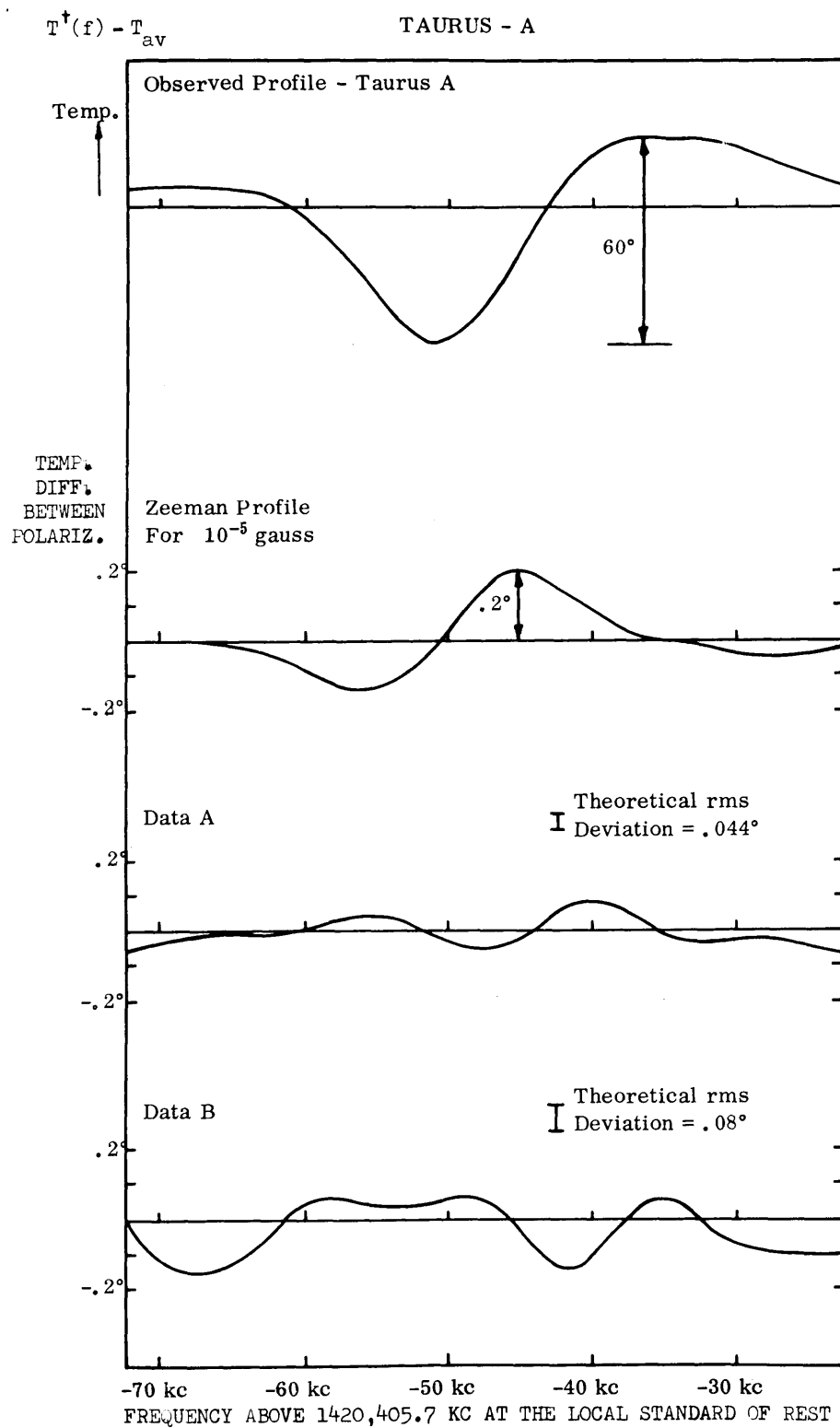


FIG. 8.2 - Results of attempt to measure Zeeman splitting of the 21-CM galactic hydrogen line observed in absorption of the Taurus A radio source.

APPENDIX A

EQUIVALENCE OF THE FILTER METHOD AND THE
AUTOCORRELATION METHOD OF SPECTRAL ANALYSIS*

Two methods of measuring the power spectrum are presented in Figure 1.2, the filter method having output, $P_F^f(i\delta f)$, and the autocorrelation method having output, $P_A^f(i\delta f)$. Each of these outputs is a set of N numbers ($i=0, N-1$) which estimate the power spectrum at N frequencies spaced δf apart. In this appendix it will be shown that the two methods are equivalent if the filter impulse responses, $h_i(t)$, are related to the autocorrelation weighting function, $w(\tau)$, in a certain manner. The equivalence of the two systems simply means that for any common input, $x(t)$, the outputs are equal, $P_F^f(i\delta f) = P_A^f(i\delta f)$.

The input-output relations of the two systems are,

$$\begin{aligned}
 P_A^f(i\delta f) &= 2\Delta\tau w(0) \frac{1}{T} \int_0^T x^2(t) dt \\
 &+ 4\Delta\tau \sum_{n=1}^{N-1} w(n\Delta\tau) \cos(2\pi i\delta f n\Delta\tau) \\
 &\cdot \frac{1}{T} \int_0^T x(t) x(t+n\Delta\tau) dt
 \end{aligned} \tag{A.1}$$

* I would like to thank R. Price, M.I. T. Lincoln Laboratory, for pointing out the relations presented in this section to me.

$$P_F'(i\delta f) = \frac{1}{T} \int_0^T \left[\int_0^T x(t) h_i(\lambda-t) dt \right]^2 d\lambda \quad (\text{A. 2})$$

We will manipulate Equation A. 2 so that it takes the form of Equation A. 1. In order to do so we must make approximations which are quite valid provided the observation time, T , is much greater than the filter time constants. In other words,

$$T \gg \tau_m$$

$$\text{where } h_i(\tau) = 0 \text{ for } \tau > \tau_m. \quad (\text{A. 3})$$

This condition is necessary in practice in order to give a meaningful spectral estimate.

After expanding the square of the integral in Equation A. 2 and interchanging the order of integration, we obtain,

$$P_F'(i\delta f) = \frac{1}{T} \int_0^T \int_0^T x(t) x(s) \int_0^T h_i(\lambda-t) \cdot h_i(\lambda-s) d\lambda ds dt \quad (\text{A. 4})$$

A change of variable, $\tau = s-t$, gives,

$$P_F'(i\delta f) = \frac{1}{T} \int_0^T \int_{-t}^{T-t} x(t) x(t+\tau) \int_0^T h_i(\lambda-t) \cdot h_i(\lambda-t-\tau) d\lambda d\tau dt \quad (\text{A. 5})$$

If the condition of Equation A. 3 is used, the integral on λ can be very closely approximated by,

$$g_i(\bar{\tau}) = \int_0^{\infty} h_i(\lambda) h_i(\lambda - \tau) d\lambda \quad (\text{A. 6})$$

to give,

$$P'_F(i\delta f) = \frac{1}{T} \int_0^T \int_{-t}^{T-t} x(t) x(t+\tau) g_i(\tau) d\tau dt \quad (\text{A. 7})$$

Upon examination of Equations (A. 1) and (A. 7) we notice that they will be similar if we require,

$$g_i(\tau) = 2\Delta\tau \sum_{n=-(N-1)}^{N-1} w(n\Delta\tau) \cos(2\pi i\delta f n\Delta\tau) \delta(\tau - n\Delta\tau) \quad (\text{A. 8})$$

Equation A. 8 is substituted into Equation A. 7; the integral on τ becomes,

$$\int_{-t}^{T-t} x(t+\tau) \delta(\tau - n\Delta\tau) d\tau = x(t+n\Delta\tau) \quad (\text{A. 9})$$

An approximation based on condition (A. 3) has again been used in Equation A. 9; the argument of the impulse function will be between the limits of integration for the range of interest, $-(N-1)\Delta\tau < n\Delta\tau < (N-1)\Delta\tau$, if (A. 3) is valid.

The result, then, of the substitution of Equation A. 8 into Equation A. 7 is,

$$P_F'(i\delta f) = P_A'(i\delta f) \quad (\text{A. 10})$$

which is what we wished to prove.

The equality required by Equation A. 8 can be more easily understood if Fourier transforms are taken of both sides of the equation. The quantity, $g_i(\tau)$, is the autocorrelation of the filter impulse response, $h_i(t)$; its Fourier transform is simply the power transfer function of the filter, $G_i(f)$. The Fourier transform of the right-hand side of Equation A. 8 can be expressed in terms of the Fourier transform, $W(f)$, of the autocorrelation weighting function, $w(\tau)$. We obtain, then,

$$G_i(f) = \sum_{k=-\infty}^{\infty} \left[W(f - i\delta f - kf_s) + W(f + i\delta f + kf_s) \right] \quad (\text{A. 11})$$

This result is illustrated in Figure 1. 3. $G_i(f)$ consists of narrow lobes centered at $\pm i\delta f$, $f_s \pm i\delta f$, $2f_s \pm i\delta f$, If the true power spectrum is zero for $|f| > f_s/2$ (in practice we will force this to be the case) then only the lobes of $G_i(f)$ at $\pm i\delta f$ are of any importance and an equivalent filter bandpass is,

$$G_i(f) = W(f - i\delta f) + W(f + i\delta f) \quad (\text{A. 12})$$

Finally, if we only consider positive frequencies which are not close to DC (see Figure 1.3), then,

$$G_1(f) = W(f - i\delta f) \quad (\text{A.13})$$

APPENDIX B

THE E1B METHOD OF AUTOCORRELATION
FUNCTION MEASUREMENT

The material presented in this section is based upon papers by Veltmann and Kwackernaak,⁹ and Jespers, Chu, and Fettweis.¹⁰ Reference (9) is in German and is not readily available. The second reference (10) is to a paper presented at a conference in Belgium; only the conference abstracts are available. For these reasons and in view of the importance of References (9) and (10) to spectral measurements, a summary of the results are given here. See Table I for a comparison of the method of this section with that (A1B) of the bulk of this paper.

Suppose we wish to measure the cross correlation functions of $x_1(t)$ and $x_2(t)$, stationary, ergodic, random signals bounded by $\pm A_1$ and $\pm A_2$, respectively. [For autocorrelation, $x_1(t) = x_2(t)$.] Two auxiliary functions, $z_1(t)$ and $z_2(t)$, having uniform probability density of $1/(2A_1)$ and $1/(2A_2)$ between $\pm A_1$ and $\pm A_2$, respectively, must be introduced. These auxiliary functions must be stationary, ergodic and statistically independent of each other, $x_1(t)$, and $x_2(t)$; that is, the joint probability density function factors,

$$p(x_1, x_2, z_1, z_2) = p(x_1, x_2) p(z_1) p(z_2) \quad (\text{B. 1})$$

$$\begin{aligned}
&= \frac{p(x_1, x_2)}{2A_1 \cdot 2A_2} && |z_1| < A_1 \\
& && |z_2| < A_2 \\
&= 0 && |z_1| > A_1 \\
& && |z_2| > A_2
\end{aligned} \tag{B.2}$$

for all arguments of x_1 , x_2 , z_1 , and z_2 .

The auxiliary functions are used as variable clipping levels for $x_1(t)$ and $x_2(t)$. The outputs of these "variable clippers" are $y_1(t)$ and $y_2(t)$, where,

$$\begin{aligned}
y_1(t) &= 1 && \text{when } x_1(t) > z_1(t) \\
y_1(t) &= -1 && \text{when } x_1(t) < z_1(t)
\end{aligned} \tag{B.3}$$

with identical equations for y_2 , x_2 , and z_2 .

Since $y_1(t)$ and $y_2(t)$ are either one of two values, their cross-correlation functions are easily calculated with a one-bit digital correlator which computes,

$$\rho_y'(n\Delta\tau) = \frac{1}{K} \sum_{k=1}^K y_1(k\Delta t) y_2(k\Delta t + n\Delta\tau) \tag{B.4}$$

for $n=0$ to $N-1$. An estimate, $R'_{12}(n\Delta\tau)$, of a point on the true cross-correlation function, $R_{12}(\tau)$, is then given as,

$$R'_{12}(n\Delta\tau) = A_1 A_2 \rho_y'(n\Delta\tau) \tag{B.5}$$

We will now prove that $R_{12}^*(n\Delta\tau)$ is an unbiased estimate of a point on the true crosscorrelation function, that is,

$$\overline{R_{12}^*(n\Delta\tau)} = R_{12}(n\Delta\tau) \quad (\text{B. 6})$$

Thus, a method is provided for estimating the crosscorrelation or autocorrelation functions of bounded signals through the use of a one-bit digital correlator.

The proof follows from simple manipulations of probability density functions. For convenience, we set $y_1(k\Delta t) = y_1$, $y_2(k\Delta t + n\Delta\tau) = y_2$ and likewise for $x_1(k\Delta t)$, $x_2(k\Delta t + n\Delta\tau)$, $z_1(k\Delta t)$, and $z_2(k\Delta t + n\Delta\tau)$. Equation B. 4 can be substituted into Equation B. 5 which, in turn, is substituted into Equation B. 6 to give,

$$\overline{R_{12}^*(n\Delta\tau)} = A_1 A_2 \overline{y_1 y_2} \quad (\text{B. 7})$$

where the stationarity of $y_1(k\Delta t)$ and $y_2(k\Delta t + n\Delta\tau)$ has been used.

The product, $y_1 y_2$, is either +1 or -1, and thus $\overline{y_1 y_2}$ can be written as,

$$\overline{y_1 y_2} = (1) [P[y_1 y_2 = 1]] + (-1) P[y_1 y_2 = -1] \quad (\text{B. 8})$$

$$= 2 P[y_1 y_2 = 1] - 1 \quad (\text{B. 9})$$

$$= 2 P[y_1 = 1, y_2 = 1] + 2 P[y_1 = -1, y_2 = -1] - 1 \quad (\text{B. 10})$$

$$= 2 P[z_1 < x_1, z_2 < x_2] + 2 P[z_1 > x_1, z_2 > x_2] - 1 \quad (\text{B. 11})$$

($P[y_1 y_2 = 1]$ means, "probability $y_1 y_2 = 1$ "). The term, $P[z_1 < x_1, z_2 < x_2]$, can be written as an integral over the joint probability density function, $p(x_1, x_2, z_1, z_2)$

$$P \left[z_1 < x_1, z_2 < x_2 \right] = \int_{-\infty}^{\infty} \int_{-\infty}^{\infty} \int_{-\infty}^{x_1} \int_{-\infty}^{x_2} p(x_1, x_2, z_1, z_2) dz_1 dz_2 dx_1 dx_2 \quad (\text{B. 12})$$

Upon substitution of Equation B. 2 into Equation B. 12 and through the use of the boundedness of x_1 and x_2 , we obtain

$$P \left[z_1 < x_1, z_2 < x_2 \right] = \frac{1}{4A_1 A_2} \int_{-A_1}^{A_1} \int_{-A_2}^{A_2} \int_{-A_1}^{x_1} \int_{-A_2}^{x_2} p(x_1, x_2, z_1, z_2) dz_1 dz_2 dx_1 dx_2 \quad (\text{B. 13})$$

$$= \frac{1}{4A_1 A_2} \int_{-A_1}^{A_1} \int_{-A_2}^{A_2} (x_1 + A_1)(x_2 + A_2) p(x_1, x_2) dx_1 dx_2 \quad (\text{B. 14})$$

$$= \frac{1}{4A_1 A_2} \left[\overline{x_1 x_2} + \overline{x_1} A_2 + \overline{x_2} A_1 + A_1 A_2 \right] \quad (\text{B. 15})$$

A similar manipulation of $p \left[z_1 > x_1, z_2 > x_2 \right]$ gives,

$$P \left[z_1 > x_1, z_2 > x_2 \right] = \frac{1}{4A_1 A_2} \left[\overline{x_1 x_2} - \overline{x_1} A_2 - \overline{x_2} A_1 + A_1 A_2 \right] \quad (\text{B. 16})$$

Equations B. 15 and B. 16 can be substituted into Equations B. 11 and B. 7 to give the desired result,

$$\overline{R_{12}^2(n\Delta\tau)} = \overline{x_1 x_2} \quad (\text{B. 17})$$

$$= \overline{R_{12}(n\Delta\tau)} \quad (\text{B. 18})$$

APPENDIX C

CALCULATION OF THE COVARIANCES OF MANY-BIT ESTIMATES
OF THE AUTOCORRELATION FUNCTION
& POWER SPECTRUM

In this appendix the covariances, $\sigma_{Pm}^2(f_1, f_2)$ and $\sigma_{Rm}^2(n, m)$, defined in Section 2.3-1, are calculated. The results are discussed in Section 2.3-2.

Calculation of $\sigma_{Rm}^2(n, m)$ proceeds by substitution of the definition of $R''(n\Delta\tau)$, Equation 2.4, into Equation 2.23, to give

$$\sigma_{Rm}^2(n, m) = \frac{1}{K^2} \sum_{k=1}^K \sum_{g=1}^K \overline{x(k\Delta t) x(k\Delta t + |n|\Delta\tau) x(g\Delta t) x(g\Delta t + |m|\Delta\tau)} - R(n\Delta\tau) R(m\Delta\tau) \quad (C.1)$$

Fortunately, for a Gaussian random process, the joint fourth moment of the process can be expressed in terms of products of autocorrelation functions (see Davenport and Root,¹ p. 108),

$$\begin{aligned} \overline{x(k\Delta t) x(k\Delta t + |n|\Delta\tau) x(g\Delta t) x(g\Delta t + |m|\Delta\tau)} &= R(n\Delta\tau) R(m\Delta\tau) \\ &+ R(i\Delta t + |n|\Delta\tau - |m|\Delta\tau) R(i\Delta t) \\ &+ R(i\Delta t + |n|\Delta\tau) R(i\Delta t - |m|\Delta\tau) \quad (C.2) \end{aligned}$$

where we have set $i = k - g$.

Substitution of Equation C. 2 into Equation C. 1 gives,

$$\sigma_{Rm}^2(n, m) = \frac{1}{K^2} \sum_{i=-K}^K (K-|i|) \left[R(i\Delta t + |n|\Delta\tau) R(i\Delta t - |m|\Delta\tau) + R(i\Delta t + |n|\Delta\tau) R(i\Delta t - |m|\Delta\tau) \right] \quad (C. 3)$$

where a change of variable ($i = k - g$) has eliminated one summation. Thus, we have found the autocorrelation covariance in terms of the autocorrelation function.

Equation C. 3 can be simplified if it is assumed that $R(i\Delta t) = 0$ for $i > i_{\max}$, where $i_{\max} \ll K$. This will be true in the practical case of interest and we obtain,

$$\sigma_{Rm}^2(n, m) = \frac{1}{K} \sum_{i=-K}^K \left[R(i\Delta t + |n|\Delta\tau - |m|\Delta\tau) R(i\Delta t) + R(i\Delta t + |n|\Delta\tau) R(i\Delta t - |m|\Delta\tau) \right] \quad (C. 4)$$

The above result will be used to calculate the spectral variance. For this purpose it is convenient to express $\sigma_{Rm}^2(n, m)$ in terms of $P(f)$ instead of $R(\tau)$. This is done by substituting the inverse transform relation, Equation 1. 14, into Equation C. 4. The result is,

$$\sigma_{Rm}^2(n, m) = \frac{1}{4K} \sum_{i=-K}^K \int_{-\infty}^{\infty} \int_{-\infty}^{\infty} P(f) P(\alpha) e^{j2\pi(f+\alpha)i\Delta t} \cdot e^{j2\pi fn\Delta\tau} \cdot \left[e^{-j2\pi fm\Delta\tau} + e^{-j2\pi\alpha m\Delta\tau} \right] df d\alpha \quad (C. 5)$$

The summation on i can be expressed in closed form as (Reference Data for Radio Engineers, ¹⁴ p. 1042),

$$\sum_{i=-K}^K e^{j2\pi(f+\alpha)i\Delta t} = \frac{\sin[\pi(f+\alpha)(2K+1)\Delta t]}{\sin[\pi(f+\alpha)\Delta t]} \quad (\text{C. 6})$$

$$\approx \frac{1}{\Delta t} \sum_{k=-\infty}^{\infty} \delta(f+\alpha - kf_t) \quad (\text{C. 7})$$

where $f_t = 1/\Delta t$.

The approximation is valid for the purpose of carrying out the integration on α in Equation C. 5 since the other terms in Equation C. 5 can be considered constant over regions of width, $1/K\Delta t$. The result of this operation is,

$$\begin{aligned} \sigma_{Rm}^2(n, m) &= \frac{1}{4K\Delta t} \sum_{k=-\infty}^{\infty} \int_{-\infty}^{\infty} P(f) P(kf_t - f) e^{j2\pi f|n|\Delta\tau} \\ &\quad \cdot \left[e^{-j2\pi f|m|\Delta\tau} + e^{-j2\pi(kf_t - f)|m|\Delta\tau} \right] df \end{aligned} \quad (\text{C. 8})$$

The spectral covariance, $\sigma_{Pm}^2(f_1, f_2)$, is given in terms of $\sigma_{Pm}^2(n, m)$ by Equation 2. 24. Before making this substitution, a great deal of complexity can be avoided by making an assumption which removes the absolute value signs in Equation C. 8. The absolute value signs arose in the definition of $R''(n\Delta\tau)$ by Equation 2. 4. They can

be removed if $|n|$ can be replaced by $-n$ in Equation 2.4 without a change; that is, we must show,

$$R''(n\Delta\tau) = \frac{1}{K} \sum_{k=1}^K x(k\Delta t) x(k\Delta t - n\Delta\tau) \quad (\text{C. 9})$$

This can be done if we assume $\Delta\tau = h\Delta t$, where h is an integer and $K \gg nh$. This assumption applies in the practical case of interest (the correlator is more complex if h is not an integer and the statistical uncertainty is large if K is not much greater than nh) and the substitution, $k' = k - nh$, leads to the proof.

Equation C.8 (with absolute value signs removed) can now be substituted into Equation 2.24 along with the following Fourier transform relations for $w(n\Delta\tau) w(m\Delta\tau)$,

$$w(n\Delta\tau) w(m\Delta\tau) = \int_{-\infty}^{\infty} \int_{-\infty}^{\infty} W(\beta) W(\gamma) e^{j2\pi\Delta\tau(n\beta+m\gamma)} d\beta d\gamma \quad (\text{C. 10})$$

The resulting expression for $\sigma_{Pm}^2(f_1, f_2)$ is rather long as it involves three summations (indices: k , n , and m) and three integrations (variables: f , β , and γ). However, two of the summations (n and m) can be expressed in terms of sums of impulses (new indices: μ and ν), which allows the integrations on β and γ to be performed. The result of these operations is,

$$\sigma_{\text{Pm}}^2(f_1, f_2) = \frac{1}{K\Delta t} \sum_{k=-\infty}^{\infty} \sum_{\mu=-\infty}^{\infty} \sum_{\nu=-\infty}^{\infty} \int_{-\infty}^{\infty} P(f) P(kf_t - f) \cdot W(f + f_1 - \mu f_s) \left[W(f - f_2 + \nu f_s) + W(f + f_2 - \nu f_s - kf_t) \right] df \quad (\text{C. 11})$$

In order to obtain minimum variance, f_t should be chosen high enough so that

$$P(f) = 0 \quad \text{for } |f| > f_t/2 \quad (\text{C. 12})$$

In this case, only the $k=0$ term is non-zero in the summation on k in Equation C. 11. The μ and ν summations can similarly be reduced if f_s is chosen large enough to avoid the spurious responses due to sampling of the autocorrelation function. The exact requirement is that f_s be chosen large enough so that,

$$\int_{-\infty}^{\infty} P^2(f) W(f+a) W(f+b) df = 0 \quad (\text{C. 13})$$

for $|a|$ and $|b| > f_s/2$.

If the requirements of Equations C. 12 and C. 13 are met, and we consider only $|f_1|$ and $|f_2| < f_s/2$, then Equation C. 11 can be simplified to,

$$\sigma_{\text{Pm}}^2(f_1, f_2) = \frac{1}{K\Delta t} \int_{-\infty}^{\infty} P^2(f) W(f+f_1) \left[W(f+f_2) + W(f-f_2) \right] df \quad (\text{C. 14})$$

In practice, f_t and f_s should both be chosen equal to $2B$, which is twice the highest frequency of a component in the power spectrum. This choice gives minimum variance and no spurious responses due to sampling. In this case conditions C. 12 and C. 13 are approximately obeyed and Equation C. 14 gives an accurate description of the spectral variance.

APPENDIX D

COMPUTER PROGRAMS

Some of the computer programs developed for this work are given here. The programs may be helpful to a reader concerned with some specific detail of the Zeeman, deuterium-line, or computer-simulation experiments and may also be of small aid to people who wish to write similar programs in the future. The programs are written in the Fortran language for use with the IBM 1620 computer.

D. 1 DOPPLER CALCULATION PROGRAM

The frequency of a spectral line received from galactic sources is Doppler shifted from the rest frequency of the line because of the following motions:

- 1) Rotation of the earth about its axis.
- 2) The orbital motion of the earth around the sun.
- 3) The motion of the sun with respect to a group of nearer stars which form a velocity reference point called the local standard of rest.
- 4) The motion of the sources of the spectral line with respect to the local standard of rest.

The program given on the next two pages calculates the line-of-sight component of the first three of the above velocities. The line-of-sight component of the last velocity is specified as data (VLSR) to the program which then gives the observed frequency, F , for a given rest frequency, F_0 .

The calculation method is that given by MacRae and Westerhout.⁴¹ For convenience in setting local oscillators, the program will calculate two linear functions of F . These are, $F1 = F \cdot Y1 + Z1$, and, $F2 = F \cdot Y2 + Z2$, where $Y1$, $Z1$, $Y2$, and $Z2$ are constants which are specified as data to the program. The following additional data must also be supplied to the program:

1) The right-ascension (RA HR, RA MIN, RA SEC) and declination (D DEG, D MIN) of the observed direction.

2) The date in units of sidereal days from November 5, 1961.

The program will then calculate the number of mean solar days from November 5, 1961 and will specify the eastern standard time when the source is at transit (right-ascension equals sidereal time). The frequency correction will then be calculated for hour angles of -6 to $+6$ in increments of HT hours, where HT is supplied as data.

3) The program assumes the observation point is Green Bank, W. Virginia. If a different observation point is used, the correct latitude must be used in the statement specifying CAT, and the correct relation between local time and sidereal time must be used in the statement specifying EST1.

41. D. A. MacRae and G. Westerhout, "Table for the Reduction of Velocities to the Local Standard of Rest," published by the Observatory, Lund, Sweden, 1956.

C DOPPLER CALCULATION PROGRAM

```

CL=2.998E+5
CAT= 3.1415926*(38.+26./60.+11./3600.)/180.
C1=(23.+56./60.+4.099/3600.)/24.
C2=(21.+40./60.+32.5/3600.)/24.
C3=3.1415926*(280.+8./60.+33.9/3600.)/180.
E=.0167268
P=3.1415926*(282.+13./60.+5./3600.)/180.
5 READ 100, RAHR, RAMIN, RASEC, DDEG, DMIN
PRINT 105, RAHR, RAMIN, RASEC, DDEG, DMIN
READ 101, F0, VLSR, T, HT, Y1, Z1, Y2, Z2, F01
PRINT 106, F0, VLSR, T, HT, Y1, Z1, Y2, Z2, F01
KT=6./HT
K1=KT+1
K2=2*KT+1
RA1=(RAHR+RAMIN/60. +RASEC/3600.)/24.
RA=2.*3.1415926*RA1
DEC=3.1415926*(DDEG/180.+DMIN/10800.)
CC=COSF(DEC)*COSF(RA)
CS=COSF(DEC)*SINF(RA)
S=SINF(DEC)
PRINT 107, CC, CS, S
PAUSE
1 RAT=T+RA1
EST1=19./24.+C1*(RAT-C2)
ND=EST1
D=ND
NH=(EST1-D)*24.
H=NH
NM=(EST1-D-H/24.)*1440.
DM=NM
NS=(EST1-D-H/24.-DM/1440.)*86400.
PRINT 102, ND, NH, NM, NS
PRINT 108, RAHR, RAMIN, RASEC
PRINT, DDEG, DMIN
PRINT, F0, VLSR
PRINT,
PRINT,
DO 4 K=1,K2
XK=K-K1
XK=HT*XK
EST2=C1*(T+RA1+XK/24.-C2)
XL=(2.*3.1415926/365.2564)*(EST2+1405.)+C3
XLAM=XL+2.*E*SINF(XL-P)+1.25*E*E*SINF(2.*(XL-P))
A=-29.804*SINF(XLAM)+.319
B=27.344*COSF(XLAM)+17.417
C=11.858*COSF(XLAM)-9.958
V=A*CC+B*CS+C*S
VE=+.465*COSF(CAT)*COSF(DEC)*SINF(3.14159*XK/12.)
V1=V+VLSR+VE
DELF=- (F0/CL)*V1
F=F01+DELF
F1=Y1*F+Z1

```

C DOPPLER CALCULATION PROGRAM CONTINUED

```

F2=Y2*F+Z2
IF (SENSE SWITCH 1) 2,3
2 PRINT 103, XK, F1, V1, VE, V
GO TO 4
3 PRINT 104, XK, F1, F2
4 CONTINUE
PRINT,
PRINT,
IF (SENSE SWITCH 2) 5,6
6 T=T+1.
GO TO 1
END

```

C DATA CARDS

C NEXT TWO CARDS FOR CAS A

23. 21. 38. 58. 35.2

1420405.73 -.8 33. .5 1. 1400000. .1 0. 20405.73

C NEXT TWO CARDS FOR TAURUS A

5. 32. 6. 22. 00.1

1420405.73 10.1 25. .5 1. 1400000. .1 0. 20405.73

C NEXT TWO CARDS FOR SAG A

17. 43. 22. -28. 57.2

1420405.73 6. 27. .5 1. 1400000. .1 0. 20405.73

TOTAL

D. 2 DEUTERIUM AND ZEEMAN DATA ANALYSIS PROGRAM

The program that is described in this section takes in as data the output of the one-bit digital correlator and produces the spectral estimate, $c(f)$, described in Section 6.5-1. The program is broken up into the following five steps:

- 1) The cos weighting function described in Section 2.2-2 is generated.
- 2) The computer reads in the digital correlator output on punch cards. The correlator output consists of 21 numbers which have accumulated in a combination of binary and decimal counters. After read-in, these numbers are converted to the computer's binary-coded-decimal number system.
- 3) The correlator output is normalized according to Equation 5.3 or 5.4 dependent on whether the radiometer was operated in the switched mode of operation (MODE = 2 in the program) or the unswitched mode of operation (MODE = 1 in the program). The switched mode of operation was used for the actual data while the unswitched mode was used to determine the receiver bandpass function, $p'_0(f)$. The autocorrelation function correction (for the effect of clipping) is programmed according to Equation 4.19 for switched mode and Equation 3.15 for the unswitched mode.
- 4) The sampled-data Fourier transform is performed as indicated by Equation 3.29.
- 5) The resulting difference spectrum, $\delta p'(f)$, is divided by the receiver bandpass function, $p'_0(f)$ [SBP(I) in the program], to give the normalized spectral estimate, $s(f)$. The slope of this spectrum is adjusted to be zero as was discussed in Section 6.5-1. The final output spectrum is then typed out and punched on cards.

C DEUTERIUM - ZEEMAN DATA ANALYSIS PROGRAM

C SENSE SWITCH 1 ON FOR PUNCH OUTPUT
C SENSE SWITCH 2 ON FOR PRINT OUTPUT

DIMENSION W(21),A(21),B(21),RBP(21),R(21),S(38),SBP(38),D(21)

C GENERATION OF WEIGHTING FUNCTION,W(K)

DO 1 K=1,21

FLO=K-1

1 W(K)=.5+.5*COSF(3.14159265*FLO/21.)

C DATA INPUT AND OCTAL - FRACTION CONVERSION.

5 READ,NRUN,MODE,SIGN

DO 6 K=1,21

6 READ,A(K),B(K)

PUNCH,NRUN,MODE,A(1),SIGN

PRINT,NRUN,MODE,A(1),SIGN

PRINT,

7 DO 14 K=1,21

OC1=0.

OC2=0.

OC3=0.

8 IF(B(K)-100.)10,9,9

9 OC1=OC1+1.

B(K)=B(K)-100.

GO TO 8

10 IF(B(K)-10.)12,11,11

11 OC2=OC2+1.

B(K)=B(K)-10.

GO TO 10

12 IF(B(K)-1.)14,13,13

13 OC3=OC3+1.

B(K)=B(K)-1.

GO TO 12

14 D(K)=OC1/8.+OC2/64.+OC3/512.+A(K)

C NORMALIZATION AND CORRECTION

C=1.5707963

IF(MODE-1)15,15,17

C MODE 1

15 DO 16 K=1,21

RBP(K)=(2.*D(K)-D(1))/D(1)

16 R(K)=SINF(C*RBP(K))

GO TO 19

C MODE 2

17 D1=D(1)

DO 18 K=1,21

18 R(K)=2.*SINF(C*(D(K)-D1)/D1)*COSF(C*RBP(K))*SIGN

19 IF(SENSE SWITCH 2) 20,220

20 DO 21 K=1,21,3

21 PRINT,R(K),R(K+1),R(K+2)

PRINT,

C DEUTERIUM - ZEEMAN DATA ANALYSIS PROGRAM CONTINUED

```
220 IF (SENSE SWITCH 1) 22,24
22 DO 23 K=1,21,3
23 PUNCH,R(K),R(K+1),R(K+2)
```

C FOURIER TRANSFORM S I OF W K R K

```
24 T=1./75.
    DF=1.0
AA=2.*T
BB=6.2831853*T*DF
DO 25 K=1,21
25 R(K)=R(K)*W(K)
CC=R(1)*T
J=0
    DO 30 I=1,38
S(I)=CC
DO 26 K=2,21
DD=(K-1)*(I-1)
26 S(I)=S(I)+AA*R(K)*COSF(BB*DD)
S1=10000.*S(I)
IF (SENSE SWITCH 2) 28,290
    28 PRINT,J,S1
290 IF (SENSE SWITCH 1) 29,30
    29 PUNCH,J,S1
PRINT,
```

C FINISHING OPERATIONS

```
IF(MODE=1)31,31,33
C MODE 1
    31 DO 32 I=1,38
32 SBP(I)=S(I)
GO TO 5
C MODE 2
    33 J=0
        DO 39 I=1,38
34 S(I)=100.*S(I)/SBP(I)
IF (SENSE SWITCH 2) 36,380
    36 PRINT,J,S(I)
380 IF (SENSE SWITCH 1) 38,39
    38 PUNCH,J,S(I)
39 J=J+1
PRINT,
IF (SENSE SWITCH 3) 141,140
141 READ,C1,C2
B1=C1/60.
A1=C2-34.*B1
PRINT,C1,C2
GO TO 142
    140 U=0
V=0.
W1=0.
```

C DEUTERIUM - ZEEMAN DATA ANALYSIS PROGRAM CONTINUED

```
X=0.
Y=0.
Z=0.
      DO 35 I=6,31
G=I
U=U+S(I)
V=V+G*S(I)
W1=W1+1.
X=X+G
Y=Y+G*G
35 Z=Z+S(I)*S(I)
D1=W1*Y-X*X
A1=(U*Y-X*V)/D1
B1=(V*W1-X*U)/D1
RMS1=SQRF(Z/W1)
H=Z-A1*A1*W1-B1*B1*Y-2.*A1*B1*X
RMS2=SQRF(H/W1)
C1=60.*B1
C2=A1+34.*B1
40 IF (SENSE SWITCH 2) 41,420
41 PRINT,RMS1,RMS2,C1,C2
PRINT,
420 IF (SENSE SWITCH 1) 42,142
42 PUNCH,RMS1,RMS2,C1,C2
142 J=0
43 DO 48 I=1,38
G=I
44 S(I)=S(I)-A1-B1*G
IF (SENSE SWITCH 2) 45,147
45 PRINT,J,S(I)
147 IF (SENSE SWITCH 4) 47,48
47 PUNCH,J,S(I)
48 J=J+1
DO 2 K=1,4
2 PRINT,
GO TO 5
END
```

TOTAL

D.3 COMPUTER SIMULATION PROGRAM

The program listed in this section was used to simulate the signal and the signal processing system. This topic was discussed in Section 6.2. A block diagram of the program is given in Figure 6.1.

The time required to run this program on the IBM 1620 computer was approximately 100 hours; however, this time did not have to be continuous. If Sense Switch 1 was turned on, the computer would punch out cards containing all of the useful results that had been computed up to that time. These cards could then be fed back into the machine at a later time. In this way the 100 hours computing time was accumulated mostly at night and on weekends.

C COMPUTER SIMULATION PROGRAM

```
DIMENSION H(40),AR(21),AS(38),SW(38,21),ARX(21),VRX(21),ARY(21)
DIMENSION VRY(21),ASX(38),VSX(38),ASY(38),VSY(38),W(40),X(21)
DIMENSION Y(21),RX(21),RY(21),SX(38),SY(38)
IM=40
NM=21
LM=38
KM=21
DO 9 I=1,IM
  9 READ,H(I)
DO 11 N=1,NM
  11 READ,AR(N)
DO 13 L=1,LM
  13 READ,AS(L)
  READ,F,F2,T2
  READ,Z1,Z2,KZ
  IF(F)17,17,28
  17 DO 21 N=1,NM
    ARX(N)=0.
    VRX(N)=0.
    ARY(N)=0.
  21 VRY(N)=0.
  DO 26 L=1,LM
    ASX(L)=0.
    VSX(L)=0.
    ASY(L)=0.
  26 VSY(L)=0.
  GO TO 32
  28 DO 29 N=1,NM
    29 READ,ARX(N),ARY(N),VRX(N),VRY(N)
  DO 31 L=1,LM
    31 READ,ASX(L),ASY(L),VSX(L),VSY(L)
  32 FKZ=KZ
  V=SQRF(3.3326563E7*FKZ)
  U=4999.5*FKZ
  IM1=IM+1
  NM1=NM+1
  PI=3.1415926
  PI1=PI*.5
  PI2=PI/21.
  PI3=2.*PI/75.
  DO 46 L=1,LM
    DO 45 K=1,KM
      SWK=K-1
      SWLK=(L-1)*(K-1)
    45 SW(L,K)=(.5+.5*COSF(PI2*SWK))*COSF(PI3*SWLK)
  46 CONTINUE
  T1=IM+NM+9
  T3=T2+T1
  A=.33
  B=.59
  49 F=F+1.
  JF=F
  PRINT,JF
```

C COMPUTER SIMULATION PROGRAM CONTINUED

```

      DO 53 I=1,IM
53  W(I)=0.
      DO 58 N=1,NM
      X(N)=0.
      Y(N)=0.
      RX(N)=0.
58  RY(N)=0.
      T=1.
60  DO 61 I=2,IM
61  W(I-1)=W(I)
      DO 64 N=2,NM
      X(N-1)=X(N)
64  Y(N-1)=Y(N)
      ZT=0.
      DO 74 K=1,KZ
      Z=Z1*Z2
      IF(Z-B)69,70,70
69  Z=Z+A.
70  Z1=Z2
      Z2=Z
      NZ=Z*1.E8
      Z=NZ
74  ZT=ZT+Z
      W(IM)=(ZT-U)/V
      X(NM)=0.
      DO 78 I=1,IM
      IM2=IM1-I
78  X(NM)=X(NM)+H(I)*W(IM2)
      IF(X(NM))83,83,85
83  Y(NM)=-1.
      GO TO 86
85  Y(NM)=1.
86  IF(T-T1)88,80,80
80  DO 81 N=1,NM
      NM2=NM1-N
      RY(N)=RY(N)+Y(NM)*Y(NM2)
81  RX(N)=RX(N)+X(NM)*X(NM2)
88  T=T+1.
      IF (SENSE SWITCH 3) 82,84
82  JT=T
      PRINT, JT
84  CONTINUE
      IF(T-T3)60,60,90
90  RX1=RX(1)*.0001
      RY1=RY(1)
      DO 98 N=1,NM
      RX(N)=RX(N)/RX1
      ARX(N)=ARX(N)+RX(N)
      VRX(N)=VRX(N)+(RX(N)-AR(N))**2
      RY(N)=SINF(PI1*RY(N)/RY1)*10000.
      ARY(N)=ARY(N)+RY(N)
98  VRY(N)=VRY(N)+(RY(N)-AR(N))**2

```

C COMPUTER SIMULATION PROGRAM CONTINUED

```
DO 101 L=1,LM
  SX(L)=0.
101 SY(L)=0.
  DO 111 L=1,LM
  DO 105 K=2,KM
  SX(L)=SX(L)+RX(K)*SW(L,K)
105 SY(L)=SY(L)+RY(K)*SW(L,K)
  SX(L)=(10000.+2.*SX(L))/75.
  ASX(L)=ASX(L)+SX(L)
  VSX(L)=VSX(L)+(SX(L)-AS(L))**2
  SY(L)=(10000.+2.*SY(L))/75.
  ASY(L)=ASY(L)+SY(L)
111 VSY(L)=VSY(L)+(SY(L)-AS(L))**2
  IF(SENSE SWITCH 2)113,120
113 PRINT,RX1,RY1
  DO 116 N=1,NM
  NTAB=N-1
116 PRINT,NTAB,RX(N),RY(N)
  DO 119 L=1,LM
  LTAB=L-1
119 PRINT,LTAB,SX(L),SY(L)
120 IF(F-F2)121,131,131
121 IF(SENSE SWITCH 1)122,49
122 PUNCH,F,F2,T2
  PUNCH,Z1,Z2,KZ
  DO 125 N=1,NM
125 PUNCH,ARX(N),ARY(N),VRX(N),VRY(N)
  DO 127 L=1,LM
127 PUNCH,ASX(L),ASY(L),VSX(L),VSY(L)
  PRINT,
  PRINT,F,F2,T2
  GO TO 135
131 PUNCH,0.,F2,T2
  PUNCH,Z1,Z2,KZ
  PRINT,
  PRINT,0.,F2,T2
135 PRINT,Z1,Z2,KZ
  PRINT,
  DO 144 N=1,NM
  ARX=ARX(N)/F
  ARY=ARY(N)/F
  VRX=SQRF(VRX(N)/F)
  VRY=SQRF(VRY(N)/F)
  IF(F-F2)143,142,143
142 PUNCH,ARX,ARY,VRX,VRY
143 NTAB=N-1
144 PRINT,NTAB,ARX,ARY,VRX,VRY
  PRINT,
  DO 153 L=1,LM
  ASX=ASX(L)/F
  ASY=ASY(L)/F
  VSX=SQRF(VSX(L)/F)/AS(L)
```

C COMPUTER SIMULATION PROGRAM CONTINUED

```

      VSY=SQRF(VSY(L)/F)/AS(L)
      IF(F-F2)152,151,152
151 PUNCH,ASX,ASY,VSX,VSY
152 LTAB=L-1
153 PRINT,LTAB,ASX,ASY,VSX,VSY
      FVSX=0.
      FVSY=0.
      DO 154 L=11,30
      FVSX=FVSX+.05*SQRF(VSX(L)/F)/AS(L)
154 FVSY=FVSY+.05*SQRF(VSY(L)/F)/AS(L)
      PRINT,
      PRINT, FVSX, FVSY
      STOP
      END

```

C DATA FOR COMPUTER SIMULATION PROGRAM

C H(I) NEXT TEN CARDS

4.0463063E-02	-.21109917	2.4860613E-07	-.52083049
-.40434399	-.46204016	-.77802933	-5.1404096E-07
-.54630318	.13955609	.17048281	-.99998148
4.6108997E-07	-3.3561187	-3.2113635	-4.7972268
-11.575174	-1.4725131E-06	-32.110496	61.544267
61.544267	-32.110496	-1.4725131E-06	-11.575174
-4.7972268	-3.2113635	-3.3561187	4.6108997E-07
-.99998148	.17048281	.13955609	-.54630318
-5.1404096E-07	-.77802933	-.46204016	-.40434399
-.52083049	2.4860613E-07	-.21109917	4.0463063E-02

C AR(N) NEXT TEN CARDS

10000.000	-.25521402	-3094.1803	-.36289696
-1801.3094	-.72864953	-501.72699	-2.9739641
210.65958	-5.8054740	242.76102	16.444171
29.214253	3.8847207	-74.478626	-3.3146357
-50.744705	-10.362919	7.3988346	-8.8327196
9.0940393	1.6463153	2.5638795	1.1505103
.29097677	.57754945	-1.1877550E-02	.27485701
.23565760	.16557374	.29605178	.12468219
.15563592	8.3742613E-02	2.7678368E-02	3.8857877E-02
-8.7503395E-03	9.2514949E-03	-3.5466145E-03	3.3990395E-04

C AS(L) IN TABLE 6.2

C Z1, Z2, KZ ON NEXT CARD

.75326499 .90037117 5

TOTAL

REFERENCES

1. W. B. Davenport and W. L. Root, Random Signals and Noise, McGraw-Hill, New York, 1958.
2. J. S. Bendat, Principles and Applications of Random Noise Theory, Wiley, New York, 1958
3. U. Grenander and M. Rosenblatt, Statistical Analysis of Stationary Time Series, Wiley, New York, 1957.
4. J. T. Tou, Digital and Sampled-Data Control Systems, McGraw-Hill, New York, 1959.
5. J. H. Van Vleck, "The Spectrum of Clipped Noise," Radio Res. Lab. Report No. 51, Harvard Univ.; July 21, 1943.
6. J. J. Faran and R. Hills, "Correlators for Signal Reception," Acoustics Res. Lab. Tech. Memo No. 27, Harvard Univ.; Sept. 1952.
7. J. F. Kaiser and R. K. Angell, "New Techniques and Equipment for Correlation Computation," Servomechanism Lab. Tech. Memo No. 7668-TM-2, M. I. T., Dec. 1957.
8. C. R. Green, "Measurement of Polarity Coincidence Correlation Functions Using Shift Register Elements," U. S. Naval Ordnance Lab. Report No. 4396, Dec. 17, 1956.
9. B. P. Veltmann and H. Kwakernaak, "Theorie und Technik der Polaritats - Korrelation fur die Dynamische Analyse Niederfrequenter Signale und Systeme," Regelungstechnik, Vol. 9, No. 9, pp. 357-364; Sept. 1961.
10. P. Jespers, P. T. Chu, and A. Fettweis, "A New Method for Computing Correlation Functions," International Symposium on Information Theory, Brussels; Sept. 3-7, 1962.

REFERENCES (Continued)

11. R. B. Blackman and J. W. Tukey, "The Measurement of Power Spectra", Dover, New York, 1958.
12. J. D. Kraus, Antennas, McGraw-Hill, New York, 1950.
13. C. L. Dolph, "A Current Distribution for Broadside Arrays which Optimizes the Relationship between Beam Width and Side-Lobe Level," Proc. IRE, Vol. 34, pp. 335-348; June, 1946.
14. Reference Data for Radio Engineers, Published by Federal Telephone and Radio, New York, 1956.
15. J. A. McFadden, "The Correlation Function of a Sine Wave Plus Noise after Extreme Clipping," IRE Transactions IT-2, pp. 66-67; June 1956.
16. H. B. Dwight, Tables of Integrals and Other Mathematical Data, 3rd Edition, Macmillan, New York, 1957.
17. J. A. McFadden, "Two Expansions for the Quadvariate Normal Integral," Biometrika, Vol. 47, pp. 325-333; 1960.
18. D. E. Norgaard, "The Phase-Shift Method of Single-Sideband Signal Reception," Proc. IRE, Vol. 44, pp. 1735-1743; December 1956.
19. D. G. C. Luck, "Properties of Some Wideband Phase-Splitting Networks," Proc. IRE, Vol. 37, pp. 147-151; February 1949.
20. R. S. Burington and D. C. May, Handbook of Probability and Statistics, Handbook Publishers, Sandusky, Ohio, 1953.
21. J. F. Kenney and E. S. Keeping, Mathematics of Statistics, 2nd Edition, Van Nostrand, Princeton, New Jersey, 1951.

REFERENCES (Continued)

22. J. Cohen and T. Orhaug, "Measurement of Output Characteristics of a Radiometer," Internal Report No. 1, National Radio Astronomy Observatory; June, 1962.
23. I. S. Shklovsky, Cosmic Radio Waves, Harvard University Press, Cambridge, Mass., 1960.
24. I. S. Shklovsky, *Astr. Zhur.*, Vol. 29, p. 144; 1952.
25. G. G. Getmanzev, K. S. Stankevitch, and V. S. Troitsky, "Detection of Monochromatic Radio Emission of Deuterium from the Center of the Galaxy on a Wavelength of 91.6 mc," *Dok. Akad. Nauk USSR*, Vol. 103, pp. 783-786; February, 1955.
26. G. J. Stanley and R. Price, "An Investigation of Monochromatic Radio Emission of Deuterium from the Galaxy," *Nature*, Vol. 177, pp. 1221-1222; June 30, 1956.
27. R. L. Adgie and J. S. Hey, "Intensity of the Radio Line of Galactic Deuterium," *Nature*, Vol. 179, p. 370; February, 1957.
28. R. L. Adgie, "An Attempt to Detect the 327 MC/S Line of Galactic Deuterium," *Paris Symposium on Radio Astronomy*, pp. 352-354; Stanford Press, 1958.
29. L. Heller, "Theories of Element Synthesis and the Abundance of Deuterium," *Astr. J.*, Vol. 126, pp. 341-355; September, 1957.
30. W. A. Fowler, "Nuclear Clues to the Early History of the Solar System," *Science*, Vol. 135, No. 3508, pp. 1037-1045; March 23, 1962.
31. W. A. Fowler, J. L. Greenstein, F. Hoyle, "Nucleosynthesis During the Early History of the Solar System," *Geophysical J. of the Roy. Astr. Soc.*, Vol. 6 No. 2, pp. 148-220; 1962.

REFERENCES (Continued)

32. S. Weinreb, "The Detection of UHF Radiation from Deuterium in Interstellar Space," B. S. Thesis, M. I. T.; June, 1958.
33. S. Chandrasekhar, Radiative Transfer, Oxford University Press, London, England, 1950.
34. G. B. Field, "Excitation of the Hydrogen 21-cm Line," Proc. IRE, Vol. 46, pp. 240-250; March, 1952.
35. J. P. Hagen, A. E. Lilley, E. F. McClain, "Absorption of 21 cm Radiation by Interstellar Hydrogen," *Astrophys. J.*, Vol. 122, pp. 361-375; November, 1958.
36. C. A. Muller, "21 cm Absorption Effects in the Spectra of Two Strong Ratio Sources," *Astrophys. J.*, Vol. 125, pp. 830-834; May, 1957.
37. B. G. Clark, V. Radhakrishnan, and R. W. Wilson, "The Hydrogen Line in Absorption," Report No. 3, California Inst. of Tech. Radio Observatory, Pasadena, Calif., 1961.
38. J. A. Galt, C. H. Slater, and W. L. H. Shuter, "An Attempt to Detect the Galactic Magnetic Field Using Zeeman Splitting of the Hydrogen Line," *Mon. Not. Royal Astro. Soc.* Vol. 120, pp. 187-192; 1962.
39. R. D. Davies, C. H. Slater, W. L. H. Shuter, and P. A. T. Wild, "A New Limit to the Galactic Magnetic Field Set by Measurements of the Zeeman Splitting of the Hydrogen Line," *Nature*, Vol. 187, pp. 1088-1089; September 24, 1960.
40. J. G. Bolton and J. P. Wild, "On the Possibility of Measuring Interstellar Magnetic Fields by 21-cm Zeeman Splitting," *Astrophys. J.*, Vol. 125, p. 296; 1957.

BIOGRAPHICAL NOTE

Sander Weinreb was born in New York, New York, on December 9, 1936. He attended secondary school in Atlanta, Georgia and received the B. S. degree in electrical engineering in 1958 from the Massachusetts Institute of Technology. He received the 1958 Boston Section IRE Student Award to the most outstanding E. E. senior at M. I. T.

Upon receiving his B. S. degree, Mr. Weinreb entered M. I. T. graduate school. Since then, he has been a research assistant at the Research Laboratory of Electronics, except during the year 1959-1960 when he was the recipient of a National Science Foundation fellowship for full time graduate study. He has engaged in part time employment with Raytheon Manufacturing Company, Radiation Inc., and the Ewen Knight Corporation, doing work in the development of communication receivers, radiometers, and parametric amplifiers. He is presently a consultant to the National Radio Astronomy Observatory and M. I. T. Lincoln Laboratory.

Mr. Weinreb is a member of the IRE, Sigma Xi, Tau Beta Pi, and Eta Kappa Nu. He has the following publications.

"Frequency Multiplication with Nonlinear Capacitors - A Circuit Analysis," (co-authored with D. B. Leeson), Proc. IRE, Vol. 47, No. 12, pp. 2076-2084; December, 1959.

"Digital Radiometer," Proc. IRE, Vol. 49, No. 6, p. 1099; June 1961.

"A New Upper Limit to the Galactic Deuterium-to-Hydrogen Ratio," Nature, Vol. 195, No. 4839, pp. 367-368; July 28, 1962.

"An Attempt to Measure Zeeman Splitting of the Galactic 21-cm Hydrogen Line," Astrophysical J., Vol. 136, No. 3; November, 1962.